Miscellaneous Paper CERC-93-3
May 1993

US Army Corps
of Engineers
Waterways Experiment
Station

Preliminary Estimates of Frequency-Direction Spectra Derived from the SAMSON Pressure Gage Array, November 1990 to May 1991

by *Charles E. Long*
Coastal Engineering Research Center

Joan M. Oltman-Shay
Quest Integrated, Inc.

Prepared for Headquarters, U.S. Army Corps of Engineers

REPORT DOCUMENTATION PAGE

Form Approved
OMB No. 0704-0188

1. AGENCY USE ONLY (Leave blank)	2. REPORT DATE	3. REPORT TYPE AND DATES COVERED
	May 1993	Final report

4. TITLE AND SUBTITLE
Preliminary Estimates of Frequency-Direction Spectra Derived from the SAMSON Pressure Gage Array November 1990 to May 1991

5. FUNDING NUMBERS
Work Unit 32484

6. AUTHOR(S)
Charles E. Long, Joan M. Oltman-Shay

7. PERFORMING ORGANIZATION NAME(S) AND ADDRESS(ES)
USAE Waterways Experiment Station
Coastal Engineering Research Center
3909 Halls Ferry Road, Vicksburg, MS 39180-6199
Northwest Research Associates, Inc.
300 120th Avenue Northeast
Bellevue, WA 98005

8. PERFORMING ORGANIZATION REPORT NUMBER
Miscellaneous Paper CERC-93-3

9. SPONSORING/MONITORING AGENCY NAME(S) AND ADDRESS(ES)
U.S. Army Corps of Engineers, Washington, D.C. 20314-1000

10. SPONSORING/MONITORING AGENCY REPORT NUMBER

11. SUPPLEMENTARY NOTES
Available from National Technical Information Service, 5285 Port Royal Road, Springfield, VA 22161.

12a. DISTRIBUTION/AVAILABILITY STATEMENT
Approved for public release; distribution is unlimited.

12b. DISTRIBUTION CODE

13. ABSTRACT *(Maximum 200 words)*

In the course of the SAMSON (Sources of Ambient Micro-Seismic Noise) experiment conducted by researchers from Scripps Institution of Oceanography at the Coastal Engineering Research Center (CERC) Field Research Facility (FRF) near Duck, NC, a two-dimensional array of 24 bottom-mounted pressure sensors was deployed near the 13-m depth contour to detect unattenuated pressure signals arising from interactions of directionally opposed wave trains. The geometry of the array was ideal for wind wave directional spectral estimation in the 0.04- to 0.24-Hz frequency band. The formal SAMSON experiment took place in October and early November 1990, but data collection continued until June 1991. Data from this post-experiment period were made available to CERC and were subsequently processed with a 360-deg Iterative Maximum Likelihood Estimation algorithm to determine the general character of the local wave field, including specifically any indications of significant seaward-propagating wind wave energy. This report contains descriptions of the SAMSON array and the type of data collected, and an estimate of error for reported reflection coefficients. It contains displays, both graphic and tabular, of relevant wind wave parameters deduced from the analysis.

14. SUBJECT TERMS
Frequency-direction spectra
Wave climate
Wave reflection
Wind waves

15. NUMBER OF PAGES
91

16. PRICE CODE

17. SECURITY CLASSIFICATION OF REPORT	18. SECURITY CLASSIFICATION OF THIS PAGE	19. SECURITY CLASSIFICATION OF ABSTRACT	20. LIMITATION OF ABSTRACT
UNCLASSIFIED	UNCLASSIFIED		

Destroy this report when no longer needed. Do not return it to the originator.

Miscellaneous Paper CERC-93-3
May 1993

Preliminary Estimates of Frequency-Direction Spectra Derived from the SAMSON Pressure Gage Array, November 1990 to May 1991

by Charles E. Long
Coastal Engineering Research Center

U.S. Army Corps of Engineers
Waterways Experiment Station
3909 Halls Ferry Road
Vicksburg, MS 39180-6199

Joan M. Oltman-Shay

Quest Integrated, Inc.
21414 68th Avenue South
Kent, WA 98032

Final report

Approved for public release; distribution is unlimited

Prepared for U.S. Army Corps of Engineers
Washington, DC 20314-1000

Under Work Unit 32484

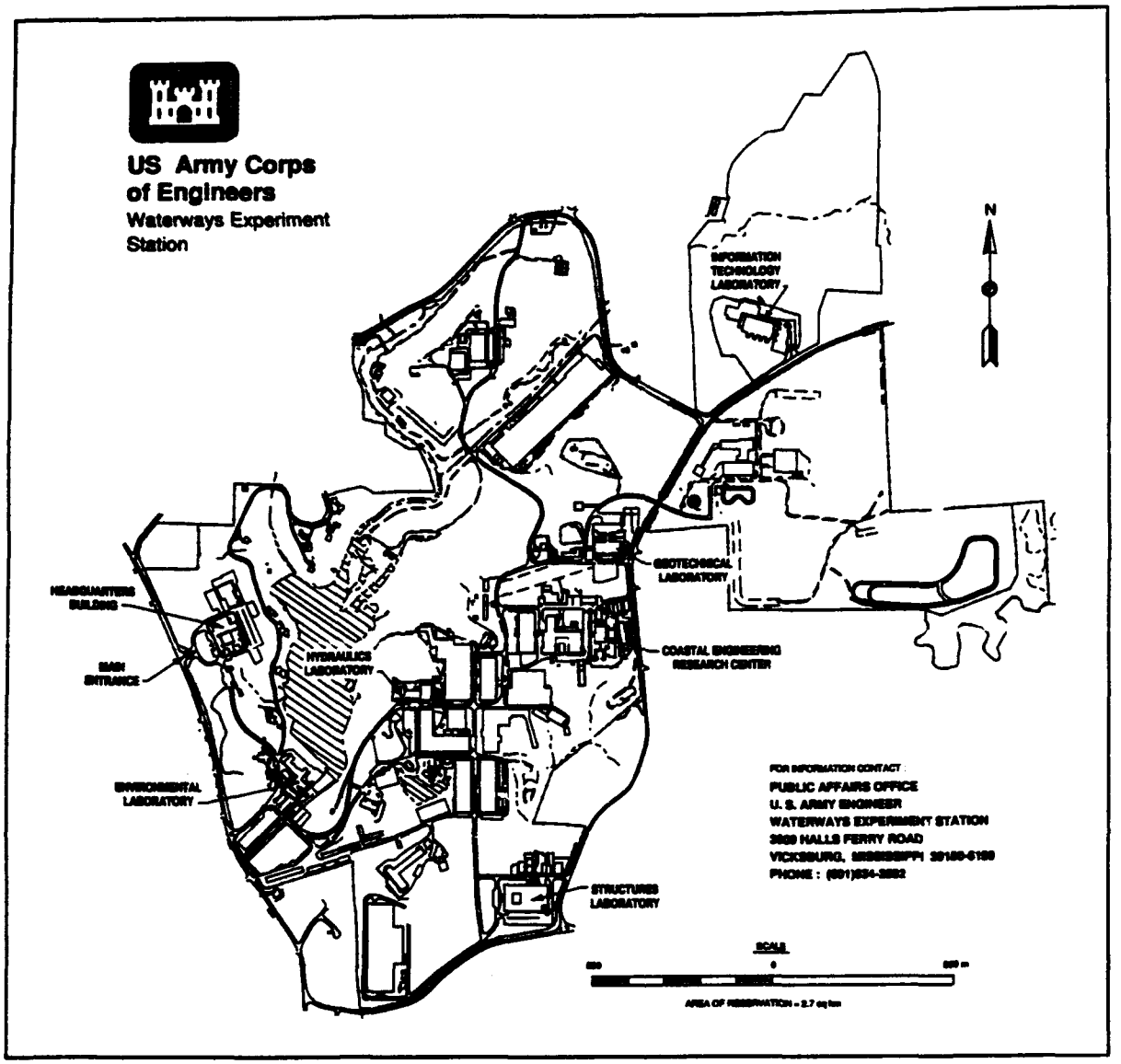

Waterways Experiment Station Cataloging-in-Publication Data

Long, Charles E.

Preliminary estimates of frequency-direction spectra derived from the SAMSON pressure gage array, November 1990 to May 1991 / by Charles E. Long, Coastal Engineering Research Center, [and] Joan M. Oltman-Shay ; prepared for U.S. Army Corps of Engineers.

91 p. : ill. ; 28 cm. — (Miscellaneous paper ; CERC-93-3)

Includes bibliographical references.

1. Ocean waves — North Carolina — Duck. 2. Water waves — Statistics. 3. Wind waves — Statistics. I. Oltman-Shay, Joan M. II. United States. Army. Corps of Engineers. III. Coastal Engineering Research Center (U.S.) IV. U.S. Army Engineer Waterways Experiment Station. V. Title. VI. Series: Miscellaneous paper (U.S. Army Engineer Waterways Experiment Station) ; CERC-93-3.

TA7 W34m no.CERC-93-3

Preface

This paper provides a summary of a series of wind wave frequency-direction spectral observations made with a two-dimensional, high-resolution directional wave gage of opportunity. These observations were the result of data shared by researchers from Scripps Institution of Oceanography (SIO) in execution of the Sources of Ambient Micro-Seismic Noise (SAMSON) experiment. The work was motivated by an opportunity to conduct a 360-deg analysis of data from a 24-gage array and thus find an extraordinary observation set of directionally distributed wave energy to augment understanding and modeling of nearshore processes that affect coastal engineering projects. This effort was authorized by Headquarters, US Army Corps of Engineers (HQUSACE), under Civil Works Research Work Unit 32484, "Directionality of Waves in Shallow Water," Coastal Flooding Program. Funds were provided through the Coastal Engineering Research Center (CERC), US Army Engineer Waterways Experiment Station (WES), under the program management of Ms. Carolyn M. Holmes, CERC. Messrs. John H. Lockhart, Jr.; John G. Housley; Barry W. Holliday; and David A. Roellig were HQUSACE Technical Monitors.

This data summary was prepared by Dr. Charles E. Long at CERC's Field Research Facility (FRF) in Duck, NC, under the direct supervision of Mr. William A. Birkemeier, Chief, FRF, and Mr. Thomas W. Richardson, Chief, Engineering Development Division, CERC; and under the general supervision of Dr. James R. Houston and Mr. Charles C. Calhoun, Jr., Director and Assistant Director, CERC, respectively.

The SAMSON experiment was planned by Drs. Robert T. Guza, SIO, and Joan M. Oltman-Shay of Quest Integrated, Inc., Kent, WA. The directional array was designed by Drs. Guza and Thomas H. C. Herbers, SIO. Data processing software was written by Dr. Oltman-Shay. The concept of continued data collection after the primary SAMSON experiment is credited to Dr. C. Linwood Vincent, CERC. The efforts of Ms. Janean Shirley, Information Technology Laboratory, in editing this report are greatly appreciated.

At the time of publication of this report, Director of WES was Dr. Robert W. Whalin. Commander was COL Leonard G. Hassell, EN.

Contents

Conversion Factors, Non-SI to SI (Metric) Units of Measurement

Non-SI units of measurement used in this report can be converted to SI (metric) units as follows:

Multiply	By	To Obtain
pounds (force) per square inch absolute	6.894757	kilopascals
fathoms	1.8288	meters

PRELIMINARY ESTIMATES OF FREQUENCY-DIRECTION SPECTRA DERIVED FROM THE SAMSON PRESSURE GAGE ARRAY, NOVEMBER 1990 TO MAY 1991

Introduction

1. During October and early November 1990, an experiment involving the detection of interacting wave trains was conducted at the Coastal Engineering Research Center Field Research Facility (FRF). Known as SAMSON (Sources of Ambient Micro-Seismic Ocean Noise), the experiment was designed to detect relatively unattenuated near-bottom pressure signals arising from nonlinear interactions of wind wave trains traveling in opposing directions. These small but detectable pressure signals are believed to initiate ocean bottom seismic waves that can propagate long distances and appear frequently in seismograms worldwide. In detecting both the presence of interacting wave trains and the resulting pressure signals, results of the SAMSON experiment can be used to test hypotheses concerning the initiation of such seismic waves near a coast where nearshore bathymetry can act as a partial reflector of ocean wind waves and thereby induce the requisite opposing wave trains. The experiment was designed and executed under the direction of Drs. Robert T. Guza and Thomas H. C. Herbers of the Center for Coastal Studies at Scripps Institution of Oceanography, University of California, San Diego, and Dr. Joan M. Oltman-Shay of Quest Integrated, Inc., Kent, Washington, with the experiment site, staging area, and logistical support provided by the FRF.

2. The primary instrument in the SAMSON experiment was a two-dimensional array of 24 bottom-mounted pressure gages located in a nominal water depth of 13 m. By design, this depth is deeper than is normally used for measurement of ocean wind waves. The idea was to let the water column act as a filter for pressure signals arising directly from wind waves above a certain cutoff frequency. In that way, any detectable pressure signal above the cutoff frequency could be interpreted as being from the wave-wave interactions sought in the experiment. At frequencies below the cutoff, the pressure gages could readily detect wind wave signals. As a result, the array of gages was an excellent directional detector for waves in the lower part of the wind wave frequency band, from about 0.04 to 0.24 Hz.

3. The SAMSON pressure gage array was deployed in September 1990 and the formal experiment took place in October and early November. Scheduling recovery of the gages immediately after the experiment was deemed unwise because of the onset of winter and the high likelihood of poor working conditions. Hence, the gages were left in place until the following spring and, because it was a fully functioning instrument set, data were collected for as long as the gages continued to function, though this was not expected to be for very long, given the harshness of the environment in which they were deployed. Curiously, 22 of the 24 gages continued to function perfectly until the first part of June 1991, at which time the gages were recovered. Data from this post-experiment phase of instrument deployment, mid-November 1990 to the end of May 1991, have been made available to the FRF for directional analysis. This report addresses the nature and results of that analysis.

4. The geometry of the SAMSON array conformed to guidelines given both by Davis and Regier (1977) for a method of wave directional detection known as Maximum Likelihood Estimation (MLE) and for an improvement on this method, known as Iterative Maximum Likelihood Estimation (IMLE), derived by Pawka (1982, 1983). Early attempts to process the SAMSON data with the MLE method were less than satisfactory for some aspects, primarily the estimation of reflection coefficients, of the analysis. Consequently, the IMLE method was employed and it provided much better results.

5. Because the SAMSON array is two-dimensional, it can detect wave energy propagating in any direction. This allows estimation of energy propagating seaward and avoids the 180-deg ambiguity present in analysis of data from the FRF linear array directional wave gage reported previously (Long and Oltman-Shay 1991, Long 1991a, 1991b). In this report, seaward-propagating energy is called "reflected" energy because reflection of incident waves from nearshore bathymetry is its most likely cause, though other processes may possibly be present. Determination of reflected directional spectra is of enormous interest in coastal research because of the myriad processes that are possible theoretically if significant reflection is present. Hence, this report is the first to describe a well-resolved estimation of the full 360-deg wave climate at the FRF.

6. The beginning text of this document describes and clarifies the substantial information contained in the appendixes. A brief overview is given of the measurement site, instrumentation, data collection, and method of

directional spectral estimation. These subjects are described in other publications to which the reader is referred for greater detail. Following the overview is a description of the archived frequency-direction spectra and some characterizing bulk parameters that can be derived from them. Appendix A is a listing of these characterizing parameters and is intended to be used as a kind of catalog of the set of spectra. Appendix B contains graphs of time series of some of these parameters as a pictorial augmentation of the information in Appendix A. Appendix C describes tests of the ability of the SAMSON array together with the IMLE algorithm to detect low levels of reflected wave energy in the presence of higher levels of incident wave energy and varying levels of background noise. It provides a measure of confidence for the reflection coefficients reported in Appendixes A and B.

Measurement Site

7. As shown in Figure 1, the FRF is located on the barrier island chain of coastal North Carolina. A detailed description of the layout, function, and capabilities of the FRF is given by Birkemeier et al. (1985). A detailed, quantitative description of the climate at the FRF, as determined from its arsenal of instrumentation and for the 11 years of its existence, is given by Leffler et al. (1992). Of particular relevance to directional wave studies are the wave-steering bathymetry and wave-generating winds.

8. As regards the former, the coastline in the vicinity of the FRF is nearly straight for several tens of kilometers north and south (Figure 1). It is oriented such that a shore-normal line (directed seaward) is very nearly 70 deg from true north. Waves and onshore winds can approach this site along an easterly 180-deg arc from 340 deg to 160 deg true. The adjacent continental shelf is wide, relatively shallow, and of somewhat complex bathymetry. The direction of nearest approach of the 100-m isobath, which indicates the shelf break, is 10 deg to 15 deg south of east and is about 80 km distant. A typical bottom slope for the shelf is 1 m/km, but this is interrupted by numerous features of 1- to 10-km horizontal scales and 10-m vertical scales scattered irregularly across the shelf.

9. Within a few kilometers of the FRF, the offshore bathymetry is more regular, with isobaths nearly shore-parallel and a bottom slope of about 2 m/km (Figure 2). Some irregularities exist. Within about 300 m of the

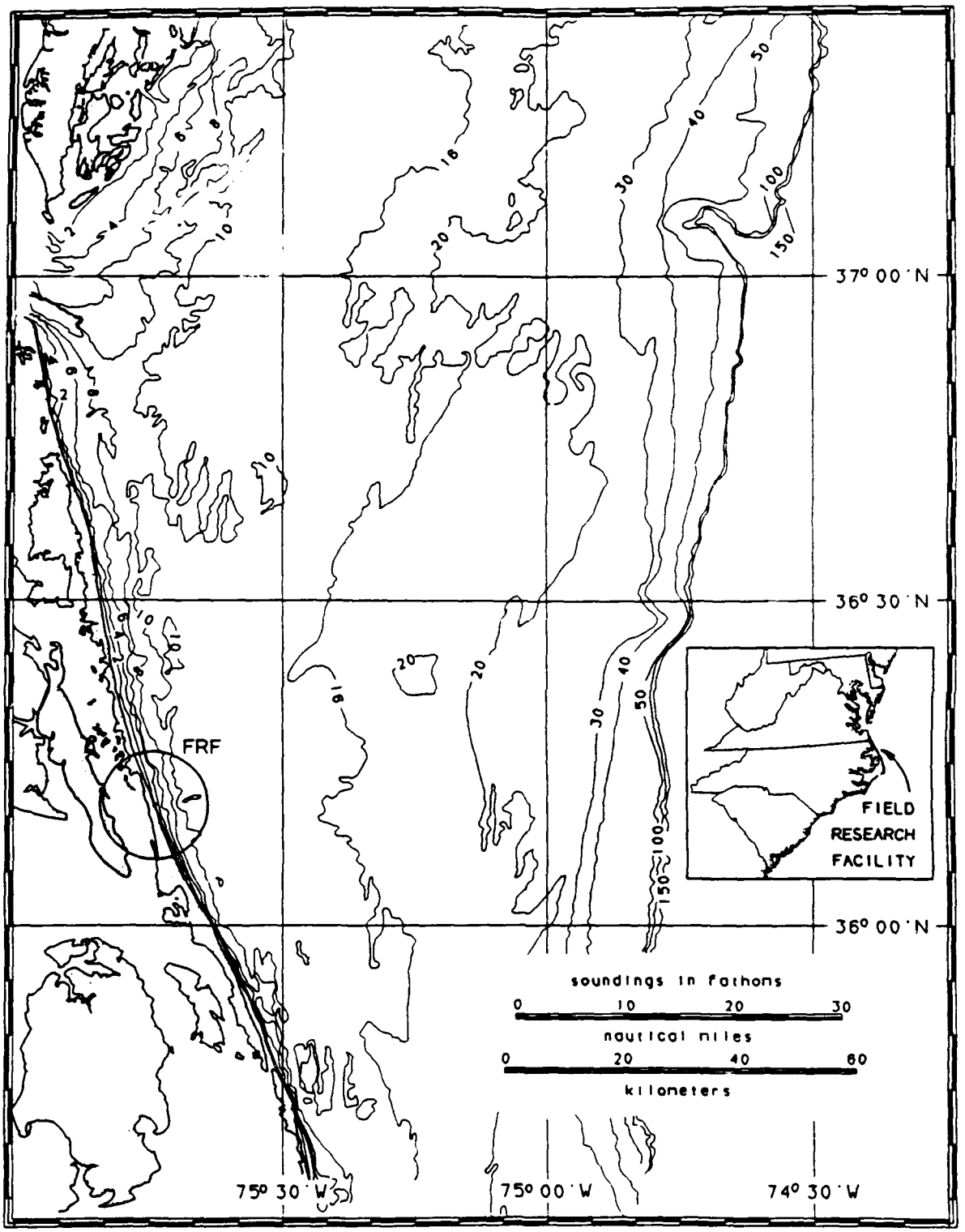

Figure 1. Location and offshore bathymetry of the FRF

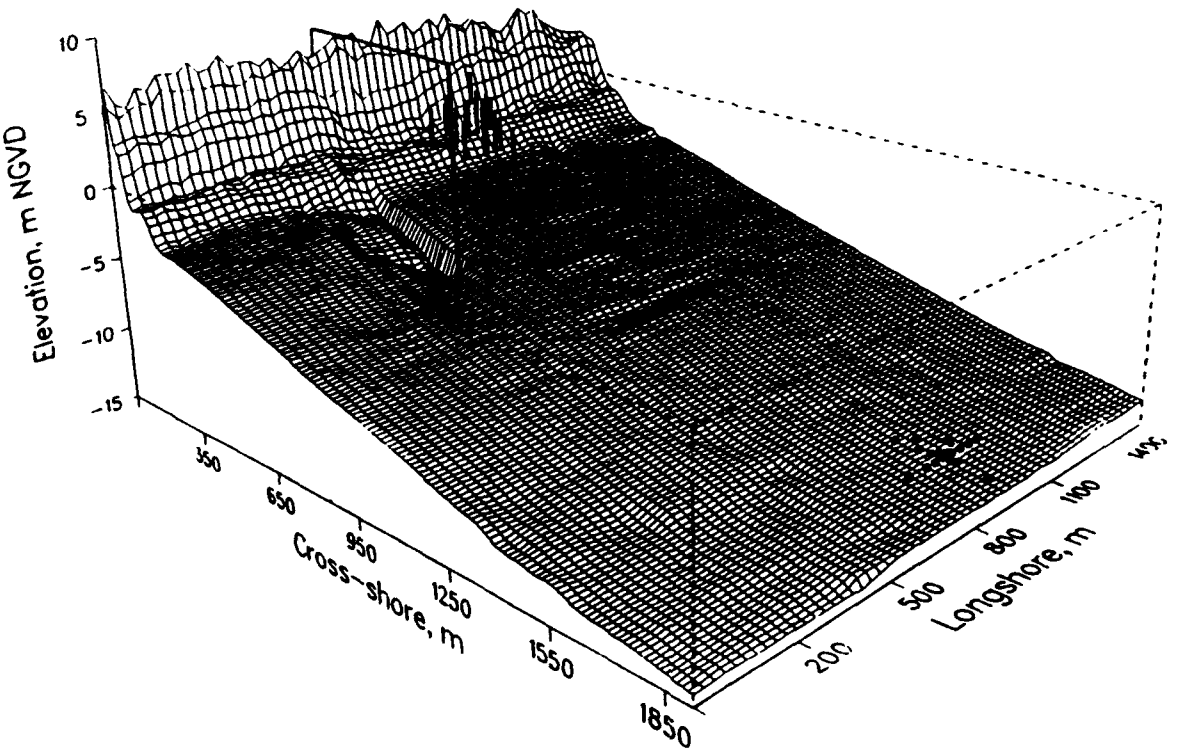

Figure 2. Approximate nearshore bathymetry and SAMSON array location (seawardmost set of dots)

shore, there exists a complex and mobile bar system (Birkemeier 1984). Furthermore, waves and currents have created some irregular bathymetry in the vicinity of the FRF research pier, which extends about 600 m offshore (Miller, Birkemeier, and DeWall 1983).

10. The site is subject to a variety of climates that give rise to a diverse set of directional wave conditions. Primary sources of high-energy waves are winds associated with hurricanes and frontal passages. Though Hurricane Lily moved up the middle Atlantic Ocean during the formal SAMSON experiment, no other hurricanes affected the FRF wave climate in the period covered by this report. Low-pressure weather fronts, of which several crossed the FRF site during this reporting period, were typically oriented northeast-southwest, with strong wave-generating winds coming from the northeast.

11. As a consequence of the complex offshore bathymetry and the close proximity of wave-generating wind systems, it is expected that directional wave spectra will exhibit a rather broad, complex structure. This expectation has been realized in studies at the FRF using a linear array directional wave gage deployed about 900 m offshore in 8 m of water (Long and Oltman-Shay 1991). With the exception of well-sorted waves from distant storms and waves in the initial growth stages under strong steady local winds, most spectra were found to be directionally broad. Because of the 180-deg ambiguity inherent in a linear array, it is possible that part of this directional spread could be due to reflected wave energy, which is folded over to appear as incident wave energy in the linear array data processing algorithm. The ability to perform a 360-deg wave analysis with the SAMSON array helps to ascertain the extent of the error induced by the 180-deg ambiguity of the linear array, in addition to estimating the amount of seaward-propagating energy.

Instrumentation

12. The primary directional wave detector used in this study was a two-dimensional array of wave gages coupled with the high-resolution IMLE algorithm for conversion of gage data to directional spectra. The array of gages sampled the near-bottom pressure field and, through linear wave theory, provided estimates of sea-surface displacement at several points in (horizontal) space. The mathematical treatment of these data to obtain estimates of wave directionality involves two tuning procedures to optimize results. One procedure is the use of subsets of gages to reduce the effective size of the array for waves with short wavelengths. The other procedure is the elimination of select gages from analysis in the event that the array provides too much redundant information in a particular observation.

Basic array

13. The SAMSON array consisted of 24 pressure gages buried about 0.1 m below the bottom in the vicinity of the 13-m isobath about 1,700 m offshore and slightly to the north of the research pier. This is shown in Figure 2 as the seawardmost set of dots. In addition to the design requirements mentioned above, its location satisfies three constraints. First, the array is generally outside the surf zone so that linear wave theory is applicable in data

processing. Second, it is in water shallow enough that signals from 4-sec waves are detectable above background noise at the bottom-mounted gages. Third, the array is located away from the irregular isobaths around the pier and in the nearshore bar system, which helps minimize bathymetrically induced inhomogeneities in the wave field.

14. Figure 3 is an enlarged view of the array layout and shows gage spacing as well as the gage numbering scheme. Spacing between the gages in the array corresponds reasonably well to the array-design criterion posed by

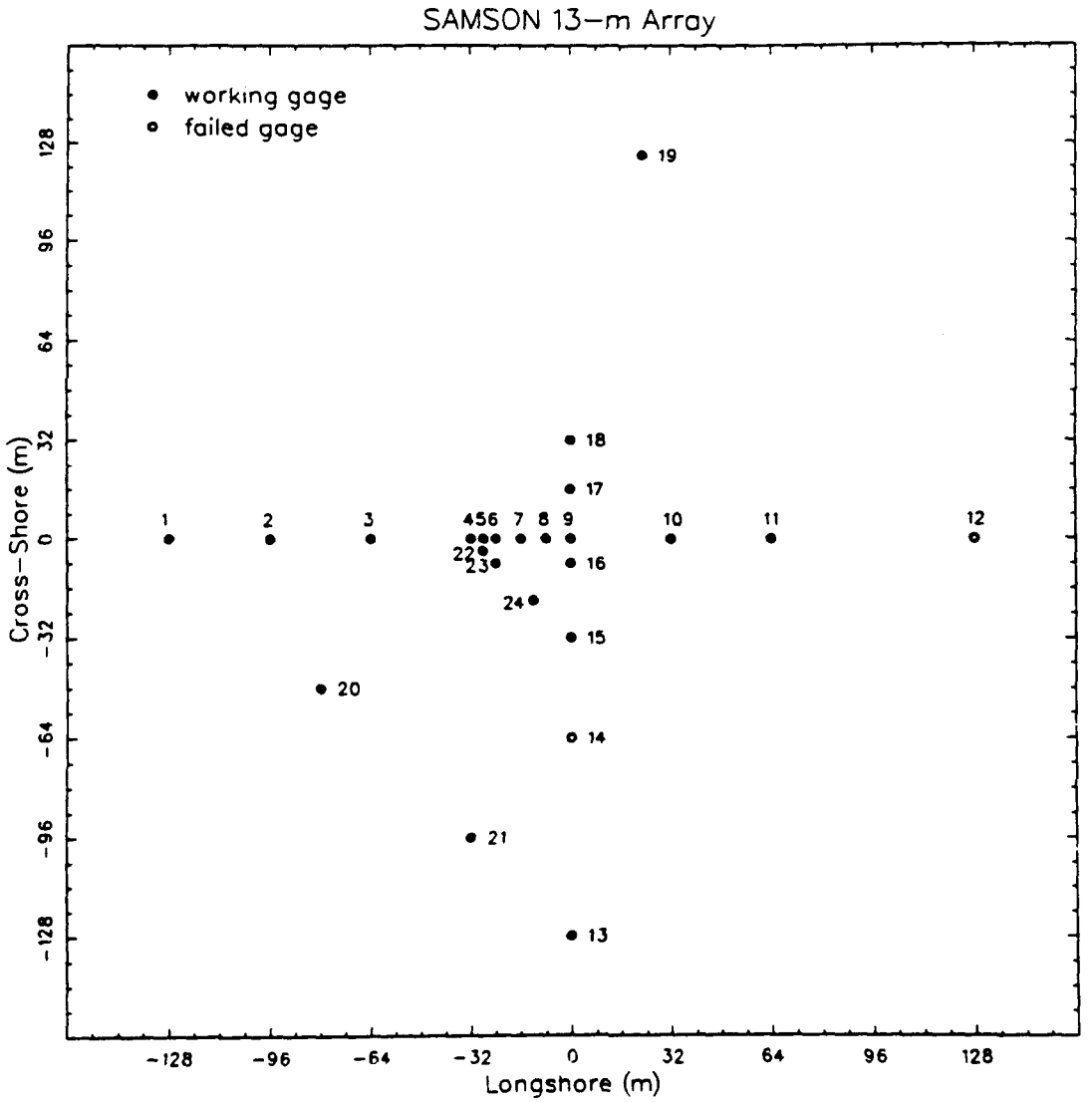

Figure 3. Layout and numbering scheme for SAMSON array

Davis and Regier (1977) that every gage pair have a unique separation or spatial lag. There are a large number of redundant lags built into the array, so that multiple estimates of cross-spectral densities can be made to check for spatial inhomogeneity in the wave field and to reduce system noise. There are more unique lags with which to fill in the spatial cross-spectral matrix from which wave direction estimates are made. Minimum gage spacing is 4 m, maximum spacing (the greatest dimension of the array) is 256 m, and intermediate gage spacings are in multiples of 4 m. Unfortunately, gages 12 and 14 were inoperative, and the loss of gage 12 reduced the longshore dimension of the array to 192 m, at some cost to direction-resolving ability for the longest (0.05-Hz) waves measured. It is noted that gage 19 appears to be offline from the basic gage pattern, and it was, in fact, slightly misplaced. However, this does not make it ineffective. In IMLE processing, it is only necessary for the true gage positions to be known, and not that they conform to any particular pattern. The SAMSON gage positions were surveyed to an accuracy of better than 1 m after the gages were in place. At worst, this uncertainty would result in a directional error of about 1.8 deg for the shortest (0.24-Hz) waves considered and about 0.6 deg for the longest (0.04-Hz) waves.

Sub-arrays

15. At sufficiently large lags, signals from a natural wave field tend to become uncorrelated. As a result, cross-spectra between widely spaced gages tend to become mostly noise. At very small lags, correlations and cross-spectra are difficult to discern from those at zero lag and so tend to become somewhat redundant. The terms large and small are generally related to the wavelengths λ^* of waves under consideration. To avoid both redundancy at small lags and the problem of noise at large lags, the SAMSON array data were processed by using subsets of gages, or sub-arrays, based on ranges of wavelengths being considered.

16. Figure 4 illustrates the sub-arrays and the ranges of wave frequency f used with each sub-array in the present analysis. Note that gages 12 and 14, from which reliable data were not obtained, are not shown. For the longest waves, all the working gages were used except those that introduced

---

* For convenience, symbols and abbreviations are listed in the Notation (Appendix D).

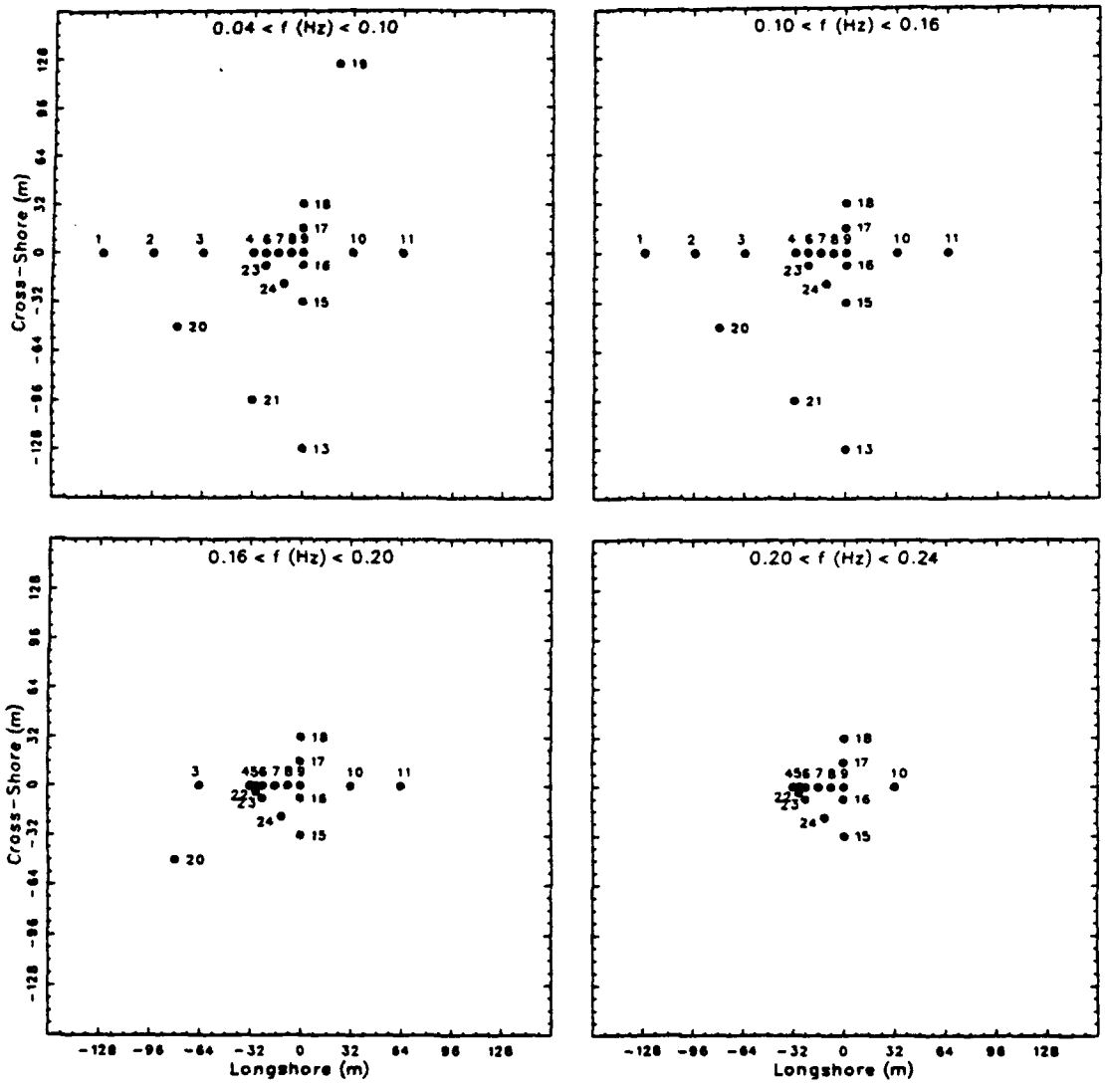

Figure 4. Sub-arrays and their associated frequency bands

the shortest (4-m) lags, i.e., gages 5 and 22. This left 20 gages for processing data in the frequency range $0.05 < f\ (Hz) < 0.10$ or wavelength range $103 < \lambda\ (m) < 220$ (assuming a nominal water depth of 13 m), and included the longest possible lags.

17. For shorter wavelengths, the selection criterion was that the longest dimension of the sub-array not exceed about three wavelengths of the shortest waves in a given band. For the low mid-range of frequencies, $0.10 < f\ (Hz) < 0.16$, corresponding to wavelengths $55 < \lambda\ (m) < 103$, this

procedure eliminated gage 19 from analysis, leaving 19 gages in the sub-array. For the high mid-range of frequencies, $0.16 < f\ (Hz) < 0.20$, or $38 < \lambda\ (m) < 55$, gages 1, 2, 13, and 21 were eliminated, but the short-lag gages 5 and 24 were included, for a total of 17 gages. For the highest frequencies, $0.20 < f\ (Hz) < 0.24$, $27 < \lambda\ (m) < 38$, gages 3, 11, and 20 were excluded from the previous set, leaving 14 gages.

Data-adaptive gage elimination

18. As noted by Davis and Regier (1977), wave fields may occur for which the cross-spectral matrix of a given array geometry contains nearly redundant information. When this happens, it becomes impossible to compute the inverse of the cross-spectral matrix, a process that is central to the IMLE algorithm, and no directional information can be found. This condition can occur when the wave field has a particularly simple directional distribution, such as a nearly unidirectional wave train, or when the wave field is more complex, but crosses the array of gages in such a way that many pairs of gages have approximately equal cross-spectral values. This condition is more likely to occur when the number of gages is large, as in the present case. One solution to this dilemma is to redeploy the gages in a pattern that does not yield so much redundant information, but such a procedure is not likely to be successful at a site, like the FRF, where the wave field is known to have quite diverse characteristics. In any case, such a procedure was not practical in the present study because gage positions were fixed before the study began.

19. The approach used here was to eliminate the data of one or more gages from analysis and try the directional computation again until success was achieved. The order of gage elimination was assigned *a priori* by examining the nature of coverage provided by a reduced array when transformed into lag coordinates. For the sub-arrays associated with long waves, gages were first eliminated that gave small lags or small lag increments, but still evenly covered the largest possible spans in both dimensions. A second criterion, to avoid aliasing, was that any remaining gages not have lag increments larger than half of the longest wavelength to be analyzed. For short-wave sub-arrays, gages were first eliminated that gave large lags. The second criterion for short waves was the same as for long waves. Table 1 lists the gages used in each frequency range and the numerical order in which they were to be eliminated. For example, for the lowest frequencies, gage 24

Table 1

Order of Gage Elimination from SAMSON Sub-Arrays

Frequency range:	0.04 < f (Hz) < 0.10
Sub-array gages:	1, 2, 3, 4, 6, 7, 8, 9, 10, 11, 13, 15, 16, 17, 18, 19, 20, 21, 23, 24
Elimination order:	24, 6, 16, 8, 23, 10, 19, 11, 1, 13, 21, 2, 20, 18, 4, 9, 17, 15, 3, 7
Frequency range:	0.10 < f (Hz) < 0.16
Sub-array gages:	1, 2, 3, 4, 6, 7, 8, 9, 10, 11, 13, 15, 16, 17, 18, 20, 21, 23, 24
Elimination order:	24, 1, 2, 13, 4, 8, 23, 11, 21, 20, 3, 15, 10, 18, 7, 16, 17, 6, 9
Frequency range:	0.16 < f (Hz) < 0.20
Sub-array gages:	3, 4, 5, 6, 7, 8, 9, 10, 11, 15, 16, 17, 18, 20, 22, 23, 24
Elimination order:	20, 11, 4, 10, 24, 8, 3, 15, 18, 16, 22, 5, 6, 23, 17, 7, 9
Frequency range:	0.20 < f (Hz) < 0.24
Sub-array gages:	4, 5, 6, 7, 8, 9, 10, 15, 16, 17, 18, 22, 23, 24
Elimination order:	18, 10, 17, 08, 15, 16, 9, 24, 7, 22, 5, 23, 4, 6

Note: Gages 12 and 14 are excluded.

is eliminated first, followed by gage 6, gage 16, gage 8, etc. Though a complete elimination order is listed, a limit was set that at least four gages must remain for a directional estimate to be made. This limit was not met in practice, though the system was occasionally reduced to five or six gages.

Pressure gages and data collection hardware

20. Each pressure gage is a Setra Systems Model 280E capacitive-type transducer having a range of 0 to 50 psia*. The manufacturer's specifications indicate an accuracy of 0.11 percent of full scale, or the pressure

* A table of factors for converting non-SI units of measurement to SI (metric) units is presented on page 3.

equivalent of ±0.037 m of water. Analog pressure signals were collected in an underwater terminal where they were discretized to 12-bit binary form, multiplexed, and encoded for transmission down a single data line. Digitization of the signal to 12-bit binary form resulted in a discretization uncertainty of the equivalent of 0.002 m of water. At the landward end of the data line, the encoded signal was decoded and sent to a parallel port on a personal computer for data acquisition. During the post-experiment period, data files from the personal computer were periodically transferred to the higher capacity hard disks of the FRF's Digital Equipment Corporation VAX 11/750 computer for accumulation and eventual archiving on magnetic media.

Data Collection

21. Signals from each of the 24 pressure gages were sampled at 4 Hz and stored in records of 768 samples. A total of 1,280 records, or 10,240 data points, were collected for each gage for an elapsed time of 2 hr 50 min 40 sec for each collection. Starting times for collections during the main SAMSON experiment were daily at 0100, 0400, 0700, 1000, 1300, 1600, 1900, and 2200 Eastern Standard Time (EST) and this pattern was continued into the post-experiment period until 1 December 1990. At that time, collection start times were set to coincide with routine FRF observations (Birkemeier et al. 1985), which occur daily at 0100, 0700, 1300, and 1900 EST. This collection pattern was maintained until the gages were disconnected for retrieval on 2 Jun 1991.

22. In the analysis presented here, only the first 2 hr 16 min 32 sec (eight records of 4,096 points) of data from each collection was used. This procedure resulted in data sets that coincided both in start times and duration with other permanent directional wave gages at the FRF. It also allowed consistency in processing some collections that were terminated early to allow time for file transfers from the data collection computer to the FRF VAX 11/750 hard disks.

Data Processing

23. Conversion of measured time series to estimates of frequency-direction spectra requires products of frequency spectral estimates from all the various gages in the array. For final results to be accurate, raw input

data must be of exceptionally high quality so that spiky or drifty data from one gage do not contaminate products of results from the other gages. Hence, the procedure for data processing is to check the raw data for errors, estimate the frequency-direction spectrum, and then compute some bulk parameters with which to characterize results.

Error checking

24. Because multiple gages were deployed in an (assumed) uniform sea, certain properties of raw data from the pressure gages should be identical. A convenient method of error checking is to compute frequency spectra of the raw time series from each of the 22 functioning gages and overplot the results on a single graph. This method was used by Drs. Guza and Herbers during the main experiment and has also been incorporated for the present analysis. Because of the depth at which the SAMSON gages were deployed, very little direct wind wave signal is expected in the frequency range from about 0.3 Hz out to the Nyquist frequency of 2.0 Hz. The frequency spectrum in this frequency band should primarily indicate system noise, which should be about the same for each gage. Excessively spiky data from one gage will raise the noise level for that gage relative to the noise levels from the other gages, so that its signature will be distinct in a collection of overplotted spectra. Strong drifts in the signal can appear in a variety of ways in corresponding spectra, but will generally give a distinct signal at low frequencies. In the pass band of wind wave frequencies for which directional estimates are computed (here 0.04 to 0.24 Hz), one expects the frequency spectra to be nearly identical.

25. Figure 5 is an example of one set of overplotted frequency spectra. Semi-logarithmic coordinates have been used and pressure gage voltages have been converted to equivalent heights of a static water column, but no other transformations have been used. As can be seen, signals in the wind wave frequency pass band are all very nearly alike, indicating that all gages are functioning reasonably well. The noise floor at high frequencies is very low relative to the wind wave signal and is nearly uniform for all gages. The spikes in the spectra at high frequencies are due to low levels of commercial 60-Hz power line noise present in the system. The inset graph in Figure 5 identifies the gages used and shows the deviations of their mean values from the median of all the mean values after adjusting for their relative depths. Also shown is the deviation of mean water level from still-water level (based

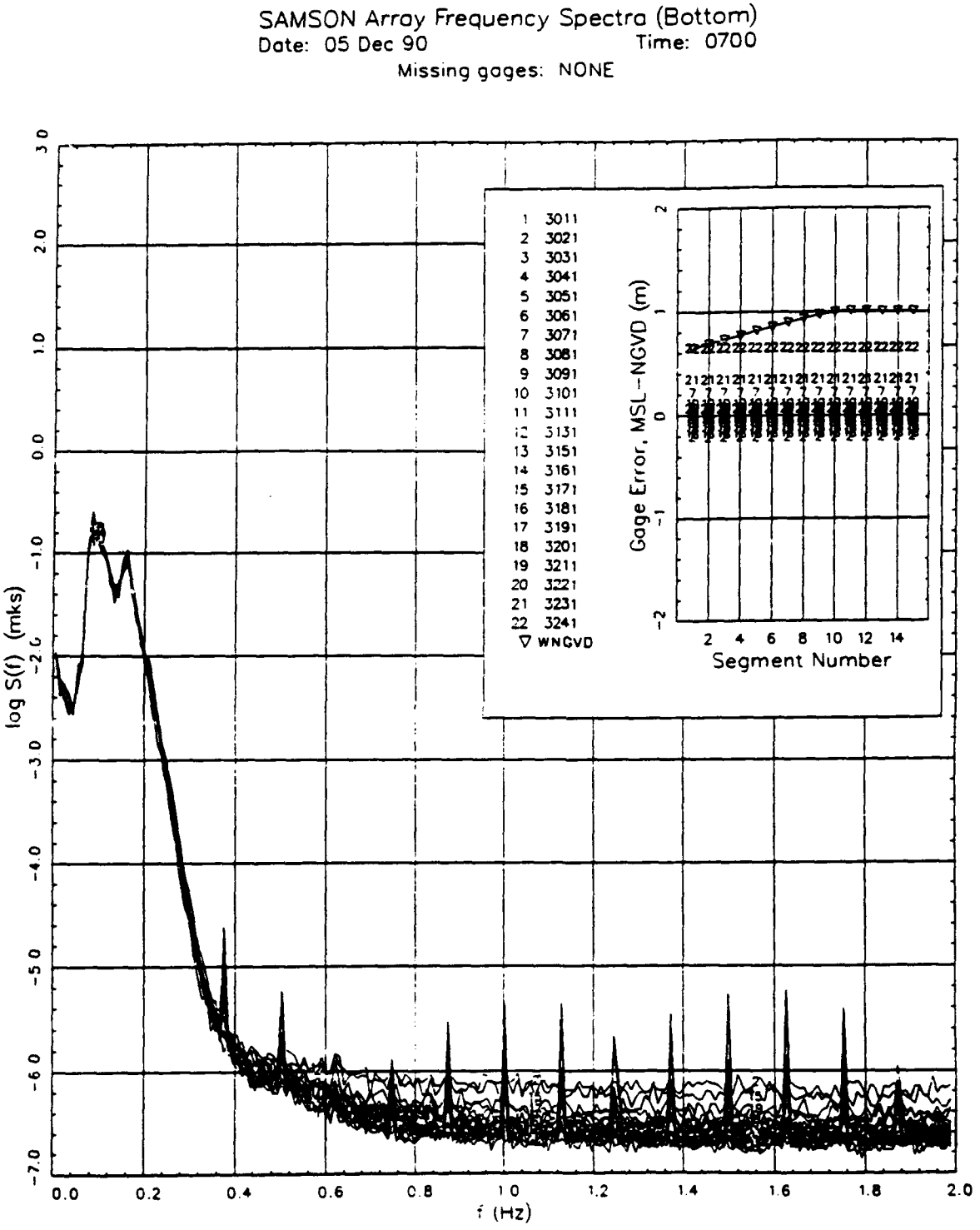

Figure 5. Example of overplotted frequency spectra

on the 1929 National Geodetic Vertical Datum) so that tidal level and tidal variation can be ascertained. If a particular gage becomes more noisy than the others, it can then be readily identified.

26. Tests with this kind of checking routine indicated that the SAMSON gages and data collection system were extremely reliable. At no time during the post-experiment period were any of the 22 functioning gages found to have any significant errors.

Frequency-direction spectra

27. Estimation of frequency-direction spectra is done in four parts. First, time series of pressure data from each gage are Fourier transformed to the frequency domain. Second, these transforms are converted to sea-surface displacement transforms. Third, cross spectra of sea-surface displacement are computed for all unique gage pairs at each frequency. Finally, an estimate is made of a directional distribution of wave energy that corresponds to the computed spatial variation in cross-spectral density for each frequency.

28. The Fourier transform is conventional. A 32,768-point time series is divided into 15 half-overlapping segments of 4,096 points. Segments are tapered with a Kaiser-Bessel window (a modified Bessel function of the first kind, compensated uniformly for loss of variance due to windowing) and fast Fourier transformed. An intermediate-resolution transform is found by averaging the 15 transformed segments, frequency by frequency. Final transforms are found by then averaging results over 10 adjacent frequency bands. Final resolution bandwidth is 0.00976 Hz, and degrees of freedom are at least 150 (assuming eight contiguous segments and ignoring any gain from lapped segments). Transform estimates are retained for 20 frequency bands with band-center frequency ranging from 0.054 to 0.240 Hz.

29. Conversion of pressure signals at depth to water-surface displacement is done through the linear wave theory pressure response factor as described in the Shore Protection Manual (SPM) (1984). After this conversion, complex cross spectra in the form of coincident and quadrature spectra are computed in the conventional way (Bendat and Piersol 1971, Jenkins and Watts 1968) for all unique gage pairs. Cross-spectral estimates at a given frequency are then stored in a matrix of complex numbers, the indices of which can be used to address data arrays containing gage position for the computation of gage separation distance, or lag space, in preparation for directional spectral estimation at that frequency.

30. As mentioned in the introduction, conversion of cross-spectral patterns in lag space to directional spectra is done with the IMLE algorithm described by Pawka (1983). The algorithm is also described in application to data from heave-pitch-roll buoys by Oltman-Shay and Guza (1984). Specifically, data were processed using Equations 1 to 4 of Pawka's (1983) paper with a convergence exponent of 1.0, a convergence coefficient of 5.0, and a maximum of 30 iterations.

31. The algorithm used here made a spectral estimate for every 1 deg of azimuthal direction. These were smoothed over 2-deg arcs to create 180 bins covering a complete circle with which to describe the directional distribution of wave energy.

32. The primary result of data processing is an estimate of the discrete frequency-direction spectrum $S(f_n,\theta_m)$, which represents the variance of sea-surface displacement per frequency resolution bandwidth df (= 0.00976 Hz) per direction resolution arc $d\theta$ (= 2 deg), where f_n is the n^{th} of $N = 21$ discrete frequencies and θ_m is the m^{th} of $M = 180$ discrete directions. In this work, direction is considered to be the angle from which wave energy is coming, measured counterclockwise from shore-normal. It is noted that parametric definitions below are given in terms of these discrete definitions rather than in terms of the continuous functions they approximate.

33. Numerical values of $S(f_n,\theta_m)$ can range over many orders of magnitude, depending on the amount of energy in a given frequency band and direction arc, and this can require space-consuming formats for archiving data. To simplify this problem, frequency-direction spectra can be saved in the form of directional distribution functions $D(f_n,\theta_m)$ defined by

$$D(f_n,\theta_m) = \frac{S(f_n,\theta_m)}{S(f_n)} \qquad (1)$$

where $S(f_n)$ is the frequency spectral density at frequency f_n. The directional distribution function has units of deg^{-1}, and its integral with respect to direction over all directions is unity.

34. The frequency spectrum in Equation 1 represents the total over all directions of sea-surface variance per frequency bandwidth and is defined in terms of the frequency-direction spectrum by

$$S(f_n) = \sum_{m=1}^{M} S(f_n, \theta_m)\, d\theta \qquad (2)$$

where $M = 180$ as mentioned above. Note that this is identical to a conventional frequency spectrum that would result from a time series of sea-surface displacements at a single point in space. Because it is an integral of the frequency-direction spectrum, it is called the integrated frequency spectrum.

35. A directional analog of the frequency spectrum is the integrated direction spectrum, found by summing the frequency-direction spectrum over all frequencies for a fixed direction arc. It is computed from

$$S(\theta_m) = \sum_{n=1}^{N} S(f_n, \theta_m)\, df \qquad (3)$$

where $N = 21$ in the present context. Figure 6 shows one way to display the frequency-direction spectrum and the corresponding integrated frequency and integrated direction spectra.

Bulk parameters

36. Several parameters have been computed to characterize the observed spectra. Five elementary types of parameter have been used here: water depth, characteristic wave height, peak period (or its inverse, peak frequency), peak direction, and reflection coefficient. There is more than one way to define some of these parameters, so definitions are presented here.

37. Water depth. Water depth is found from the median of the mean depths from all 22 gages in the array after adjusting for their relative deployment depths and applied at the location of gage 1, which is used as a reference gage. No compensation for variations in atmospheric pressure was done. Water depth represents a water level that varies with low frequency processes like tides. Because variations in mean water level adjust intersections of the water surface with nearshore bathymetry, it may be an important variable in accounting for the amount of observed reflected energy.

38. Characteristic wave height. Characteristic wave heights from spectral observations are most frequently given as H_{mo}, which is four times the standard deviation of sea-surface displacement. It can be determined from the volume under the frequency-direction spectrum by the equation

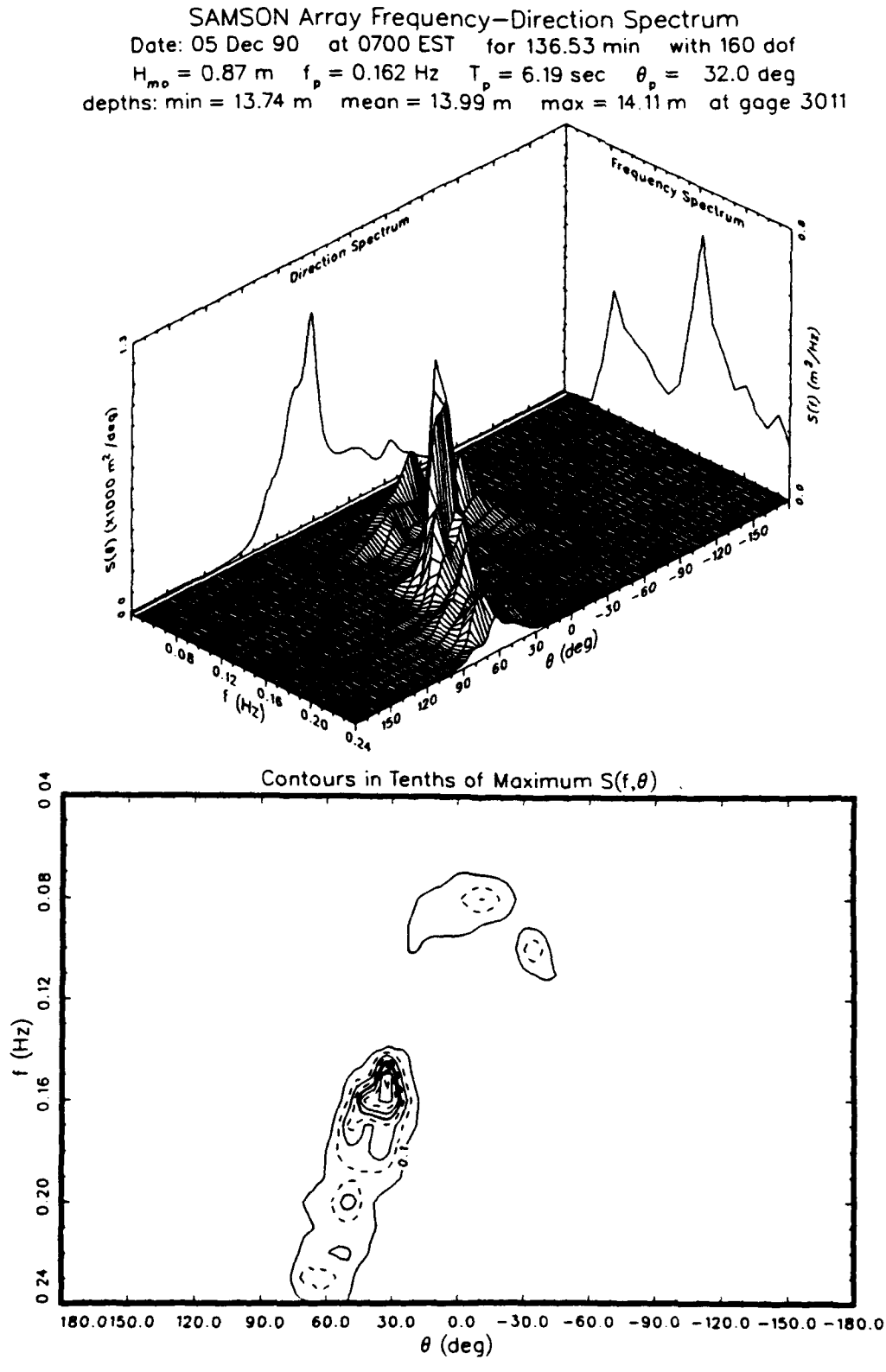

Figure 6. Sample displays of frequency spectrum, direction spectrum, and frequency-direction spectrum

$$H_{mo}^2 = 16 \sum_{n=1}^{N} \sum_{m=1}^{M} S(f_n, \theta_m)\, d\theta\, df \tag{4}$$

It can be found equivalently from the integrated frequency spectrum by

$$H_{mo}^2 = 16 \sum_{n=1}^{N} S(f_n)\, df \tag{5}$$

which is its conventional definition, or from the integrated direction spectrum by

$$H_{mo}^2 = 16 \sum_{m=1}^{M} S(\theta_m)\, d\theta \tag{6}$$

39. Because the analysis yields a 360-deg distribution of wave energy, it is reasonable to distinguish between incident wave energy and outgoing wave energy, which here is arbitrarily called reflected wave energy. Characteristic wave heights can be assigned for both incident and reflected energies, and the ratio of these wave heights is an estimate of the overall reflection coefficient. Such a ratio is rather sensitive to noise in the directional distribution estimate on which it is based, so an attempt is made here to reduce the noise level for parameters involved with wave reflection. It is noted that the tails of the integrated direction spectrum in Figure 6 do not go to zero, but appear to level off at some finite value that persists over all directions. While it is possible that some wave energy propagates in all directions, it is not likely. It is assumed, therefore, that the small persistent level of the spectrum represents the accumulation of instrument, system, and analysis noise S_N. In this report, its value is estimated as the average of the 10 smallest values of the discrete integrated direction spectrum and it is assumed to be constant for all directions.

40. A characteristic incident wave height $H_{mo,I}$ can be identified from the volume under the frequency-direction spectrum for waves approaching from directions in the range -90 deg < θ < 90 deg or, equivalently, the area under the integrated direction spectrum over the same range of directions after the removal of noise. Discrete directions in the present analysis are defined by

$$\theta_m = 180 \text{ deg} - (m - 1)\, 2 \text{ deg} \tag{7}$$

If half the energy in the 90-deg and -90-deg bins and all the energy in the

intervening directional bins is attributed to incident energy plus noise, a characteristic incident wave height is the sum of the spectral estimates reduced by the estimated noise, or

$$H_{mo,i}^2 = 8\,[S(\theta_{46}) - S_N]\,d\theta + 16 \sum_{m=47}^{135} [S(\theta_m) - S_N]\,d\theta + 8\,[S(\theta_{136}) - S_N]\,d\theta \qquad (8)$$

In a similar fashion, if the other half of the energy in the 90-deg and -90-deg bins and the remainder of the offshore propagating energy is attributed to reflected energy, a characteristic reflected wave height $H_{mo,r}$ is given by

$$H_{mo,r}^2 = 16 \sum_{m=1}^{45} [S(\theta_m) - S_N]\,d\theta + 16\left[\frac{1}{2} S(\theta_{46}) + \frac{1}{2} S(\theta_{136}) - S_N\right] d\theta + 16 \sum_{m=137}^{180} [S(\theta_m) - S_N]\,d\theta \qquad (9)$$

41. Peak frequency. Peak frequency, which has the generic notation f_p, can be defined at least two ways. One way is to find the frequency (and direction) at which the frequency-direction spectrum is maximum. Another way is to find the frequency at which the integrated frequency spectrum is maximum. This is the more conventional definition and is the basic definition used here. As with characteristic wave height, a distinction is made between peak frequencies associated with incident and reflected wave energy. The peak frequency of the incident wave spectrum $f_{p,i}$ is defined as the frequency of the maximum of the integrated incident frequency spectrum $S_i(f_n)$ defined following the notation above for H_{mo} (and without removing any noise estimate) as

$$S_i(f_n) = \frac{1}{2} S(f_n, \theta_{46})\,d\theta + \sum_{m=47}^{135} S(f_n, \theta_m)\,d\theta + \frac{1}{2} S(f_n, \theta_{136})\,d\theta \qquad (10)$$

In a similar manner, the integrated reflected wave spectrum $S_r(f_n)$ is given by

$$S_r(f_n) = \sum_{m=1}^{45} S(f_n, \theta_m)\,d\theta + \frac{1}{2}\left[S(f_n, \theta_{46}) + S(f_n, \theta_{136})\right] d\theta + \sum_{m=137}^{180} S(f_n, \theta_m)\,d\theta \qquad (11)$$

However, this spectrum was not used to find the reflected peak frequency because of the propensity for the tails of the incident peaks to cross the shore-parallel azimuths (±90 deg) and dominate the usually weaker reflected energy. For example, the spectral surface in Figure 6 crosses the 90-deg azimuth at $f = 0.24$ Hz and clearly has more energy than anywhere else along the reflection arc, even though that surface is associated with the incident spectrum. To avoid this effect in the definition of the reflected peak frequency $f_{p,r}$, an auxiliary frequency spectrum $S_a(f_n)$ was computed using only those parts of $S(f_n,\theta_m)$ for which $|\theta| \geq 120$ deg, or

$$S_a(f_n) = \sum_{m=1}^{30} S(f_n,\theta_m)\,d\theta + \sum_{m=152}^{180} S(f_n,\theta_m)\,d\theta \qquad (12)$$

The frequency at which $S_a(f_n)$ is a maximum is then identified as $f_{p,r}$.

42. The distinction between $f_{p,i}$ and $f_{p,r}$ may be important. Unless there are very strong reflections, the incident peak frequency is virtually the same as the peak frequency one would obtain from a time series at a single point in space. If the beach is uniformly reflective (the same for all frequencies), reflected peak frequency will be the same as incident peak frequency. If the two frequencies are not equal, the beach may be significantly more reflective for certain frequencies other than the peak, a situation of no small dynamic importance in nearshore processes.

43. Peak period. Peak period T_p is the characteristic wave period associated with spectral peak frequency. As simply inverses of peak frequencies, there are two peak periods associated with a directional spectrum corresponding to the two peak frequencies defined above. The incident peak period is $T_{p,i} = 1/f_{p,i}$ and the reflected peak period is $T_{p,r} = 1/f_{p,r}$.

44. Peak direction. Peak direction is the direction at which the most energy occurs. Given the generic symbol θ_p, it is defined as the peak of the directional distribution associated with a peak frequency. As with the other parameters there is an incident peak direction $\theta_{p,i}$ and a reflected peak direction $\theta_{p,r}$. Incident peak direction is the direction of the maximum of $S(f_{p,i},\theta_m)$ in the range of directions for which $-90 \text{ deg} < \theta < 90 \text{ deg}$ or for which index m is in the range $46 < m < 136$. Reflected peak direction is the maximum of $S(f_{p,r},\theta_m)$ for directions satisfying $\theta < -90$ deg and $\theta > 90$ deg or direction indices in the ranges $1 < m < 46$ and $136 < m < 180$. Note that all reflected directions are searched for $\theta_{p,r}$

and not just those outside the 120-deg azimuths that were used to search for $f_{p,r}$. This avoids biasing $\theta_{p,r}$, but does allow peaks occasionally to exist at ±90 deg due to the tails of incident directional distributions, as discussed above.

45. Reflection coefficient. Following notation and definitions given in the SPM, reflection coefficients χ are generally defined as ratios of reflected to incident wave heights. Coefficients indicating ratios of energy would then vary as the squares of height-based coefficients defined here. Three reflection coefficients are identified. The first is a bulk parameter that characterizes total reflected to total incident energy. These two energies are the volumes under the reflected and incident spectra, respectively, and, after removal of estimated noise, are the sources of the definitions of $H_{mo,r}$ and $H_{mo,i}$. Because it is a wave-height ratio that is used in the definition, a bulk reflection coefficient χ_{mo} is simply

$$\chi_{mo} = \frac{H_{mo,r}}{H_{mo,i}} \tag{13}$$

The other two reflection coefficients are frequency specific. One is based on the square root of the ratio of reflected to incident energy at the peak frequency of the incident spectrum and suggests how much of the energy at the frequency spectral peak is reflected. Denoted $\chi_{p,i}$, it is defined from the incident and reflected frequency spectra given by Equations 10 and 11, respectively, and modified for noise removal, as

$$\chi_{p,i} = \left[\frac{S_r(f_{p,i}) - S_N(f_{p,i})\cdot 180^\circ}{S_i(f_{p,i}) - S_N(f_{p,i})\cdot 180^\circ}\right]^{\frac{1}{2}} \tag{14}$$

where the noise estimate $S_N(f_{p,i})$ is the average of the smallest 10 values of $S(f_{p,i},\theta_m)$ and the product with 180 deg yields the area under the directional distribution attributed to noise. Because the peak in the reflected energy may not occur at the peak frequency of the incident spectrum, a third reflection coefficient is defined from the ratio of frequency spectral energies at the peak frequency of the reflected spectrum, with a correction for estimated noise. Denoted $\chi_{p,r}$, it is defined by

$$\chi_{p,r} = \left[\frac{S_r(f_{p,r}) - S_N(f_{p,r}) \cdot 180^\circ}{S_i(f_{p,r}) - S_N(f_{p,r}) \cdot 180^\circ} \right]^{\frac{1}{2}} \qquad (15)$$

where $S_N(f_{p,r})$ is the average of the 10 smallest values of $S(f_{p,r}, \theta_m)$.

46. Together, these parameters give a bulk characterization of some properties of a frequency-direction spectrum. There are, of course, many other parameters that can be defined, but the present set is simple and is adequate for this preliminary analysis.

Archived Results

47. A magnetic storage medium containing the set of observed frequency-direction spectra has been prepared for copying and distribution. These spectra are immediately available to researchers within the US Army Corps of Engineers and are available to the general public after June 1994. They can be obtained by communicating with:

Chief, Field Research Facility
1261 Duck Road
Kitty Hawk, NC 27949-4471
Phone: (919) 261-3511
Fax: (919) 261-4432

48. Appendix A contains a listing of the date, starting time (EST), and the characterizing parameters defined previously for each case. It is intended to be used as a kind of index or catalog of the set of cases. Dates are given in the form yymmdd , where yy is a two-digit year indicator (e.g., 90 means 1990), mm is the numeric index of the calendar month (i.e, 01 is January, 12 is December, etc.), and dd is the day of the month. A 24-hr clock is used.

49. Some of the bulk parameters defined above are plotted as functions of time in Appendix B. One graph is shown for each month of the post-experiment period. Shown are H_{mo} , $H_{mo,i}$, $H_{mo,r}$, depth, $\theta_{p,i}$, a modified form of $\theta_{p,r}$, $T_{p,i}$, $T_{p,r}$, χ_{mo} , $\chi_{p,i}$, and $\chi_{p,r}$. The modification to $\theta_{p,r}$ is a shift of 180 deg so that, in the figures, this variable represents direction <u>toward which</u> reflected waves propagate. The variable $\theta_{p,i}$ continues to represent direction <u>from which</u> incident waves arrive.

Discussion

50. The intent of this report is to indicate that additional frequency-direction spectral observations have been added to the already extensive FRF database and to characterize these observations with some simple parameters. There is clearly much more work to be done with this extraordinary data set, including scientific interpretation, but that is beyond the scope of this document. The descriptive parameters used here are defined simply to be preliminary indicators of the nature of the data. Close examination of the parameters displayed in Appendix B indicates that the rudimentary definitions used here may be somewhat misleading. Hence, a few warnings follow.

51. In plots of characteristic wave height, it is clear that most of the total wave energy, characterized by H_{mo}, is in the incident spectrum, which is characterized by $H_{mo,i}$. The so-called reflected energy, indicated by $H_{mo,r}$, is small, but is very seldom zero. It is possible that some energy always reflects from the FRF beach, but a more likely reason is that the tails of directional distributions for incident waves extend beyond the arbitrarily assigned 90-deg limit for incident energy, as mentioned in the paragraphs describing peak frequency. Consequently, $H_{mo,r}$ and all the reflection coefficients are affected by this characteristic. Reflection coefficients are legitimate estimators of seaward-propagating energy when defined in the simple way used here, but a more elaborate scheme is required to distinguish directionally broad incident spectra from true reflected spectra.

52. An attempt has been made to deal with the low, persistent levels of energy, interpreted here as noise, in all the directional spectra. If this interpretation is correct, and other sources of noise are not dominant, an approximate confidence level can be assigned to the reflection coefficients reported here. Appendix C describes an analysis using artificial directional distributions that include directionally broad noise at various levels, as well as incident spectra with tails that cross the 90-deg azimuth. The results of Appendix C suggest that, for noise-to-signal (N/S) ratios estimated from the present data set to be in the range 0.01 to 0.1, moderate to high estimated reflection coefficients can be low by as much as 25 percent and high by as much as 50 percent, with more probable errors in the range of 5 percent to 20 percent high for high-wave (small N/S) conditions. Small reflection coefficients (order 0.1) reported for low-wave conditions can be in error by a

factor of 2 or more. Because the results of Appendix C are based on rather clean synthetic data and because there may be other types of noise in real data, reflection coefficients reported here must be considered rough first approximations.

53. These observations qualify, but do not preclude, the usefulness of the parameters defined here. High energy conditions are readily identified, as are primary directions and periods. In high-energy conditions, reflected wave heights rise sufficiently above the background level to suggest the existence of legitimately quantified reflected energy. For the data set as a whole, however, more elegant definitions clearly are required for sound scientific interpretation, a task reserved for future work.

Summary

54. Data from the post-experiment period of the SAMSON project have provided an opportunity to add to the FRF database of high-resolution, directional-spectral observations. Processed data have been put in a form that will be highly accessible to researchers interested in nearshore processes. Directional gage, directional analysis algorithms, and definitions of characterizing parameters are described. The parameters used here are first approximations, but adequate for case distinction in this preliminary analysis. More refined parametric definitions will be necessary for proper scientific interpretation of the data.

References

Bendat, J. S., and Piersol, A. G. 1971. Random Data: Analysis and Measurement Procedures, Wiley-Interscience, New York.

Birkemeier, W. A. 1984. "Time Scales of Nearshore Profile Changes," Proceedings of the 19th Coastal Engineering Conference, American Society of Civil Engineers, 3-7 September 1984, Houston, TX, pp 1507-1521.

Birkemeier, W. A., Miller, H. C., Wilhelm, S. D., DeWall, A. E., and Gorbics, C. S. 1985. "A User's Guide to the Coastal Engineering Research Center's (CERC's) Field Research Facility," Technical Report CERC-85-1, US Army Engineer Waterways Experiment Station, Vicksburg, MS.

Davis, R. E., and Regier, L. A. 1977. "Methods for Estimating Directional Wave Spectra from Multi-Element Arrays," Journal of Marine Research, Vol 35, pp 453-477.

Jenkins, G. M., and Watts, D. G. 1968. Spectral Analysis and Its Applications, Holden-Day, Oakland, CA.

Leffler, M. W., Baron C. F., Scarborough, B. L., Hathaway, K. K., and Hayes, R. T. 1992. "Annual Data Summary for 1990, CERC Field Research Facility," Technical Report CERC-92-3, US Army Engineer Waterways Experiment Station, Vicksburg, MS.

Long, C. E. 1991a. "Index and Bulk Parameters for Frequency-Direction Spectra Measured at CERC Field Research Facility, September 1986 to August 1987," Miscellaneous Paper CERC-91-6, US Army Engineer Waterways Experiment Station, Vicksburg, MS.

_____. 1991b. "Index and Bulk Parameters for Frequency-Direction Spectra Measured at CERC Field Research Facility, September 1987 to August 1988," Miscellaneous Paper CERC-91-7, US Army Engineer Waterways Experiment Station, Vicksburg, MS.

Long, C. E., and Oltman-Shay, J. M. 1991. "Directional Characteristics of Waves in Shallow Water," Technical Report CERC-91-1, US Army Engineer Waterways Experiment Station, Vicksburg, MS.

Miller, H. C., Birkemeier, W. A., and DeWall, A. E. 1983. "Effects of CERC Research Pier on Nearshore Processes," Proceedings of Coastal Structures '83, American Society of Civil Engineers, March 9-11, 1983, Arlington, VA, pp 769-784.

Munk, W. H., Miller, G. R., Snodgrass, F. E., and Barber, N. F. 1963. "Directional Recording of Swell from Distant Storms," Proceedings of the Royal Society of London, Series A, Vol 255, pp 505-584.

Oltman-Shay, J., and Guza, R. T. 1984. "A Data-Adaptive Ocean Wave Directional-Spectrum Estimator for Pitch and Roll Type Measurements," Journal of Physical Oceanography, Vol 14, pp 1800-1810.

Pawka, S. S. 1982. "Wave Directional Characteristics on a Partially Sheltered Coast," Ph.D. dissertation, Scripps Institution of Oceanography, University of California, San Diego.

_____. 1983. "Island Shadows in Wave Directional Spectra," Journal of Geophysical Research, Vol 88, pp 2579-2591.

Shore Protection Manual. 1984. 4th Edition, 2 Vols, US Army Engineer Waterways Experiment Station, Coastal Engineering Research Center, US Government Printing Office, Washington, DC.

Appendix A: Table of Collection Times and Bulk Parameters

Bulk Parameters of Observed Frequency-Direction Spectra*

Date	Time EST	Wave Height H_{mo} m	$H_{mo,i}$ m	$H_{mo,r}$ m	Direction $\theta_{p,i}$ deg	$\theta_{p,r}$ deg	Period $T_{p,i}$ sec	$T_{p,r}$ sec	Reflection X_{mo}	$X_{p,i}$	$X_{p,r}$	Depth m
901112	1600	0.67	0.65	0.09	16.0	178.0	7.56	7.56	0.145	0.152	0.152	13.37
901112	1900	0.65	0.63	0.08	44.0	90.0	5.83	5.24	0.130	0.082	0.194	12.78
901112	2200	0.70	0.68	0.08	18.0	162.0	8.16	8.16	0.122	0.118	0.118	12.69
901113	0100	1.02	1.00	0.12	24.0	156.0	7.56	7.56	0.119	0.119	0.119	13.32
901113	0400	1.21	1.20	0.15	22.0	150.0	6.59	7.56	0.122	0.078	0.136	13.65
901113	0700	1.10	1.08	0.12	30.0	152.0	6.59	7.56	0.111	0.071	0.123	13.09
901113	1600	1.06	1.04	0.15	38.0	148.0	6.59	7.04	0.141	0.109	0.151	13.48
901113	1900	0.89	0.88	0.12	34.0	90.0	6.59	5.24	0.131	0.078	0.166	13.06
901114	0100	1.33	1.31	0.17	32.0	152.0	6.59	7.56	0.126	0.067	0.122	13.35
901114	0400	1.42	1.40	0.19	36.0	150.0	6.59	7.04	0.138	0.088	0.150	13.87
901114	0700	1.48	1.45	0.21	24.0	146.0	7.56	7.56	0.147	0.099	0.099	13.45
901114	1300	1.32	1.30	0.16	24.0	90.0	6.59	7.56	0.125	0.074	0.123	13.19
901114	1600	1.23	1.19	0.22	22.0	-180.0	8.16	9.71	0.183	0.103	0.185	13.64
901114	1900	1.04	1.01	0.18	14.0	170.0	8.16	8.87	0.178	0.160	0.181	13.32
901114	2200	0.92	0.90	0.11	18.0	90.0	7.56	5.52	0.122	0.081	0.132	12.84
901115	0100	0.79	0.77	0.12	22.0	-174.0	7.56	7.56	0.157	0.174	0.174	13.23
901115	0400	0.70	0.68	0.13	18.0	-168.0	7.04	8.16	0.186	0.164	0.297	13.89
901115	0700	0.56	0.53	0.10	22.0	174.0	6.59	5.24	0.184	0.138	0.327	13.62
901115	1000	0.48	0.46	0.08	-2.0	-178.0	9.71	8.87	0.178	0.202	0.266	12.91
901115	1300	0.46	0.44	0.08	-8.0	146.0	8.87	9.71	0.172	0.153	0.208	13.00
901115	1600	0.41	0.40	0.07	6.0	170.0	8.16	8.16	0.173	0.182	0.182	13.55
901115	1900	0.34	0.33	0.07	4.0	154.0	8.16	8.16	0.210	0.227	0.227	13.35
901115	2200	0.32	0.30	0.07	-6.0	174.0	8.16	8.87	0.228	0.165	0.307	12.79
901116	0100	0.30	0.29	0.07	-6.0	152.0	7.56	8.16	0.245	0.149	0.239	12.97
901116	0400	0.28	0 27	0.07	-4.0	-174.0	8.16	15.63	0.268	0.228	0.527	13.64
901116	0700	0.25	0.23	0.07	-6.0	-132.0	8.16	8.87	0.297	0.219	0.324	13.58
901116	1900	0.20	0.18	0.07	-44.0	174.0	8.87	13.56	0.388	0.427	0.709	13.31
901116	2200	0.19	0.17	0.06	-36.0	-176.0	8.87	15.63	0.327	0.270	0.452	12.76
901117	0100	0.19	0.16	0.07	-4.0	-172.0	15.63	15.63	0.446	0.659	0.659	12.78
901117	0400	0.20	0.17	0.09	-4.0	-176.0	15.63	15.63	0.502	0.617	0.617	13.48
901117	0700	0.20	0.17	0.07	-6.0	142.0	15.63	15.63	0.442	0.658	0.658	13.71
901117	1000	0.93	0.89	0.24	54.0	90.0	4.98	4.17	0.264	0.296	0.351	13.14
901117	1300	1.28	1.25	0.25	50.0	90.0	5.52	4.17	0.202	0.145	0.386	12.91
901117	1600	1.39	1.35	0.27	48.0	90.0	6.19	6.19	0.201	0.116	0.116	13.50
901117	1900	1.67	1.63	0.33	38.0	90.0	6.59	4.17	0.202	0.106	0.311	13.77
901117	2200	2.21	2.15	0.46	28.0	90.0	7.04	4.17	0.213	0.103	0.340	13.39
901118	0100	2.32	2.24	0.52	30.0	90.0	7.56	6.19	0.231	0.123	0.296	13.20
901118	0400	2.26	2.16	0.57	32.0	90.0	6.59	6.19	0.263	0.214	0.313	13.84
901118	0700	2.30	2.19	0.57	20.0	118.0	6.19	4.17	0.258	0.278	0.396	14.25
901118	1000	2.26	2.17	0.50	32.0	90.0	6.59	4.17	0.229	0.193	0.358	13.72
901118	1300	2.02	1.95	0.40	34.0	90.0	6.59	4.17	0.205	0.143	0.380	13.26
901118	1600	1.84	1.80	0.29	2.0	90.0	9.71	4.17	0.162	0.118	0.281	13.56
901118	1900	1.84	1.80	0.28	4.0	-162.0	9.71	10.72	0.155	0.126	0.131	13.92
901118	2200	1.82	1.78	0.24	6.0	-166.0	9.71	10.72	0.133	0.085	0.155	13.56
901119	0100	1.85	1.81	0.20	6.0	90.0	10.72	4.17	0.111	0.099	0.285	13.23
901119	0400	1.88	1.85	0.18	12.0	-170.0	10.72	11.98	0.098	0.100	0.085	13.66
901119	0700	1.82	1.77	0.23	-8.0	-168.0	11.98	13.56	0.133	0.133	0.189	14.16
901119	1300	1.90	1.86	0.21	6.0	-168.0	11.98	13.56	0.114	0.077	0.117	13.15
901119	1600	1.81	1.78	0.20	2.0	-166.0	11.98	11.98	0.110	0.104	0.104	13.36

(Continued)

* See Notation (Appendix D) for definitions of terms

(Continued)

Date	Time EST	Wave Height H_{mo} m	$H_{mo,i}$ m	$H_{mo,r}$ m	Direction $\theta_{p,i}$ deg	$\theta_{p,r}$ deg	Period $T_{p,i}$ sec	$T_{p,r}$ sec	Reflection X_{mo}	$X_{p,i}$	$X_{p,r}$	Depth m
901119	1900	1.47	1.44	0.18	0.0	-174.0	11.98	13.56	0.126	0.115	0.133	13.79
901119	2200	1.31	1.28	0.18	6.0	172.0	11.98	10.72	0.137	0.101	0.118	13.55
901120	0100	1.20	1.17	0.14	4.0	-164.0	11.98	11.98	0.119	0.111	0.111	13.16
901120	0400	1.12	1.09	0.15	6.0	-166.0	10.72	11.98	0.140	0.131	0.168	13.47
901120	0700	1.07	1.03	0.19	14.0	-170.0	10.72	11.98	0.183	0.208	0.222	14.06
901120	1000	0.93	0.90	0.15	12.0	-176.0	10.72	11.98	0.171	0.154	0.207	13.85
901120	1300	0.95	0.92	0.10	6.0	166.0	10.72	10.72	0.113	0.114	0.114	13.23
901120	1600	0.99	0.96	0.10	-6.0	-174.0	10.72	11.98	0.105	0.133	0.192	13.26
901120	1900	1.01	0.99	0.11	6.0	172.0	10.72	10.72	0.112	0.143	0.143	13.71
901120	2200	1.04	1.02	0.12	4.0	-178.0	10.72	10.72	0.119	0.155	0.155	13.63
901121	0100	1.22	1.20	0.13	28.0	-162.0	5.83	10.72	0.107	0.077	0.158	13.21
901121	0400	1.16	1.14	0.11	28.0	-176.0	5.83	10.72	0.097	0.069	0.129	13.33
901121	0700	1.13	1.10	0.12	20.0	-166.0	5.83	8.87	0.111	0.084	0.182	13.89
901121	1000	1.02	1.00	0.13	20.0	-166.0	6.19	10.72	0.128	0.098	0.187	13.85
901121	1300	1.03	1.01	0.11	16.0	-166.0	7.04	10.72	0.113	0.092	0.178	13.25
901121	1600	1.01	0.99	0.09	32.0	90.0	6.59	5.52	0.094	0.073	0.106	13.16
901121	1900	0.87	0.84	0.11	8.0	-158.0	8.16	8.87	0.134	0.178	0.253	13.55
901121	2200	0.77	0.75	0.10	28.0	-172.0	6.59	7.56	0.133	0.104	0.174	13.59
901122	0100	0.69	0.67	0.08	-10.0	148.0	9.71	8.16	0.122	0.113	0.204	13.18
901122	0400	0.66	0.64	0.09	4.0	-154.0	8.87	8.87	0.145	0.264	0.264	13.15
901122	0700	0.64	0.62	0.10	-8.0	-142.0	8.87	8.87	0.159	0.206	0.206	13.65
901122	1000	0.60	0.58	0.09	-22.0	-170.0	8.87	8.16	0.164	0.131	0.201	13.80
901122	1300	0.56	0.53	0.09	10.0	-150.0	8.87	8.87	0.171	0.168	0.168	13.30
901122	1600	0.54	0.52	0.09	-24.0	-152.0	8.16	8.87	0.168	0.162	0.248	13.05
901122	1900	0.54	0.52	0.10	0.0	-162.0	7.56	8.16	0.196	0.204	0.227	13.41
901122	2200	0.49	0.47	0.08	-10.0	-170.0	7.56	8.16	0.171	0.210	0.219	13.61
901123	0100	0.47	0.45	0.09	6.0	-176.0	8.16	8.16	0.197	0.209	0.209	13.25
901123	0400	0.48	0.46	0.10	-4.0	-168.0	7.56	8.16	0.210	0.149	0.212	13.04
901123	0700	0.51	0.48	0.12	0.0	-162.0	7.56	8.87	0.249	0.217	0.300	13.44
901123	1000	0.47	0.45	0.09	-24.0	-174.0	8.87	8.16	0.191	0.130	0.239	13.73
901123	1300	0.42	0.40	0.09	-24.0	-180.0	8.87	8.87	0.221	0.195	0.195	13.35
901123	1600	0.41	0.38	0.10	-10.0	-150.0	8.16	8.87	0.251	0.226	0.310	12.97
901123	1900	0.46	0.44	0.09	-6.0	-138.0	8.87	8.87	0.218	0.224	0.224	13.21
901123	2200	0.40	0.38	0.08	-28.0	-170.0	8.87	8.16	0.203	0.156	0.211	13.56
901124	0100	0.34	0.31	0.07	0.0	-166.0	8.87	8.87	0.219	0.261	0.261	13.33
901124	0400	0.29	0.27	0.07	-24.0	-178.0	9.71	10.72	0.265	0.216	0.340	13.00
901124	0700	0.28	0.25	0.06	4.0	-174.0	10.72	10.72	0.249	0.338	0.338	13.28
901124	1000	0.29	0.27	0.06	22.0	-168.0	10.72	10.72	0.229	0.274	0.274	13.69
901124	1300	0.31	0.29	0.07	6.0	-160.0	10.72	10.72	0.228	0.326	0.326	13.43
901124	1600	0.32	0.30	0.08	22.0	-166.0	10.72	11.98	0.256	0.216	0.404	12.95
901124	1900	0.34	0.30	0.09	8.0	156.0	10.72	10.72	0.308	0.385	0.385	13.01
901124	2200	0.34	0.31	0.09	14.0	-164.0	10.72	10.72	0.284	0.309	0.309	13.41
901125	0100	0.30	0.28	0.07	12.0	-174.0	10.72	10.72	0.269	0.316	0.316	13.32
901125	0400	0.29	0.26	0.07	16.0	-160.0	10.72	10.72	0.272	0.288	0.288	12.88
901125	0700	0.25	0.22	0.07	6.0	-176.0	10.72	9.71	0.314	0.326	0.371	12.91
901125	1000	0.24	0.22	0.06	-4.0	-168.0	9.71	10.72	0.270	0.208	0.397	13.33
901125	1300	0.24	0.22	0.05	8.0	-166.0	10.72	10.72	0.221	0.285	0.285	13.33
901125	1600	0.24	0.23	0.05	10.0	-168.0	9.71	9.71	0.238	0.291	0.291	12.86
901125	1900	0.26	0.24	0.07	-26.0	-130.0	10.72	15.63	0.286	0.345	0.577	12.77
901125	2200	0.28	0.26	0.06	-34.0	-130.0	9.71	15.63	0.217	0.259	0.424	13.25
901126	0100	0.26	0.25	0.05	-34.0	-170.0	9.71	15.63	0.209	0.174	0.424	13.43
901126	0400	0.26	0.24	0.06	-42.0	-130.0	15.63	15.63	0.261	0.523	0.523	13.04

(Continued)

(Continued)

Date	Time EST	Wave Height H_{mo} m	$H_{mo,i}$ m	$H_{mo,r}$ m	Direction $\theta_{p,i}$ deg	$\theta_{p,r}$ deg	Period $T_{p,i}$ sec	$T_{p,r}$ sec	Reflection x_{mo}	$x_{p,i}$	$x_{p,r}$	Depth m
901126	0700	0.25	0.22	0.08	-36.0	-132.0	15.63	15.63	0.336	0.558	0.558	12.86
901126	1000	0.26	0.24	0.09	4.0	-170.0	18.45	18.45	0.372	0.660	0.660	13.26
901126	1300	0.31	0.27	0.10	-6.0	-180.0	18.45	18.45	0.356	0.534	0.534	13.48
901126	1600	0.33	0.29	0.11	0.0	-174.0	18.45	18.45	0.369	0.476	0.476	13.08
901126	1900	0.34	0.29	0.12	2.0	176.0	18.45	18.45	0.415	0.555	0.555	12.78
901126	2200	0.40	0.35	0.14	-6.0	-174.0	18.45	18.45	0.387	0.396	0.396	13.24
901127	0100	0.40	0.35	0.14	-6.0	-180.0	18.45	18.45	0.398	0.470	0.470	13.65
901127	0400	0.42	0.36	0.14	-2.0	-180.0	18.45	18.45	0.394	0.419	0.419	13.35
901127	0700	0.40	0.35	0.13	-2.0	-170.0	18.45	18.45	0.375	0.414	0.414	12.94
901127	1000	0.41	0.35	0.13	22.0	-178.0	15.63	18.45	0.387	0.362	0.655	13.18
901127	1300	0.40	0.36	0.13	-4.0	-178.0	15.63	18.45	0.369	0.384	0.617	13.58
901127	1600	0.45	0.41	0.12	-2.0	-162.0	15.63	18.45	0.300	0.331	0.409	13.30
901127	1900	0.42	0.38	0.11	2.0	-178.0	15.63	18.45	0.299	0.283	0.431	12.77
901127	2200	0.47	0.43	0.12	-2.0	-176.0	15.63	15.63	0.271	0.330	0.330	13.01
901128	0100	0.45	0.41	0.12	-42.0	-170.0	13.56	15.63	0.290	0.345	0.472	13.65
901128	0400	0.44	0.41	0.11	-38.0	-172.0	13.56	15.63	0.266	0.267	0.447	13.52
901128	0700	0.45	0.42	0.11	6.0	-132.0	13.56	13.56	0.249	0.343	0.343	12.95
901128	1000	0.55	0.51	0.12	8.0	-166.0	5.24	13.56	0.234	0.133	0.395	12.97
901128	1300	0.54	0.51	0.12	2.0	-178.0	5.24	15.63	0.246	0.231	0.446	13.47
901128	1600	0.58	0.55	0.12	-70.0	-164.0	5.52	15.63	0.212	0.132	0.376	13.42
901128	1900	0.48	0.45	0.11	-8.0	-168.0	13.56	15.63	0.234	0.289	0.466	12.76
901128	2200	0.46	0.43	0.11	10.0	-148.0	13.56	13.56	0.250	0.341	0.341	12.76
901129	0100	0.53	0.51	0.11	-54.0	-172.0	5.24	13.56	0.207	0.173	0.317	13.48
901129	0400	0.56	0.53	0.13	-44.0	-172.0	5.24	13.56	0.237	0.249	0.258	13.63
901129	0700	0.52	0.50	0.10	-56.0	-142.0	5.83	13.56	0.205	0.129	0.323	12.97
901129	1000	1.11	1.07	0.27	56.0	90.0	5.24	4.75	0.247	0.101	0.289	12.74
901129	1300	1.69	1.66	0.27	48.0	90.0	6.19	4.35	0.163	0.086	0.315	13.39
901129	1600	1.67	1.61	0.37	36.0	90.0	5.83	4.17	0.230	0.174	0.348	13.70
901129	1900	1.76	1.70	0.41	34.0	90.0	5.83	4.17	0.244	0.169	0.393	13.21
901129	2200	1.95	1.88	0.46	36.0	90.0	6.19	5.83	0.247	0.221	0.329	12.97
901130	0100	2.38	2.30	0.55	26.0	90.0	7.04	4.17	0.241	0.119	0.442	13.71
901130	0400	2.13	2.05	0.50	34.0	90.0	7.04	4.17	0.246	0.134	0.383	14.24
901130	0700	1.86	1.80	0.41	38.0	90.0	6.59	4.17	0.229	0.164	0.355	13.73
901130	1000	1.68	1.64	0.27	30.0	90.0	7.04	4.17	0.167	0.098	0.287	13.03
901130	1300	1.47	1.44	0.22	34.0	90.0	7.04	4.17	0.154	0.088	0.272	13.31
901130	1600	1.30	1.27	0.20	32.0	106.0	7.04	7.56	0.158	0.134	0.196	13.85
901130	1900	1.14	1.11	0.16	16.0	90.0	8.16	4.98	0.143	0.093	0.207	13.40
901130	2200	1.01	0.99	0.11	14.0	90.0	8.16	7.56	0.113	0.095	0.131	12.78
901201	0100	0.88	0.86	0.13	14.0	152.0	7.04	8.87	0.147	0.108	0.256	13.30
901201	0400	0.76	0.73	0.13	22.0	-168.0	6.19	7.56	0.181	0.151	0.220	14.13
901201	0700	0.63	0.59	0.13	14.0	158.0	7.56	8.87	0.213	0.219	0.288	13.79
901201	1300	0.51	0.49	0.08	-28.0	160.0	9.71	10.72	0.167	0.142	0.401	12.82
901201	1900	0.46	0.43	0.10	-28.0	-166.0	9.71	11.98	0.233	0.143	0.292	13.39
901202	0117	0.48	0.45	0.11	10.0	-172.0	10.72	13.56	0.244	0.225	0.408	12.92
901202	0700	0.41	0.37	0.11	-26.0	-170.0	9.71	11.98	0.293	0.170	0.376	13.92
901202	1300	0.39	0.37	0.08	-32.0	-162.0	9.71	11.98	0.224	0.134	0.310	12.61
901202	1900	0.41	0.38	0.10	-32.0	-160.0	9.71	10.72	0.254	0.245	0.245	13.66
901203	0117	0.46	0.42	0.09	-8.0	-168.0	9.71	11.98	0.222	0.126	0.325	12.89
901203	0700	1.02	0.98	0.09	12.0	170.0	4.98	10.72	0.090	0.100	0.195	14.28
901203	1300	1.10	1.08	0.10	0.0	-90.0	5.83	4.98	0.090	0.067	0.116	12.79
901203	1900	1.37	1.34	0.16	-54.0	-90.0	7.56	5.52	0.119	0.078	0.144	13.86

(Continued)

(Continued)

Date	Time EST	Wave Height H_{mo} m	$H_{mo,i}$ m	$H_{mo,r}$ m	Direction $\theta_{p,i}$ deg	$\theta_{p,r}$ deg	Period $T_{p,i}$ sec	$T_{p,r}$ sec	Reflection x_{mo}	$x_{p,i}$	$x_{p,r}$	Depth m
901204	0117	1.56	1.51	0.28	-52.0	-174.0	7.56	15.63	0.185	0.062	0.134	12.67
901204	0700	1.62	1.56	0.32	-38.0	-178.0	8.87	15.63	0.208	0.124	0.231	14.07
901204	1300	1.09	1.05	0.16	-2.0	-90.0	13.56	6.59	0.155	0.109	0.305	12.78
901204	1900	0.78	0.74	0.14	2.0	-150.0	13.56	10.72	0.195	0.208	0.263	13.78
901205	0117	0.85	0.82	0.12	6.0	-180.0	11.98	13.56	0.150	0.154	0.214	12.84
901205	0700	0.87	0.85	0.12	32.0	-160.0	6.19	11.98	0.135	0.108	0.156	13.99
901205	1300	0.80	0.79	0.11	40.0	-168.0	6.19	11.98	0.140	0.079	0.174	12.98
901205	1900	0.57	0.55	0.08	36.0	172.0	5.83	10.72	0.152	0.119	0.222	13.50
901206	0117	0.49	0.47	0.08	-10.0	-172.0	11.98	15.63	0.177	0.223	0.484	12.86
901206	0700	0.48	0.45	0.09	6.0	-176.0	10.72	11.98	0.189	0.249	0.297	13.57
901206	1300	0.46	0.43	0.09	0.0	-174.0	13.56	13.56	0.215	0.265	0.265	13.09
901206	1900	0.41	0.38	0.10	-4.0	-180.0	13.56	15.63	0.276	0.233	0.501	13.12
901207	0117	0.39	0.37	0.09	-4.0	-172.0	13.56	13.56	0.234	0.216	0.216	13.09
901207	0700	0.36	0.33	0.08	6.0	-166.0	13.56	13.56	0.249	0.261	0.261	13.32
901207	1300	0.37	0.35	0.08	6.0	-166.0	13.56	13.56	0.245	0.250	0.250	13.49
901207	1900	0.39	0.37	0.09	-12.0	-166.0	11.98	11.98	0.232	0.211	0.211	13.20
901208	0117	0.76	0.74	0.08	38.0	-154.0	4.35	11.98	0.112	0.111	0.135	13.69
901208	0700	1.55	1.51	0.24	12.0	90.0	5.24	4.17	0.158	0.136	0.262	13.34
901208	1300	2.06	2.01	0.31	6.0	90.0	6.19	4.17	0.156	0.118	0.347	13.83
901208	1900	2.03	1.99	0.22	8.0	90.0	6.59	4.17	0.111	0.071	0.254	13.27
901209	0117	2.07	2.02	0.28	24.0	90.0	6.59	4.17	0.136	0.095	0.289	13.98
901209	0700	2.08	2.03	0.28	4.0	90.0	7.56	4.17	0.139	0.051	0.332	13.32
901209	1300	1.74	1.70	0.21	14.0	-170.0	8.16	8.87	0.123	0.078	0.134	13.92
901209	1900	1.27	1.25	0.11	4.0	166.0	8.16	5.24	0.092	0.078	0.145	13.08
901210	0117	0.92	0.88	0.18	4.0	148.0	8.87	8.16	0.210	0.120	0.335	13.82
901210	0700	0.72	0.69	0.09	-2.0	156.0	8.87	10.72	0.129	0.084	0.171	13.00
901210	1300	0.54	0.51	0.11	-20.0	170.0	10.72	10.72	0.210	0.218	0.218	13.53
901210	1900	0.51	0.48	0.10	-8.0	-160.0	9.71	11.98	0.212	0.106	0.267	12.80
901211	0117	1.35	1.33	0.16	34.0	90.0	5.52	4.98	0.120	0.077	0.165	13.76
901211	0700	1.26	1.24	0.16	40.0	90.0	6.19	4.17	0.126	0.090	0.257	13.15
901211	1300	1.19	1.17	0.13	28.0	150.0	6.59	7.56	0.115	0.091	0.137	13.58
901211	1900	0.91	0.89	0.09	10.0	-168.0	7.04	13.56	0.102	0.065	0.180	13.01
901212	0117	0.72	0.70	0.09	26.0	-166.0	5.83	13.56	0.126	0.073	0.245	13.72
901212	0700	0.59	0.56	0.08	-12.0	-162.0	11.98	13.56	0.149	0.176	0.320	13.16
901212	1300	0.49	0.46	0.09	-8.0	-170.0	13.56	13.56	0.199	0.256	0.256	13.38
901212	1900	0.43	0.40	0.08	-12.0	-176.0	13.56	13.56	0.212	0.303	0.303	13.01
901213	0117	0.45	0.42	0.10	-16.0	-162.0	4.98	11.98	0.228	0.216	0.335	13.46
901213	1300	0.40	0.37	0.08	-68.0	-168.0	6.19	10.72	0.204	0.162	0.444	13.07
901213	1900	0.34	0.32	0.06	-24.0	-164.0	6.59	11.98	0.197	0.237	0.358	13.06
901214	0117	1.34	1.30	0.28	34.0	90.0	4.98	4.54	0.215	0.225	0.240	13.48
901214	0700	2.16	2.12	0.33	36.0	90.0	7.04	4.17	0.154	0.058	0.285	13.76
901214	1300	1.54	1.52	0.16	8.0	90.0	7.04	4.17	0.106	0.075	0.195	13.30
901214	1900	1.24	1.22	0.13	22.0	90.0	8.16	5.24	0.107	0.072	0.173	13.44
901215	0117	1.19	1.17	0.10	10.0	90.0	5.52	5.24	0.090	0.075	0.146	13.35
901215	0700	1.01	0.97	0.10	6.0	90.0	5.52	4.98	0.107	0.128	0.204	13.66
901215	1300	1.04	1.02	0.09	24.0	-90.0	6.19	6.19	0.084	0.081	0.081	12.98
901215	1900	1.08	1.05	0.15	-58.0	-90.0	6.59	4.98	0.143	0.117	0.213	13.41

(Continued)

(Continued)

Date	Time EST	Wave Height H_{mo} m	$H_{mo,i}$ m	$H_{mo,r}$ m	Direction $\theta_{p,i}$ deg	$\theta_{p,r}$ deg	Period $T_{p,i}$ sec	$T_{p,r}$ sec	Reflection x_{mo}	$x_{p,i}$	$x_{p,r}$	Depth m
901216	0117	0.82	0.80	0.10	-44.0	-90.0	7.04	5.52	0.131	0.103	0.212	13.02
901216	0700	0.62	0.60	0.12	-52.0	-132.0	7.04	8.16	0.201	0.188	0.234	13.58
901216	1300	0.36	0.34	0.06	-54.0	-128.0	7.04	9.71	0.187	0.153	0.293	12.75
901216	1900	0.48	0.46	0.06	40.0	90.0	4.17	4.17	0.133	0.173	0.173	13.47
901217	0117	0.52	0.51	0.05	64.0	-138.0	4.17	7.56	0.091	0.112	0.092	13.03
901217	0700	0.77	0.75	0.08	44.0	90.0	5.83	5.24	0.110	0.109	0.156	13.78
901217	1300	0.63	0.62	0.06	20.0	164.0	5.83	11.98	0.091	0.056	0.228	12.75
901217	1900	0.58	0.56	0.06	20.0	170.0	5.83	5.52	0.114	0.093	0.181	13.45
901218	0117	0.55	0.53	0.04	20.0	-170.0	6.59	5.83	0.077	0.067	0.130	12.83
901218	0700	0.46	0.43	0.07	-20.0	-146.0	7.56	8.16	0.159	0.172	0.224	13.75
901218	1300	0.40	0.38	0.06	-18.0	-124.0	8.16	11.98	0.169	0.149	0.372	12.65
901218	1900	0.54	0.52	0.12	-62.0	-90.0	4.17	5.24	0.232	0.373	0.285	13.30
901219	0117	0.54	0.52	0.09	-48.0	-90.0	8.16	5.52	0.165	0.112	0.270	12.65
901219	0700	0.53	0.51	0.09	-40.0	-130.0	9.71	9.71	0.179	0.161	0.161	13.69
901219	1300	0.50	0.49	0.05	-32.0	178.0	9.71	11.98	0.102	0.070	0.319	12.86
901219	1900	1.05	1.02	0.10	2.0	-146.0	4.98	8.87	0.100	0.098	0.258	13.64
901220	0117	1.17	1.15	0.14	14.0	90.0	5.52	4.17	0.121	0.111	0.168	13.02
901220	0700	1.45	1.43	0.14	24.0	90.0	5.52	4.75	0.098	0.067	0.176	13.95
901220	1300	1.52	1.50	0.13	38.0	90.0	6.19	4.17	0.087	0.054	0.134	13.13
901220	1900	1.57	1.55	0.11	16.0	148.0	6.59	7.56	0.068	0.054	0.116	13.67
901221	0117	1.55	1.52	0.10	16.0	142.0	7.04	8.16	0.068	0.042	0.079	13.09
901221	0700	1.52	1.48	0.12	-8.0	-140.0	7.04	8.16	0.082	0.067	0.096	13.79
901221	1300	1.54	1.50	0.11	-12.0	-90.0	8.16	5.52	0.071	0.047	0.156	13.13
901221	1900	1.56	1.53	0.14	-8.0	-90.0	7.56	5.52	0.089	0.067	0.140	13.48
901222	0117	1.35	1.32	0.13	-26.0	-90.0	8.16	5.83	0.099	0.055	0.159	13.14
901222	0700	1.34	1.31	0.15	-8.0	-130.0	8.16	8.16	0.113	0.112	0.112	13.54
901222	1300	1.05	1.02	0.13	-8.0	-164.0	8.16	11.98	0.126	0.078	0.172	13.17
901222	1900	1.03	1.01	0.12	-6.0	-106.0	7.04	8.16	0.116	0.069	0.108	13.30
901223	0117	0.89	0.86	0.12	-8.0	-146.0	9.71	10.72	0.143	0.101	0.143	13.19
901223	0700	1.10	1.07	0.14	-58.0	-90.0	6.59	5.24	0.131	0.075	0.253	13.21
901223	1300	1.01	0.98	0.14	-42.0	-120.0	7.04	11.98	0.149	0.089	0.231	13.14
901223	1900	0.91	0.88	0.12	-14.0	-116.0	10.72	10.72	0.133	0.133	0.133	12.96
901224	0117	0.81	0.79	0.12	-26.0	-90.0	10.72	5.83	0.157	0.113	0.367	13.18
901224	0700	0.90	0.87	0.14	-34.0	-90.0	10.72	5.83	0.161	0.114	0.196	12.91
901224	1300	0.91	0.87	0.14	-16.0	-152.0	10.72	10.72	0.157	0.155	0.155	13.25
901224	1900	1.84	1.82	0.25	38.0	90.0	6.59	4.17	0.139	0.053	0.293	13.14
901225	0100	1.55	1.51	0.24	30.0	90.0	6.59	4.17	0.159	0.070	0.330	13.69
901225	0700	1.17	1.15	0.15	50.0	90.0	5.52	4.17	0.132	0.075	0.256	13.03
901225	1300	1.09	1.06	0.13	-14.0	138.0	10.72	10.72	0.122	0.108	0.108	13.45
901225	1900	1.05	1.02	0.11	-16.0	-90.0	11.98	11.98	0.104	0.082	0.082	12.85
901226	0117	1.02	0.98	0.14	-22.0	-160.0	11.98	13.56	0.141	0.118	0.247	13.72
901226	0700	0.93	0.90	0.11	-8.0	-90.0	11.98	11.98	0.117	0.095	0.095	13.03
901226	1300	1.16	1.12	0.13	-6.0	90.0	11.98	4.54	0.120	0.110	0.169	13.65
901226	1900	1.21	1.17	0.13	16.0	90.0	5.24	4.75	0.107	0.094	0.159	12.94
901227	0117	1.37	1.34	0.14	12.0	90.0	5.24	4.75	0.106	0.095	0.154	13.94
901227	0700	1.65	1.61	0.24	16.0	100.0	5.52	4.75	0.148	0.137	0.305	13.15
901227	1300	1.91	1.87	0.23	8.0	90.0	6.19	6.19	0.123	0.162	0.162	13.70
901227	1900	1.79	1.77	0.12	14.0	90.0	6.59	4.98	0.066	0.046	0.145	13.02

(Continued)

(Sheet 5 of 18)

(Continued)

Date	Time EST	Wave Height H_{mo} m	$H_{mo,i}$ m	$H_{mo,r}$ m	Direction $\theta_{p,i}$ deg	$\theta_{p,r}$ deg	Period $T_{p,i}$ sec	$T_{p,r}$ sec	Reflection x_{mo}	$x_{p,i}$	$x_{p,r}$	Depth m
901228	0100	1.88	1.83	0.16	4.0	-144.0	7.56	8.16	0.088	0.078	0.078	13.94
901228	0700	1.60	1.56	0.12	4.0	-166.0	8.87	8.16	0.076	0.046	0.067	13.30
901228	1300	1.29	1.24	0.15	-8.0	-174.0	8.87	8.16	0.118	0.085	0.121	13.64
901228	1900	1.01	0.97	0.09	6.0	150.0	8.87	8.16	0.094	0.046	0.110	13.13
901229	0117	1.05	1.00	0.13	-2.0	-172.0	9.71	8.16	0.134	0.137	0.152	13.87
901229	0700	1.07	1.02	0.14	4.0	160.0	9.71	10.72	0.141	0.092	0.209	13.57
901229	1300	1.15	1.11	0.10	2.0	140.0	10.72	11.98	0.087	0.104	0.153	13.39
901229	1900	1.05	1.02	0.11	16.0	-144.0	10.72	10.72	0.109	0.111	0.111	13.28
901230	0117	1.00	0.97	0.15	4.0	164.0	10.72	11.98	0.154	0.103	0.207	13.43
901230	0700	0.88	0.83	0.16	14.0	172.0	10.72	11.98	0.196	0.171	0.185	13.61
901230	1300	0.82	0.79	0.10	4.0	-128.0	10.72	9.71	0.132	0.079	0.118	12.82
901230	1900	0.75	0.72	0.15	-20.0	-124.0	10.72	11.98	0.203	0.150	0.246	13.19
901231	0100	0.66	0.62	0.10	-8.0	-138.0	10.72	10.72	0.165	0.178	0.178	12.68
901231	1300	1.65	1.62	0.24	46.0	90.0	6.19	4.17	0.146	0.096	0.249	12.79
901231	1900	1.44	1.41	0.20	18.0	90.0	6.59	4.17	0.138	0.061	0.253	13.76
910101	0100	1.38	1.35	0.19	48.0	90.0	5.52	4.35	0.144	0.073	0.225	12.88
910101	0700	1.40	1.36	0.21	18.0	-170.0	5.83	11.98	0.154	0.109	0.144	14.23
910101	1300	1.15	1.13	0.13	12.0	134.0	6.19	11.98	0.111	0.071	0.118	12.84
910101	1900	1.17	1.13	0.10	-8.0	148.0	5.52	11.98	0.089	0.091	0.229	13.92
910102	0117	1.03	1.00	0.10	-24.0	144.0	10.72	4.35	0.098	0.087	0.144	12.82
910102	0700	1.15	1.10	0.14	-14.0	-160.0	6.19	11.98	0.131	0.151	0.331	14.25
910102	1300	1.15	1.12	0.15	24.0	90.0	4.35	4.17	0.131	0.226	0.232	12.86
910102	1900	1.26	1.22	0.11	26.0	-160.0	5.83	10.72	0.093	0.087	0.267	13.94
910103	0117	0.92	0.91	0.07	34.0	-114.0	5.83	8.87	0.079	0.068	0.103	12.80
910103	0700	0.78	0.75	0.12	18.0	-162.0	5.83	8.16	0.163	0.140	0.279	14.05
910103	1300	0.63	0.61	0.08	-2.0	138.0	8.16	8.16	0.127	0.120	0.120	12.89
910103	1900	0.72	0.69	0.11	-38.0	-140.0	9.71	8.87	0.165	0.198	0.226	13.78
910104	0100	0.57	0.54	0.09	-34.0	162.0	9.71	10.72	0.162	0.087	0.227	13.04
910104	0700	1.20	1.18	0.15	28.0	90.0	4.98	4.17	0.129	0.138	0.226	13.95
910104	1300	1.34	1.31	0.17	26.0	90.0	5.83	4.35	0.130	0.068	0.199	13.23
910104	1900	1.05	1.03	0.10	8.0	90.0	5.52	4.35	0.093	0.065	0.155	13.64
910105	0117	1.06	1.04	0.10	12.0	90.0	5.52	4.17	0.097	0.088	0.102	13.30
910105	0700	1.17	1.15	0.13	4.0	90.0	4.98	5.24	0.109	0.141	0.127	13.62
910105	1300	1.02	1.00	0.09	0.0	90.0	5.52	4.98	0.093	0.065	0.144	13.37
910105	1900	0.96	0.93	0.08	-14.0	-170.0	6.59	8.87	0.089	0.072	0.153	13.36
910106	0117	0.73	0.70	0.11	-22.0	-124.0	6.59	8.16	0.160	0.131	0.256	13.46
910106	0700	0.61	0.59	0.08	-4.0	-90.0	6.19	5.52	0.132	0.117	0.155	13.22
910106	1300	0.47	0.44	0.10	-34.0	-90.0	9.71	5.52	0.218	0.149	0.347	13.40
910106	1900	0.50	0.47	0.07	-36.0	-178.0	8.87	18.45	0.144	0.136	0.582	13.06
910107	0117	0.51	0.48	0.10	-38.0	-90.0	9.71	8.87	0.217	0.181	0.272	13.63
910107	0700	0.50	0.47	0.09	-40.0	-180.0	9.71	18.45	0.188	0.172	0.707	13.22
910107	1300	1.96	1.91	0.30	34.0	90.0	6.59	4.54	0.157	0.089	0.241	13.83
910107	1900	2.89	2.85	0.34	8.0	90.0	8.16	4.17	0.120	0.083	0.262	13.44
910108	0117	2.99	2.93	0.41	10.0	90.0	8.16	4.17	0.139	0.084	0.339	14.17
910108	0700	2.73	2.68	0.29	0.0	90.0	8.87	4.17	0.109	0.066	0.272	13.47
910108	1300	3.00	2.96	0.25	4.0	130.0	8.16	4.17	0.085	0.054	0.238	13.98
910108	1900	2.81	2.76	0.25	4.0	132.0	10.72	4.17	0.090	0.071	0.311	13.36

(Continued)

(Continued)

Date	Time EST	Wave Height H_{mo} m	$H_{mo,i}$ m	$H_{mo,r}$ m	Direction $\theta_{p,i}$ deg	$\theta_{p,r}$ deg	Period $T_{p,i}$ sec	$T_{p,r}$ sec	Reflection X_{mo}	$X_{p,i}$	$X_{p,r}$	Depth m
910109	0117	3.05	2.97	0.26	2.0	132.0	10.72	4.17	0.086	0.044	0.399	14.17
910109	0700	2.69	2.63	0.31	-6.0	90.0	11.98	4.17	0.118	0.046	0.476	13.45
910109	1300	2.59	2.53	0.26	-2.0	146.0	11.98	10.72	0.105	0.042	0.092	13.88
910109	1900	1.83	1.78	0.14	-2.0	142.0	11.98	11.98	0.077	0.070	0.070	13.32
910110	0117	1.66	1.60	0.21	6.0	166.0	10.72	10.72	0.132	0.128	0.128	14.03
910110	0700	1.51	1.46	0.16	-20.0	174.0	9.71	10.72	0.112	0.071	0.134	13.46
910110	1300	1.49	1.45	0.18	10.0	-162.0	10.72	10.72	0.123	0.175	0.175	13.73
910110	1900	1.15	1.11	0.13	8.0	-154.0	10.72	10.72	0.116	0.172	0.172	13.29
910111	0117	1.49	1.45	0.17	4.0	-172.0	5.24	10.72	0.120	0.119	0.164	13.92
910111	0700	1.62	1.58	0.15	20.0	-178.0	6.59	10.72	0.093	0.067	0.192	13.52
910111	1300	1.56	1.52	0.16	8.0	-170.0	7.04	9.71	0.106	0.060	0.165	13.50
910111	1900	1.99	1.93	0.20	-6.0	-90.0	8.16	8.87	0.105	0.079	0.077	13.28
910112	0117	2.35	2.30	0.26	-32.0	-90.0	8.87	8.16	0.111	0.060	0.116	13.60
910112	0700	1.66	1.60	0.22	-30.0	176.0	9.71	10.72	0.140	0.097	0.174	13.53
910112	1300	1.40	1.35	0.20	-32.0	-116.0	8.87	8.16	0.149	0.088	0.150	13.33
910112	1900	1.15	1.09	0.21	-32.0	-164.0	8.87	10.72	0.189	0.112	0.260	13.41
910113	0117	1.21	1.13	0.14	-32.0	90.0	8.87	4.17	0.126	0.102	0.269	13.58
910113	0700	1.42	1.36	0.26	28.0	90.0	5.52	4.35	0.192	0.154	0.299	13.81
910113	1300	1.13	1.09	0.13	32.0	90.0	5.83	4.75	0.117	0.073	0.201	13.29
910113	1900	1.07	1.03	0.18	34.0	152.0	5.83	4.54	0.179	0.132	0.294	13.58
910114	0117	0.87	0.84	0.11	30.0	90.0	5.83	4.75	0.133	0.077	0.229	13.44
910114	0700	0.74	0.69	0.12	26.0	176.0	5.83	5.24	0.161	0.154	0.206	13.87
910114	1300	0.55	0.52	0.08	-28.0	-178.0	9.71	15.63	0.152	0.096	0.342	13.04
910114	1900	0.53	0.50	0.11	-6.0	-134.0	15.63	18.45	0.223	0.265	0.566	13.46
910115	0117	0.49	0.46	0.09	-6.0	-178.0	15.63	15.63	0.200	0.236	0.236	13.01
910115	0700	0.45	0.41	0.11	-8.0	-174.0	15.63	15.63	0.253	0.256	0.256	13.75
910115	1300	0.46	0.41	0.11	-8.0	-172.0	15.63	15.63	0.256	0.375	0.375	12.86
910115	1900	0.45	0.42	0.10	6.0	-180.0	13.56	15.63	0.243	0.239	0.388	13.60
910116	0117	0.45	0.42	0.08	-6.0	-174.0	13.56	13.56	0.202	0.255	0.255	13.02
910116	0700	1.74	1.67	0.33	-20.0	-126.0	8.16	8.16	0.200	0.152	0.152	13.86
910116	1300	1.42	1.38	0.17	-34.0	-90.0	8.87	8.16	0.124	0.079	0.133	12.83
910116	1900	1.07	1.02	0.23	-56.0	-90.0	8.16	8.16	0.225	0.216	0.216	13.68
910117	0117	0.76	0.72	0.14	-38.0	-146.0	8.87	10.72	0.200	0.142	0.321	12.92
910117	0700	0.65	0.61	0.17	-40.0	-148.0	9.71	10.72	0.284	0.218	0.353	13.90
910117	1300	0.45	0.42	0.08	-38.0	-152.0	8.87	10.72	0.187	0.111	0.301	12.84
910117	1900	0.43	0.40	0.09	-32.0	-90.0	8.87	8.87	0.237	0.236	0.236	13.70
910118	0117	0.36	0.33	0.06	-34.0	168.0	8.87	10.72	0.194	0.116	0.325	12.83
910118	0700	0.37	0.34	0.06	-34.0	-122.0	9.71	8.16	0.186	0.171	0.288	13.75
910118	1300	0.30	0.27	0.05	8.0	170.0	10.72	10.72	0.184	0.279	0.279	12.71
910118	1900	0.25	0.21	0.06	-2.0	-178.0	9.71	18.45	0.282	0.414	0.715	13.54
910119	0117	0.18	0.16	0.04	-32.0	-176.0	9.71	18.45	0.249	0.233	0.512	12.70
910119	0700	0.21	0.18	0.06	28.0	-176.0	6.19	18.45	0.362	0.155	0.755	13.60
910119	1300	0.25	0.23	0.04	-34.0	-180.0	9.71	15.63	0.193	0.185	0.518	12.75
910119	1900	0.28	0.25	0.06	14.0	-176.0	6.19	18.45	0.239	0.123	0.672	13.37
910120	0117	0.25	0.23	0.05	0.0	-176.0	15.63	18.45	0.236	0.374	0.613	12.80
910120	0700	0.47	0.43	0.11	32.0	-180.0	4.17	15.63	0.251	0.222	0.655	13.53
910120	1300	0.76	0.73	0.10	22.0	90.0	4.54	4.54	0.130	0.160	0.160	12.97
910120	1900	0.62	0.58	0.14	-38.0	-128.0	9.71	11.98	0.244	0.205	0.552	13.46

(Continued)

(Continued)

Date	Time	Wave Height			Direction		Period		Reflection			Depth
		H_{mo}	$H_{mo,i}$	$H_{mo,r}$	$\theta_{p,i}$	$\theta_{p,r}$	$T_{p,i}$	$T_{p,r}$	x_{mo}	$x_{p,i}$	$x_{p,r}$	
	ZST	m	m	m	deg	deg	sec	sec				m
910121	0117	0.55	0.50	0.16	-20.0	-130.0	10.72	10.72	0.321	0.470	0.470	13.17
910121	0700	0.46	0.43	0.11	-24.0	-136.0	10.72	9.71	0.261	0.242	0.297	13.39
910121	1300	0.52	0.49	0.12	60.0	90.0	4.35	4.17	0.252	0.339	0.382	13.26
910121	1900	1.44	1.39	0.32	32.0	90.0	5.83	4.98	0.233	0.181	0.307	13.65
910122	0117	1.33	1.27	0.30	30.0	90.0	6.19	4.17	0.238	0.157	0.319	13.75
910122	0700	1.59	1.53	0.33	30.0	106.0	5.52	4.98	0.218	0.130	0.356	13.63
910122	1300	1.64	1.59	0.32	40.0	90.0	6.59	4.17	0.204	0.103	0.402	13.69
910122	1900	1.29	1.25	0.21	14.0	152.0	7.56	8.16	0.168	0.158	0.238	13.44
910123	0117	0.93	0.90	0.15	32.0	144.0	7.04	7.56	0.165	0.130	0.211	13.82
910123	0700	0.70	0.68	0.12	-8.0	-178.0	8.87	8.16	0.176	0.183	0.242	13.28
910123	1300	0.56	0.53	0.10	-6.0	168.0	8.87	10.72	0.194	0.154	0.257	13.56
910123	1900	0.52	0.49	0.08	10.0	172.0	8.87	10.72	0.171	0.134	0.321	12.97
910124	0117	0.38	0.36	0.08	-4.0	-160.0	9.71	11.98	0.237	0.139	0.293	13.65
910124	0700	0.36	0.33	0.07	-8.0	172.0	10.72	11.98	0.215	0.212	0.284	12.90
910124	1300	0.36	0.33	0.08	2.0	160.0	10.72	10.72	0.245	0.288	0.288	13.42
910124	1900	0.36	0.34	0.07	-20.0	178.0	10.72	10.72	0.215	0.249	0.249	12.76
910125	0117	0.35	0.33	0.07	-14.0	-166.0	10.72	11.98	0.219	0.206	0.249	13.84
910125	0700	1.82	1.78	0.33	36.0	90.0	6.19	5.83	0.184	0.116	0.187	13.19
910125	1300	1.56	1.51	0.32	26.0	90.0	5.52	4.17	0.214	0.180	0.341	13.71
910125	1900	1.09	1.06	0.18	18.0	90.0	7.56	4.98	0.168	0.076	0.305	12.94
910126	0117	0.89	0.85	0.15	32.0	160.0	6.59	5.52	0.172	0.133	0.239	13.91
910126	0700	0.75	0.72	0.12	-4.0	164.0	8.16	8.87	0.167	0.131	0.211	13.15
910126	1300	0.67	0.64	0.10	32.0	-180.0	6.59	8.16	0.157	0.117	0.234	13.50
910126	1900	0.55	0.51	0.09	4.0	178.0	7.56	5.83	0.167	0.128	0.235	12.92
910127	0117	0.44	0.41	0.08	-50.0	-172.0	7.56	8.16	0.184	0.158	0.217	13.69
910127	0700	0.34	0.31	0.07	-14.0	-124.0	7.56	6.59	0.210	0.193	0.339	13.24
910127	1300	0.33	0.31	0.07	-54.0	-108.0	7.04	8.16	0.219	0.183	0.269	13.27
910127	1900	0.36	0.34	0.06	-50.0	-106.0	7.56	6.59	0.185	0.119	0.288	13.08
910128	0117	0.53	0.49	0.11	-22.0	-90.0	7.56	5.24	0.218	0.239	0.326	13.42
910128	0700	0.63	0.58	0.15	-14.0	-90.0	7.56	5.24	0.251	0.221	0.355	13.50
910128	1300	0.51	0.47	0.08	-42.0	-90.0	7.56	5.52	0.166	0.162	0.202	12.99
910128	1900	0.63	0.60	0.15	-44.0	-128.0	8.87	9.71	0.256	0.216	0.269	13.35
910129	0117	0.62	0.59	0.12	-38.0	-124.0	9.71	9.71	0.196	0.183	0.183	13.20
910129	0700	0.61	0.57	0.14	-40.0	-128.0	8.87	9.71	0.241	0.193	0.234	13.92
910129	1300	0.68	0.65	0.06	-12.0	140.0	8.87	8.87	0.100	0.133	0.133	12.91
910129	1900	0.69	0.66	0.11	-52.0	-90.0	7.56	5.83	0.160	0.149	0.216	13.71
910130	0117	0.85	0.82	0.10	-6.0	-90.0	6.19	5.24	0.125	0.127	0.189	12.96
910130	0700	0.71	0.67	0.12	0.0	142.0	6.59	8.87	0.184	0.124	0.338	14.04
910201	1300	0.81	0.80	0.07	36.0	132.0	6.59	8.87	0.091	0.065	0.118	12.63
910201	1900	0.66	0.63	0.09	8.0	154.0	6.19	8.87	0.142	0.166	0.215	13.66
910202	0117	0.54	0.53	0.07	26.0	138.0	6.59	10.72	0.133	0.062	0.194	12.68
910202	0700	0.55	0.51	0.07	-30.0	-114.0	9.71	10.72	0.145	0.132	0.270	13.67
910202	1300	0.52	0.50	0.08	-32.0	-90.0	9.71	6.59	0.155	0.096	0.208	12.75
910202	1900	0.54	0.51	0.10	-36.0	-120.0	9.71	9.71	0.187	0.188	0.188	13.50
910203	0117	0.50	0.46	0.10	-8.0	-90.0	9.71	9.71	0.221	0.237	0.237	12.89
910203	0700	0.51	0.47	0.11	-40.0	-112.0	9.71	8.16	0.234	0.219	0.242	13.41
910203	1300	0.45	0.41	0.11	-38.0	-148.0	9.71	10.72	0.256	0.152	0.415	12.89

(Continued)

(Continued)

Date	Time EST	Wave Height H_{mo} m	$H_{mo,i}$ m	$H_{mo,r}$ m	Direction $\theta_{p,i}$ deg	$\theta_{p,r}$ deg	Period $T_{p,i}$ sec	$T_{p,r}$ sec	Reflection X_{mo}	$X_{p,i}$	$X_{p,r}$	Depth m
910203	1900	0.54	0.50	0.12	-42.0	-118.0	8.87	6.19	0.239	0.183	0.450	13.23
910204	0117	0.46	0.43	0.12	-36.0	-138.0	9.71	10.72	0.271	0.219	0.295	13.07
910204	0700	0.46	0.43	0 09	-34.0	-122.0	9.71	6.59	0.209	0.204	0.333	13.17
910204	1300	0.36	0.33	0.08	-34.0	-140.0	9.71	10.72	0.254	0.222	0.375	13.09
910204	1900	0.41	0.39	0.08	-38.0	-122.0	8.87	6.59	0.208	0.150	0.392	13.10
910205	0117	0.41	0.38	0.10	-44.0	-126.0	8.87	9.71	0.250	0.178	0.228	13.38
910205	0700	0.43	0.40	0.08	-38.0	-122.0	9.71	9.71	0.202	0.191	0.191	13.18
910205	1300	0.48	0.44	0.11	-32.0	-132.0	9.71	8.16	0.256	0.202	0.347	13.40
910205	1900	0.51	0.48	0.10	-38.0	-126.0	8.87	10.72	0.203	0.162	0.302	13.16
910206	0117	0.60	0.56	0.17	-38.0	-130.0	8.87	9.71	0.298	0.224	0.306	13.66
910206	0700	0.62	0.59	0.11	-34.0	-128.0	8.87	10.72	0.190	0.156	0.326	13.14
910206	1300	0.56	0.52	0.14	-34.0	-106.0	8.87	8.16	0.262	0.178	0.324	13.47
910206	1900	0.53	0.50	0.12	-16.0	-130.0	8.16	8.16	0.232	0.280	0.280	13.08
910207	0100	0.51	0.48	0.14	-38.0	-132.0	8.87	7.56	0.283	0.186	0.367	13.73
910207	0700	0.51	0.47	0.10	-14.0	-134.0	8.16	8.16	0.211	0.230	0.230	13.14
910207	1900	0.56	0.53	0.10	-32.0	-130.0	8.87	6.59	0.192	0.149	0.280	13.13
910208	0117	0.66	0.61	0.09	-34.0	164.0	8.87	5.83	0.140	0.151	0.406	13.89
910208	0700	1.96	1.89	0.44	24.0	108.0	5.83	4.75	0.233	0.200	0.386	13.39
910209	1317	1.30	1.25	0.26	16.0	-180.0	8.16	8.16	0.208	0.172	0.172	13.52
910209	1900	0.90	0.87	0.12	-2.0	166.0	8.16	8.87	0.136	0.145	0.202	13.19
910210	0117	0.70	0.66	0.09	4.0	-178.0	8.16	8.16	0.143	0.216	0.216	13.68
910210	0700	0.67	0.64	0.09	-4.0	178.0	8.87	8.16	0.147	0.137	0.166	13.37
910211	1317	0.65	0.63	0.08	18.0	90.0	4.17	4.17	0.121	0.178	0.178	13.35
910211	1900	0.56	0.53	0.09	-6.0	164.0	6.19	4.35	0.171	0.127	0.183	13.44
910212	0117	1.15	1.09	0.29	18.0	104.0	4.75	4.98	0.265	0.306	0.378	13.51
910212	0700	1.68	1.64	0.27	22.0	90.0	6.59	4.17	0.167	0.109	0.294	13.80
910212	1300	1.15	1.13	0.15	30.0	90.0	5.83	4.17	0.135	0.096	0.221	13.26
910212	1900	0.91	0.89	0.12	22.0	156.0	6.59	8.16	0.136	0.095	0.198	13.55
910213	0117	0.63	0.61	0.08	12.0	170.0	8.16	5.24	0.129	0.101	0.208	13.15
910213	0700	0.49	0.46	0.08	8.0	-164.0	7.56	8.87	0.175	0.137	0.276	13.56
910213	1300	0.35	0.32	0.05	-20.0	150.0	4.98	9.71	0.162	0.209	0.387	12.78
910213	1900	0.27	0.25	0.05	-6.0	140.0	9.71	11.98	0.214	0.226	0.393	13.46
910214	0117	0.44	0.40	0.08	-52.0	-104.0	7.56	8.87	0.202	0.134	0.318	12.97
910214	0700	0.62	0.57	0.19	-54.0	-116.0	10.72	10.72	0.338	0.473	0.473	13.71
910214	1300	0.66	0.62	0.14	-22.0	-90.0	11.98	11.98	0.227	0.315	0.315	12.78
910214	1900	0.63	0.58	0.16	-38.0	-92.0	9.71	10.72	0.282	0.239	0.344	13.73
910215	0117	0.53	0.49	0.10	-18.0	-118.0	10.72	11.98	0.207	0.200	0.351	12.91
910215	0700	0.41	0.37	0.10	-14.0	-148.0	11.98	10.72	0.271	0.343	0.342	13.84
910215	1300	0.39	0.37	0.07	-2.0	-114.0	10.72	10.72	0.177	0.300	0.300	12.78
910215	1900	0.84	0.80	0.19	64.0	-108.0	4.98	10.72	0.238	0.279	0.268	13.80
910216	0100	0.95	0.91	0.22	52.0	90.0	5.24	4.54	0.240	0.126	0.352	12.88
910216	0700	0.94	0.91	0.19	50.0	-166.0	5.52	10.72	0.208	0.108	0.230	13.89
910216	1300	0.78	0.76	0.16	54.0	90.0	5.24	4.35	0.207	0.101	0.349	12.81
910216	1900	0.66	0.64	0.10	54.0	164.0	5.52	7.04	0.155	0.093	0.221	13.78
910217	0117	0.38	0.37	0.06	6.0	154.0	11.98	11.98	0.168	0.184	0.184	12.67

(Continued)

(Continued)

Date	Time EST	Wave Height H_{mo} m	$H_{mo,i}$ m	$H_{mo,r}$ m	Direction $\theta_{p,i}$ deg	$\theta_{p,r}$ deg	Period $T_{p,i}$ sec	$T_{p,r}$ sec	Reflection χ_{mo}	$\chi_{p,i}$	$\chi_{p,r}$	Depth m
910217	0700	0.29	0.25	0.07	-10.0	160.0	11.98	10.72	0.260	0.286	0.502	13.57
910217	1300	0.25	0.23	0.04	-4.0	168.0	10.72	11.98	0.190	0.170	0.244	12.49
910217	1900	0.29	0.26	0.07	18.0	166.0	11.98	11.98	0.251	0.446	0.446	13.54
910218	0117	0.31	0.28	0.06	-12.0	-178.0	10.72	15.63	0.200	0.161	0.343	12.73
910218	0700	0.28	0.26	0.07	0.0	156.0	11.98	10.72	0.256	0.269	0.431	13.58
910219	1300	0.45	0.42	0.09	-38.0	-90.0	5.52	5.24	0.203	0.271	0.269	13.05
910219	1900	0.47	0.43	0.09	-32.0	-90.0	5.83	5.52	0.205	0.132	0.256	13.48
910220	0117	0.44	0.41	0.08	-34.0	-90.0	5.83	5.52	0.200	0.175	0.241	13.16
910220	0700	0.44	0.41	0.07	-26.0	-90.0	5.83	5.24	0.175	0.188	0.276	13.07
910220	1300	0.40	0.38	0.07	-42.0	-90.0	6.59	6.19	0.177	0.136	0.267	12.94
910220	1900	0.39	0.37	0.06	-24.0	154.0	6.59	10.72	0.161	0.199	0.292	13.01
910221	0117	0.40	0.38	0.06	-50.0	-90.0	7.04	5.83	0.168	0.180	0.247	13.38
910221	0700	0.56	0.55	0.06	20.0	-90.0	6.59	5.83	0.103	0.080	0.158	13.01
910221	1300	0.65	0.64	0.08	14.0	-90.0	6.59	5.83	0.130	0.077	0.195	13.28
910221	1900	0.57	0.56	0.07	-38.0	-90.0	8.87	6.19	0.117	0.092	0.136	12.95
910222	0117	0.65	0.62	0.10	-38.0	-128.0	8.87	8.16	0.159	0.160	0.251	13.57
910222	0700	0.52	0.50	0.07	-32.0	174.0	8.87	5.83	0.130	0.073	0.203	12.82
910222	1300	0.44	0.41	0.09	-32.0	-134.0	9.71	9.71	0.207	0.213	0.213	13.35
910222	1900	0.37	0.35	0.05	-36.0	-90.0	8.87	10.72	0.148	0.109	0.194	12.74
910223	0117	1.22	1.14	0.38	14.0	90.0	4.75	4.17	0.333	0.352	0.402	13.84
910223	0700	2.28	2.24	0.32	38.0	90.0	6.59	4.17	0.144	0.088	0.259	13.17
910223	1300	2.19	2.13	0.37	20.0	90.0	6.59	4.17	0.173	0.087	0.275	13.77
910223	1900	2.41	2.36	0.33	16.0	90.0	7.56	4.17	0.139	0.050	0.294	13.10
910224	0117	1.54	1.50	0.19	38.0	90.0	6.59	4.98	0.127	0.086	0.209	13.95
910224	0700	1.37	1.35	0.15	12.0	90.0	6.59	5.24	0.112	0.064	0.165	13.12
910224	1300	1.41	1.38	0.17	14.0	-178.0	7.04	8.16	0.121	0.076	0.118	13.54
910224	1900	1.79	1.75	0.19	-30.0	130.0	8.87	4.35	0.107	0.060	0.239	13.02
910225	0117	1.67	1.64	0.15	-28.0	132.0	8.87	4.17	0.094	0.059	0.172	13.83
910225	0700	1.21	1.18	0.13	-20.0	-180.0	8.87	8.16	0.113	0.059	0.126	13.32
910225	1300	1.26	1.23	0.15	-4.0	172.0	7.56	8.16	0.119	0.085	0.147	13.44
910225	1900	1.09	1.07	0.15	16.0	118.0	7.56	8.16	0.137	0.079	0.156	13.24
910226	0117	1.02	0.99	0.12	2.0	160.0	7.56	8.87	0.120	0.107	0.175	13.62
910226	0700	1.62	1.57	0.33	12.0	90.0	5.52	4.35	0.208	0.151	0.256	13.63
910226	1300	1.44	1.40	0.24	20.0	90.0	5.83	4.54	0.172	0.116	0.288	13.38
910226	1900	1.06	1.03	0.17	22.0	90.0	5.83	4.35	0.161	0.135	0.245	13.59
910227	0117	0.79	0.76	0.12	14.0	176.0	7.56	4.17	0.158	0.136	0.293	13.36
910227	0700	0.82	0.79	0.15	0.0	166.0	8.87	8.16	0.193	0.159	0.195	13.83
910227	1300	0.57	0.55	0.07	12.0	114.0	8.16	8.16	0.133	0.145	0.145	13.01
910227	1900	0.44	0.43	0.07	2.0	130.0	8.87	9.71	0.175	0.134	0.178	13.75
910228	0117	0.36	0.33	0.08	12.0	154.0	8.87	8.87	0.255	0.339	0.339	12.98
910228	0700	0.30	0.27	0.07	0.0	156.0	9.71	8.87	0.256	0.284	0.324	13.88
910228	1300	0.35	0.32	0.06	0.0	110.0	9.71	10.72	0.180	0.128	0.265	12.75
910228	1900	0.47	0.44	0.08	14.0	136.0	10.72	10.72	0.191	0.211	0.211	13.79
910301	0100	0.45	0.42	0.06	16.0	144.0	10.72	10.72	0.149	0.140	0.140	12.74
910301	0700	0.66	0.61	0.14	-38.0	-90.0	5.52	5.24	0.226	0.246	0.345	13.91
910301	1300	0.62	0.60	0.07	-16.0	154.0	9.71	10.72	0.122	0.077	0.120	12.71
910301	1900	0.66	0.61	0.11	-32.0	-90.0	9.71	5.24	0.185	0.127	0.302	13.94

(Continued)

(Continued)

Date	Time EST	Wave Height H_{mo} m	$H_{mo,i}$ m	$H_{mo,r}$ m	Direction $\theta_{p,i}$ deg	$\theta_{p,r}$ deg	Period $T_{p,i}$ sec	$T_{p,r}$ sec	Reflection x_{mo}	$x_{p,i}$	$x_{p,r}$	Depth m
910302	0117	1.11	1.09	0.14	-38.0	-90.0	7.04	6.19	0.127	0.057	0.201	12.71
910302	0700	1.38	1.34	0.22	-50.0	-90.0	8.16	8.16	0.162	0.140	0.140	13.77
910302	1300	1.14	1.12	0.16	-34.0	-90.0	8.87	8.16	0.148	0.074	0.175	12.55
910302	1900	1.01	0.96	0.16	-36.0	-112.0	8.87	8.16	0.169	0.135	0.210	13.77
910303	0117	0.92	0.90	0.13	-28.0	-106.0	9.71	8.16	0.142	0.077	0.159	12.68
910303	0700	1.00	0.96	0.17	-34.0	-112.0	8.87	8.16	0.175	0.120	0.208	13.63
910303	1300	0.86	0.83	0.13	-32.0	-108.0	8.87	8.16	0.156	0.073	0.162	12.71
910303	1900	1.33	1.28	0.21	-34.0	-114.0	8.87	8.16	0.161	0.094	0.205	13.61
910304	0117	1.28	1.24	0.23	-32.0	-90.0	9.71	4.98	0.189	0.103	0.311	12.73
910304	0700	1.17	1.11	0.22	-36.0	-90.0	10.72	5.52	0.201	0.153	0.326	13.36
910304	1300	1.14	1.11	0.19	-24.0	-114.0	10.72	10.72	0.169	0.138	0.138	12.76
910304	1900	1.11	1.05	0.25	-52.0	-144.0	10.72	10.72	0.242	0.222	0.222	13.49
910305	0117	0.99	0.95	0.20	-22.0	138.0	11.98	11.98	0.208	0.182	0.182	13.14
910305	0700	0.95	0.91	0.16	-28.0	-110.0	10.72	11.98	0.171	0.152	0.205	13.48
910305	1300	0.88	0.83	0.14	-20.0	136.0	10.72	11.98	0.168	0.164	0.257	13.20
910305	1900	0.87	0.83	0.13	-34.0	-132.0	9.71	10.72	0.152	0.113	0.154	13.42
910306	0117	0.76	0.72	0.15	-30.0	-142.0	9.71	10.72	0.208	0.139	0.259	13.27
910306	0700	0.81	0.77	0.12	-30.0	-136.0	9.71	10.72	0.158	0.107	0.188	13.16
910306	1300	0.79	0.75	0.14	-30.0	-132.0	9.71	10.72	0.191	0.119	0.239	13.15
910306	1900	0.80	0.77	0.14	-26.0	-142.0	9.71	10.72	0.181	0.116	0.162	13.09
910307	0117	0.82	0.76	0.19	-32.0	-142.0	9.71	10.72	0.249	0.161	0.258	13.24
910307	0700	0.71	0.67	0.15	-30.0	-90.0	9.71	5.52	0.219	0.100	0.434	12.94
910307	1300	0.55	0.51	0.13	-24.0	-144.0	10.72	10.72	0.262	0.241	0.241	13.30
910307	1900	0.48	0.45	0.09	-10.0	-118.0	10.72	10.72	0.200	0.306	0.306	13.14
910308	0100	0.58	0.55	0.08	-36.0	-122.0	9.71	11.98	0.138	0.126	0.322	13.66
910308	0700	1.01	0.98	0.16	24.0	90.0	5.24	4.98	0.158	0.117	0.212	13.15
910308	1300	0.90	0.87	0.16	34.0	90.0	5.24	4.17	0.186	0.178	0.294	13.40
910308	1900	0.85	0.81	0.14	28.0	90.0	5.52	4.75	0.177	0.164	0.222	13.01
910309	0117	0.79	0.76	0.13	32.0	90.0	5.24	4.17	0.178	0.189	0.272	13.59
910309	0700	1.23	1.20	0.19	18.0	90.0	6.19	4.17	0.155	0.093	0.281	13.06
910309	1300	1.08	1.04	0.17	14.0	90.0	5.24	4.17	0.168	0.164	0.304	13.47
910309	1900	0.92	0.89	0.13	10.0	90.0	7.56	4.17	0.151	0.099	0.249	13.02
910310	0117	0.77	0.74	0.10	16.0	168.0	7.04	5.24	0.141	0.110	0.225	13.61
910310	0700	1.12	1.10	0.14	12.0	90.0	5.52	4.75	0.126	0.102	0.219	13.11
910310	1300	1.17	1.13	0.14	16.0	90.0	6.59	4.54	0.127	0.077	0.220	13.58
910310	1900	1.19	1.16	0.20	18.0	164.0	5.83	4.35	0.169	0.128	0.293	13.25
910311	0117	1.31	1.25	0.26	34.0	90.0	6.59	5.52	0.211	0.142	0.237	13.92
910311	0700	1.43	1.40	0.23	34.0	90.0	6.59	4.98	0.161	0.099	0.359	13.45
910311	1300	1.65	1.61	0.24	22.0	90.0	7.04	4.17	0.151	0.100	0.369	13.67
910311	1900	1.32	1.28	0.22	24.0	164.0	7.04	4.17	0.170	0.110	0.352	13.39
910312	0117	1.40	1.35	0.25	34.0	90.0	6.59	4.17	0.186	0.112	0.325	13.82
910312	0700	1.26	1.22	0.18	32.0	134.0	7.04	8.16	0.148	0.098	0.156	13.54
910312	1300	1.10	1.07	0.15	30.0	90.0	6.59	4.35	0.139	0.080	0.237	13.55
910312	1900	0.87	0.83	0.12	16.0	136.0	8.16	10.72	0.149	0.143	0.197	13.44
910313	0117	0.81	0.77	0.13	2.0	178.0	9.71	9.71	0.167	0.233	0.233	13.55
910313	0700	0.88	0.84	0.15	2.0	156.0	13.56	10.72	0.184	0.169	0.208	13.55
910313	1300	1.00	0.97	0.09	4.0	144.0	13.56	10.72	0.095	0.076	0.116	13.29
910313	1900	1.08	1.04	0.14	0.0	146.0	11.98	11.98	0.134	0.135	0.135	13.47

(Continued)

(Continued)

Date	Time EST	Wave Height H_{mo} m	$H_{mo,i}$ m	$H_{mo,r}$ m	Direction $\theta_{p,i}$ deg	$\theta_{p,r}$ deg	Period $T_{p,i}$ sec	$T_{p,r}$ sec	Reflection x_{mo}	$x_{p,i}$	$x_{p,r}$	Depth m
910314	0117	0.96	0.92	0.11	8.0	138.0	11.98	11.98	0.114	0.143	0.143	13.38
910314	0700	1.18	1.13	0.15	2.0	-174.0	7.56	10.72	0.132	0.138	0.224	13.71
910314	1300	0.93	0.90	0.11	10.0	138.0	8.16	8.87	0.117	0.091	0.173	13.22
910314	1900	0.96	0.90	0.20	2.0	90.0	8.87	4.17	0.227	0.113	0.441	13.81
910315	0117	1.24	1.20	0.18	4.0	168.0	9.71	10.72	0.149	0.103	0.157	13.39
910315	0700	1.46	1.41	0.25	14.0	168.0	10.72	10.72	0.180	0.176	0.176	14.03
910315	1300	1.63	1.59	0.25	0.0	90.0	9.71	4.35	0.156	0.071	0.307	13.28
910315	1900	1.77	1.71	0.32	18.0	166.0	10.72	10.72	0.186	0.134	0.134	14.12
910316	0100	1.82	1.78	0.24	2.0	90.0	10.72	4.35	0.134	0.081	0.271	13.25
910316	0700	1.70	1.64	0.24	16.0	138.0	11.98	11.98	0.148	0.171	0.171	14.14
910316	1300	1.46	1.42	0.17	-10.0	150.0	11.98	10.72	0.120	0.110	0.122	13.14
910316	1900	1.35	1.29	0.17	4.0	170.0	11.98	10.72	0.130	0.099	0.175	14.16
910317	0100	1.30	1.27	0.13	10.0	142.0	11.98	11.98	0.104	0.088	0.088	12.98
910317	0700	1.29	1.25	0.17	8.0	146.0	11.98	13.56	0.138	0.123	0.140	14.01
910317	1300	1.19	1.16	0.12	14.0	-118.0	11.98	10.72	0.102	0.078	0.118	12.91
910317	1900	1.29	1.25	0.19	2.0	-180.0	13.56	13.56	0.154	0.162	0.162	14.12
910318	0117	1.30	1.27	0.13	10.0	-90.0	11.98	10.72	0.105	0.090	0.109	12.86
910318	0700	1.20	1.14	0.17	14.0	-136.0	11.98	11.98	0.146	0.134	0.134	13.87
910318	1300	1.41	1.38	0.16	-2.0	-90.0	13.56	5.52	0.118	0.046	0.258	12.74
910318	1900	1.52	1.47	0.23	10.0	-142.0	11.98	10.72	0.155	0.118	0.167	14.03
910319	0117	1.17	1.14	0.13	0.0	-108.0	11.98	10.72	0.115	0.076	0.109	12.92
910319	0700	0.96	0.92	0.17	-34.0	-130.0	9.71	10.72	0.185	0.138	0.222	13.80
910319	1300	0.95	0.91	0.17	18.0	-116.0	11.98	10.72	0.182	0.120	0.161	12.95
910319	1900	0.84	0.77	0.15	16.0	-142.0	10.72	10.72	0.189	0.284	0.284	14.01
910320	0117	0.61	0.58	0.12	20.0	142.0	11.98	11.98	0.200	0.172	0.172	13.06
910320	0700	0.52	0.48	0.10	-6.0	130.0	11.98	10.72	0.201	0.186	0.318	13.54
910320	1300	0.44	0.41	0.07	12.0	-142.0	11.98	10.72	0.174	0.174	0.178	13.00
910320	1900	0.46	0.42	0.10	20.0	176.0	11.98	15.63	0.237	0.261	0.406	13.63
910321	0117	0.48	0.45	0.10	8.0	-180.0	11.98	18.45	0.230	0.164	0.581	13.24
910321	0700	0.52	0.47	0.10	6.0	178.0	13.56	13.56	0.218	0.292	0.292	13.32
910321	1300	0.51	[illegible]	0.09	6.0	140.0	13.56	11.98	0.196	0.143	0.179	13.18
910321	1900	0.51	0.48	0.09	10.0	-178.0	11.98	18.45	0.181	0.153	0.640	13.31
910322	0117	0.48	0.44	0.09	16.0	174.0	11.98	15.63	0.215	0.151	0.334	13.43
910322	0700	0.44	0.41	0.08	-10.0	146.0	11.98	15.63	0.194	0.197	0.244	13.08
910323	1317	0.82	0.78	0.15	10.0	90.0	7.56	5.83	0.195	0.143	0.361	13.69
910323	1900	0.99	0.96	0.14	26.0	-90.0	8.87	5.83	0.148	0.045	0.298	13.06
910324	0117	0.86	0.81	0.13	4.0	-90.0	9.71	6.19	0.164	0.116	0.261	13.91
910324	0700	0.80	0.76	0.11	2.0	152.0	8.87	10.72	0.139	0.061	0.129	13.07
910324	1300	0.83	0.78	0.15	-2.0	166.0	8.87	10.72	0.194	0.120	0.252	13.70
910324	1900	0.69	0.65	0.11	-26.0	-90.0	8.87	8.16	0.163	0.095	0.144	13.02
910325	0100	0.92	0.88	0.16	18.0	90.0	4.35	4.35	0.187	0.261	0.261	13.95
910325	0700	0.91	0.89	0.10	20.0	90.0	5.83	4.98	0.113	0.091	0.194	13.08
910325	1300	0.69	0.67	0.08	-2.0	160.0	9.71	10.72	0.120	0.128	0.191	13.66
910325	1900	0.48	0.46	0.06	24.0	152.0	10.72	10.72	0.138	0.188	0.188	13.06
910326	0117	0.48	0.45	0.07	20.0	132.0	10.72	11.98	0.145	0.155	0.268	13.88
910326	0700	0.43	0.39	0.07	10.0	150.0	10.72	11.98	0.178	0.175	0.277	13.33
910326	1300	0.54	0.51	0.09	14.0	138.0	10.72	10.72	0.180	0.168	0.168	13.65

(Continued)

(Continued)

Date	Time EST	Wave Height H_{mo} m	$H_{mo,i}$ m	$H_{mo,r}$ m	Direction $\theta_{p,i}$ deg	$\theta_{p,r}$ deg	Period $T_{p,i}$ sec	$T_{p,r}$ sec	Reflection X_{mo}	$X_{p,i}$	$X_{p,r}$	Depth m
910326	1900	0.54	0.51	0.09	18.0	130.0	10.72	10.72	0.185	0.241	0.241	13.36
910327	0117	0.66	0.63	0.11	12.0	166.0	10.72	10.72	0.169	0.194	0.194	13.67
910327	0700	0.73	0.69	0.13	16.0	168.0	10.72	10.72	0.189	0.181	0.181	13.43
910327	1300	0.81	0.78	0.11	-12.0	138.0	10.72	10.72	0.136	0.093	0.093	13.32
910327	1900	0.73	0.69	0.14	-12.0	-150.0	10.72	10.72	0.201	0.193	0.193	13.39
910328	0117	0.63	0.60	0.10	-8.0	152.0	11.98	10.72	0.163	0.134	0.156	13.14
910328	0700	0.64	0.59	0.13	12.0	-170.0	11.98	11.98	0.214	0.225	0.225	13.40
910328	1300	0.55	0.52	0.08	-6.0	118.0	11.98	10.72	0.149	0.152	0.202	12.92
910328	1900	0.51	0.47	0.12	10.0	-170.0	11.98	11.98	0.264	0.257	0.257	13.56
910329	0117	0.47	0.44	0.07	6.0	156.0	10.72	10.72	0.153	0.237	0.237	12.93
910329	0700	0.50	0.46	0.11	10.0	-158.0	11.98	10.72	0.250	0.235	0.268	13.64
910329	1300	0.69	0.64	0.17	-50.0	-90.0	7.04	4.35	0.266	0.145	0.449	12.83
910329	1900	0.76	0.69	0.25	-56.0	-90.0	7.56	4.35	0.364	0.209	0.463	13.82
910330	0117	0.82	0.78	0.16	-56.0	-90.0	7.56	5.24	0.201	0.136	0.327	12.85
910330	0700	0.85	0.80	0.21	-38.0	-154.0	9.71	11.98	0.258	0.215	0.253	13.91
910330	1300	1.84	1.78	0.41	28.0	90.0	5.83	4.35	0.234	0.157	0.334	13.15
910330	1900	1.58	1.51	0.27	22.0	90.0	7.56	4.17	0.180	0.135	0.302	14.27
910331	0117	1.06	1.04	0.11	-40.0	150.0	8.16	10.72	0.110	0.107	0.145	13.03
910331	0700	1.14	1.09	0.17	0.0	-158.0	8.16	8.87	0.154	0.115	0.235	13.98
910331	1300	1.19	1.16	0.15	6.0	90.0	4.98	4.17	0.125	0.164	0.211	12.98
910331	1900	1.28	1.24	0.17	6.0	138.0	5.52	8.87	0.139	0.114	0.194	14.12
910401	0100	1.03	1.01	0.11	-26.0	90.0	8.87	4.75	0.107	0.080	0.200	12.94
910401	0700	1.01	0.98	0.15	-2.0	164.0	8.16	8.16	0.148	0.140	0.140	13.81
910401	1300	0.78	0.76	0.08	2.0	144.0	8.16	10.72	0.103	0.080	0.114	12.87
910401	1900	0.66	0.63	0.12	-6.0	-178.0	10.72	8.87	0.182	0.220	0.279	13.93
910402	0117	0.64	0.62	0.06	-10.0	-136.0	9.71	8.16	0.104	0.067	0.134	12.93
910402	0700	0.77	0.74	0.11	4.0	138.0	8.87	8.87	0.150	0.197	0.197	13.69
910402	1300	0.55	0.54	0.07	2.0	-178.0	8.16	8.87	0.129	0.125	0.113	12.96
910402	1900	0.51	0.49	0.06	0.0	168.0	7.56	7.56	0.123	0.133	0.133	13.81
910403	0117	0.51	0.48	0.06	-2.0	116.0	9.71	8.16	0.126	0.079	0.129	13.05
910403	0700	0.56	0.54	0.06	-4.0	-142.0	9.71	8.16	0.119	0.111	0.166	13.55
910403	1300	0.49	0.47	0.06	-2.0	-140.0	8.87	8.16	0.129	0.105	0.161	13.10
910403	1900	0.53	0.51	0.08	16.0	146.0	8.87	8.87	0.149	0.203	0.203	13.60
910404	0117	0.56	0.53	0.06	2.0	154.0	8.87	10.72	0.120	0.136	0.250	13.16
910404	0700	0.60	0.57	0.08	2.0	154.0	10.72	10.72	0.135	0.209	0.209	13.28
910404	1300	0.55	0.52	0.07	-6.0	-90.0	10.72	10.72	0.129	0.142	0.142	13.14
910404	1900	0.57	0.54	0.08	6.0	-106.0	10.72	10.72	0.150	0.193	0.193	13.39
910405	0117	0.53	0.49	0.10	-2.0	-144.0	10.72	10.72	0.198	0.171	0.171	13.27
910405	0700	0.52	0.50	0.08	-22.0	-90.0	10.72	11.98	0.160	0.127	0.173	13.07
910405	1300	0.56	0.54	0.09	-32.0	142.0	10.72	11.98	0.177	0.116	0.198	13.16
910405	1900	0.51	0.48	0.07	-20.0	-90.0	10.72	4.98	0.155	0.141	0.373	13.09
910406	0117	0.44	0.41	0.10	-32.0	-154.0	10.72	11.98	0.234	0.222	0.311	13.31
910406	0700	0.44	0.41	0.07	-30.0	-124.0	10.72	10.72	0.172	0.192	0.192	12.93
910406	1300	0.50	0.47	0.10	-30.0	-148.0	9.71	10.72	0.203	0.181	0.218	13.27
910406	1900	0.50	0.48	0.07	-36.0	-90.0	9.71	5.83	0.143	0.128	0.237	13.05
910407	0117	0.47	0.44	0.11	-32.0	-134.0	9.71	5.83	0.239	0.176	0.420	13.46
910407	0700	0.40	0.37	0.06	-36.0	-94.0	9.71	8.87	0.161	0.146	0.193	12.93

(Continued)

(Continued)

Date	Time EST	Wave Height H_{mo} m	$H_{mo,i}$ m	$H_{mo,r}$ m	Direction $\theta_{p,i}$ deg	$\theta_{p,r}$ deg	Period $T_{p,i}$ sec	$T_{p,r}$ sec	Reflection x_{mo}	$x_{p,i}$	$x_{p,r}$	Depth m
910407	1300	0.36	0.33	0.07	-36.0	-152.0	9.71	8.87	0.223	0.188	0.347	13.38
910407	1900	0.35	0.33	0.06	-38.0	-114.0	8.87	10.72	0.170	0.101	0.263	12.99
910408	0117	0.36	0.34	0.08	-20.0	-90.0	8.87	9.71	0.226	0.226	0.229	13.52
910408	0700	0.33	0.32	0.05	-40.0	146.0	8.87	13.56	0.149	0.102	0.283	12.90
910408	1300	0.33	0.31	0.07	-26.0	-92.0	8.87	8.87	0.226	0.264	0.264	13.43
910408	1900	0.34	0.33	0.06	-40.0	-126.0	8.87	13.56	0.171	0.106	0.321	12.96
910409	0117	0.38	0.35	0.09	-42.0	-126.0	8.87	9.71	0.253	0.140	0.258	13.55
910409	0700	0.47	0.45	0.09	-72.0	-90.0	6.19	5.83	0.199	0.203	0.292	12.89
910409	1300	0.50	0.47	0.10	-36.0	-90.0	6.19	5.83	0.211	0.229	0.278	13.39
910409	1900	0.51	0.48	0.08	-36.0	-90.0	8.87	5.52	0.176	0.101	0.231	12.91
910410	0117	0.51	0.47	0.12	-46.0	-90.0	6.59	5.83	0.263	0.211	0.443	13.43
910410	0700	0.45	0.42	0.08	-44.0	-90.0	7.04	8.87	0.199	0.143	0.257	12.91
910410	1300	0.39	0.36	0.08	-40.0	-90.0	8.87	6.19	0.232	0.199	0.267	13.39
910410	1900	0.38	0.35	0.07	-26.0	-90.0	8.87	5.52	0.209	0.179	0.332	13.14
910411	0100	0.70	0.66	0.18	42.0	90.0	4.17	4.17	0.276	0.324	0.324	13.58
910411	0700	1.83	1.77	0.41	36.0	90.0	6.19	5.83	0.230	0.180	0.271	13.48
910411	1300	0.97	0.94	0.15	26.0	90.0	6.19	4.54	0.159	0.123	0.201	13.55
910411	1900	0.55	0.52	0.10	36.0	164.0	6.59	5.24	0.197	0.148	0.297	13.34
910412	0117	0.48	0.46	0.05	-18.0	-180.0	6.19	5.83	0.114	0.097	0.229	13.31
910412	0700	0.76	0.74	0.14	16.0	90.0	4.75	4.17	0.190	0.219	0.179	13.43
910412	1300	1.40	1.38	0.16	18.0	90.0	6.19	6.19	0.115	0.118	0.118	13.36
910412	1900	1.03	1.00	0.14	32.0	90.0	6.19	4.54	0.138	0.124	0.192	13.62
910413	0117	1.08	1.06	0.12	12.0	90.0	5.52	5.24	0.116	0.079	0.164	13.19
910413	0700	0.85	0.83	0.11	12.0	-90.0	5.83	5.24	0.134	0.126	0.190	13.50
910413	1300	0.80	0.78	0.09	6.0	90.0	6.19	5.24	0.118	0.091	0.169	13.10
910413	1900	0.83	0.79	0.12	22.0	-90.0	6.59	5.52	0.151	0.087	0.211	13.76
910414	0117	0.76	0.74	0.09	6.0	-90.0	5.83	5.24	0.120	0.092	0.188	13.01
910414	0700	0.64	0.61	0.08	-14.0	-90.0	6.19	5.83	0.135	0.131	0.229	13.74
910414	1300	0.53	0.51	0.07	-8.0	-90.0	10.72	5.52	0.145	0.145	0.217	13.12
910414	1900	1.51	1.45	0.24	22.0	146.0	7.56	7.56	0.162	0.146	0.146	14.21
910415	0117	1.32	1.31	0.11	2.0	90.0	8.87	8.16	0.087	0.035	0.065	12.98
910415	0700	1.28	1.25	0.13	4.0	152.0	8.87	5.83	0.105	0.080	0.178	13.82
910415	1300	0.99	0.97	0.10	-8.0	116.0	8.87	10.72	0.108	0.043	0.119	12.84
910415	1900	0.83	0.78	0.11	-24.0	158.0	8.87	10.72	0.146	0.109	0.221	14.05
910416	0117	0.70	0.68	0.08	-22.0	-90.0	9.71	5.52	0.122	0.061	0.211	12.72
910416	0700	0.68	0.64	0.13	-24.0	-90.0	8.87	5.52	0.208	0.092	0.367	13.80
910416	1300	0.53	0.51	0.08	-6.0	-90.0	8.16	8.16	0.149	0.136	0.136	12.76
910416	1900	0.61	0.59	0.10	-42.0	-90.0	8.16	5.83	0.170	0.142	0.276	14.07
910417	0117	0.57	0.56	0.07	-12.0	-90.0	6.59	5.83	0.134	0.081	0.174	12.68
910417	0700	0.59	0.55	0.10	-6.0	-90.0	6.19	15.63	0.175	0.165	0.512	13.63
910417	1300	0.46	0.44	0.07	-40.0	-90.0	6.59	15.63	0.147	0.079	0.237	12.68
910417	1900	0.47	0.44	0.11	-58.0	-134.0	7.56	15.63	0.250	0.171	0.616	13.93
910418	0717	1.16	1.11	0.24	18.0	90.0	4.17	4.17	0.217	0.223	0.223	13.84
910418	1300	1.68	1.63	0.35	20.0	90.0	5.83	4.17	0.214	0.200	0.308	13.32
910418	1900	1.65	1.62	0.25	24.0	90.0	6.59	4.35	0.153	0.092	0.248	14.06
910419	0117	1.79	1.76	0.27	14.0	90.0	5.83	4.17	0.154	0.162	0.263	13.51
910419	0700	1.72	1.68	0.23	20.0	90.0	5.83	4.75	0.136	0.102	0.259	13.66

(Continued)

(Continued)

Date	Time EST	Wave Height H_{mo} m	$H_{mo,i}$ m	$H_{mo,r}$ m	Direction $\theta_{p,i}$ deg	$\theta_{p,r}$ deg	Period $T_{p,i}$ sec	$T_{p,r}$ sec	Reflection x_{mo}	$x_{p,i}$	$x_{p,r}$	Depth m
910419	1300	1.51	1.48	0.19	0.0	90.0	9.71	4.17	0.128	0.058	0.232	13.46
910419	1900	1.57	1.54	0.17	-6.0	90.0	9.71	5.52	0.113	0.058	0.164	13.67
910420	0100	1.59	1.56	0.16	14.0	-90.0	7.04	5.24	0.100	0.048	0.198	13.79
910420	0700	1.83	1.80	0.18	16.0	-100.0	7.04	4.17	0.099	0.048	0.233	13.41
910420	1300	2.56	2.51	0.24	-28.0	-90.0	8.87	4.17	0.095	0.037	0.236	13.72
910420	1900	3.07	2.99	0.51	8.0	90.0	8.16	4.17	0.170	0.096	0.404	13.52
910421	0117	2.09	2.04	0.29	4.0	126.0	8.16	4.17	0.144	0.066	0.360	14.02
910421	0700	1.65	1.62	0.19	10.0	90.0	8.16	4.17	0.118	0.077	0.358	13.29
910421	1300	1.36	1.32	0.18	8.0	-172.0	8.16	10.72	0.136	0.091	0.165	13.88
910421	1900	0.85	0.82	0.13	30.0	-92.0	8.16	5.24	0.157	0.104	0.399	13.18
910422	0117	0.60	0.57	0.11	0.0	156.0	8.87	10.72	0.191	0.154	0.226	13.91
910422	0700	0.44	0.42	0.06	4.0	150.0	8.16	10.72	0.142	0.181	0.207	12.96
910422	1300	0.48	0.44	0.10	-36.0	148.0	8.87	6.59	0.224	0.194	0.365	13.70
910422	1900	0.49	0.46	0.08	-42.0	154.0	8.87	10.72	0.174	0.095	0.214	12.85
910423	0117	0.56	0.52	0.11	-36.0	-112.0	8.87	8.16	0.221	0.162	0.291	13.76
910423	0700	0.47	0.44	0.06	-42.0	154.0	8.87	10.72	0.141	0.123	0.163	12.93
910423	1300	0.46	0.42	0.09	-48.0	-166.0	8.16	10.72	0.206	0.170	0.223	13.78
910423	1900	0.47	0.44	0.06	-4.0	148.0	8.16	8.87	0.132	0.146	0.218	13.02
910424	0117	0.51	0.48	0.10	-48.0	-146.0	8.16	8.16	0.203	0.202	0.202	13.71
910424	0700	0.54	0.50	0.07	16.0	132.0	8.16	11.98	0.129	0.111	0.253	13.01
910425	1317	0.46	0.44	0.07	4.0	142.0	8.16	11.98	0.149	0.119	0.217	13.56
910425	1900	0.45	0.42	0.07	12.0	178.0	11.98	11.98	0.158	0.205	0.205	13.49
910426	0117	0.46	0.43	0.06	14.0	146.0	10.72	10.72	0.130	0.195	0.195	13.34
910426	0700	0.46	0.44	0.09	18.0	-148.0	10.72	10.72	0.209	0.259	0.259	13.43
910426	1300	0.50	0.48	0.08	-2.0	-128.0	7.04	10.72	0.166	0.105	0.286	13.27
910426	1900	0.43	0.40	0.09	10.0	170.0	10.72	11.98	0.230	0.207	0.294	13.67
910427	0117	0.42	0.39	0.06	2.0	158.0	10.72	10.72	0.166	0.207	0.207	13.11
910427	0700	0.43	0.40	0.09	-16.0	-152.0	9.71	8.87	0.230	0.130	0.215	13.54
910427	1300	0.55	0.51	0.08	8.0	152.0	10.72	10.72	0.151	0.165	0.165	13.06
910427	1900	0.56	0.52	0.12	14.0	166.0	10.72	10.72	0.240	0.220	0.220	13.81
910428	0100	0.63	0.60	0.09	6.0	150.0	13.56	13.56	0.155	0.151	0.151	12.87
910428	0700	0.59	0.56	0.12	-6.0	154.0	11.98	10.72	0.209	0.168	0.219	13.62
910428	1300	0.56	0.52	0.09	-6.0	164.0	11.98	11.98	0.180	0.140	0.140	12.92
910428	1900	0.52	0.48	0.11	4.0	166.0	11.98	11.98	0.224	0.220	0.220	13.99
910429	0100	0.51	0.48	0.08	0.0	-90.0	10.72	5.52	0.171	0.153	0.296	13.00
910429	0700	0.79	0.76	0.11	-30.0	-90.0	5.83	5.52	0.149	0.110	0.171	13.87
910430	1317	0.64	0.61	0.07	18.0	-90.0	7.04	5.52	0.120	0.085	0.207	12.97
910430	1900	0.53	0.50	0.10	-2.0	-170.0	13.56	13.56	0.202	0.241	0.241	13.96
910501	0100	0.46	0.43	0.07	0.0	-180.0	13.56	13.56	0.173	0.216	0.216	12.96
910501	0700	0.41	0.38	0.07	-10.0	178.0	13.56	13.56	0.191	0.223	0.223	13.70
910501	1300	0.40	0.37	0.08	-10.0	156.0	13.56	11.98	0.205	0.288	0.369	13.04
910501	1900	0.38	0 35	0.07	-20.0	168.0	11.98	13.56	0.212	0.209	0.270	13.91
910502	0117	0.33	0.30	0.08	-16.0	-174.0	11.98	13.56	0.253	0.275	0.338	13.04
910502	0700	0.33	0.30	0.05	6.0	136.0	11.98	11.98	0.150	0.190	0.190	13.61
910502	1300	0.34	0.31	0.06	8.0	136.0	11.98	13.56	0.192	0.264	0.287	13.11
910502	1900	0.37	0.34	0.06	0.0	-146.0	13.56	8.87	0.161	0.213	0.200	13.75

(Continued)

(Sheet 15 of 18)

(Continued)

Date	Time EST	Wave Height H_{mo} m	$H_{mo,i}$ m	$H_{mo,r}$ m	Direction $\theta_{p,i}$ deg	$\theta_{p,r}$ deg	Period $T_{p,i}$ sec	$T_{p,r}$ sec	Reflection x_{mo}	$x_{p,i}$	$x_{p,r}$	Depth m
910503	0700	0.31	0.28	0.05	6.0	156.0	11.98	11.98	0.190	0.262	0.262	13.43
910503	1300	0.42	0.39	0.09	28.0	90.0	4.17	4.17	0.241	0.280	0.280	13.25
910503	1900	0.56	0.55	0.07	50.0	90.0	5.24	4.98	0.122	0.110	0.175	13.61
910504	0100	0.41	0.40	0.06	42.0	140.0	5.52	11.98	0.159	0.140	0.311	13.34
910504	0700	0.30	0.28	0.05	50.0	162.0	4.17	11.98	0.181	0.154	0.327	13.31
910504	1300	0.30	0.28	0.04	32.0	-90.0	5.24	5.24	0.139	0.191	0.191	13.32
910504	1900	0.30	0.28	0.04	20.0	-156.0	4.98	10.72	0.150	0.171	0.359	13.40
910505	0117	0.40	0.37	0.07	12.0	-90.0	5.83	5.52	0.175	0.192	0.228	13.36
910505	0700	0.40	0.38	0.06	16.0	-90.0	5.24	5.24	0.147	0.172	0.172	13.16
910505	1300	0.36	0.34	0.06	-14.0	130.0	6.59	11.98	0.179	0.110	0.268	13.43
910505	1900	0.40	0.38	0.07	-34.0	-90.0	5.24	5.24	0.189	0.221	0.221	13.34
910506	0117	0.50	0.47	0.12	-18.0	-90.0	4.98	5.24	0.247	0.317	0.312	13.59
910506	0700	0.67	0.64	0.10	-16.0	-90.0	5.52	5.24	0.163	0.148	0.255	13.12
910506	1900	0.39	0.37	0.05	-24.0	-90.0	5.83	6.59	0.140	0.143	0.147	13.10
910507	0117	0.40	0.38	0.07	-56.0	-90.0	6.59	5.83	0.199	0.129	0.265	13.55
910507	0700	0.35	0.33	0.05	-54.0	134.0	7.04	13.56	0.150	0.131	0.430	13.07
910507	1300	0.67	0.65	0.11	32.0	90.0	4.17	4.17	0.176	0.224	0.224	13.72
910507	1900	0.50	0.48	0.09	32.0	-90.0	4.75	5.24	0.194	0.205	0.241	13.13
910508	0117	0.45	0.42	0.06	-62.0	172.0	6.59	11.98	0.135	0.122	0.315	13.61
910508	0700	0.41	0.39	0.06	-52.0	156.0	7.04	10.72	0.148	0.100	0.258	12.95
910508	1300	0.40	0.38	0.07	-8.0	158.0	10.72	6.59	0.180	0.174	0.323	13.66
910508	1900	0.40	0.38	0.06	8.0	160.0	10.72	10.72	0.150	0.222	0.222	13.03
910509	0117	0.42	0.39	0.09	-12.0	-90.0	5.52	5.83	0.239	0.287	0.299	13.62
910509	0700	0.41	0.39	0.06	-16.0	158.0	5.24	10.72	0.142	0.150	0.214	12.93
910509	1300	0.38	0.35	0.06	-6.0	-142.0	10.72	9.71	0.173	0.218	0.196	13.68
910509	1900	0.40	0.38	0.05	4.0	-90.0	9.71	5.24	0.131	0.123	0.165	13.13
910510	0117	0.46	0.43	0.07	-6.0	-90.0	4.98	4.98	0.159	0.188	0.188	13.64
910510	0700	0.46	0.44	0.07	-10.0	-90.0	4.98	5.24	0.163	0.157	0.253	13.03
910510	1300	0.44	0.41	0.09	-56.0	-106.0	7.56	6.59	0.214	0.285	0.329	13.62
910510	1900	0.39	0.37	0.08	-50.0	-150.0	7.56	8.87	0.215	0.249	0.247	13.28
910511	0100	0.92	0.89	0.11	14.0	90.0	4.54	4.54	0.120	0.118	0.118	13.50
910511	0700	0.95	0.93	0.10	8.0	90.0	5.24	4.54	0.103	0.078	0.114	13.24
910511	1300	0.92	0.89	0.09	-2.0	156.0	8.16	5.24	0.100	0.096	0.137	13.52
910511	1900	0.68	0.65	0.08	6.0	114.0	7.56	8.87	0.120	0.091	0.161	13.46
910512	0100	0.73	0.71	0.08	-8.0	-134.0	8.87	8.16	0.111	0.085	0.099	13.15
910512	0700	0.73	0.70	0.12	-18.0	-166.0	8.87	8.16	0.168	0.093	0.172	13.26
910512	1300	0.78	0.75	0.10	-22.0	-96.0	9.71	10.72	0.134	0.099	0.178	13.18
910512	1900	0.62	0.58	0.14	-26.0	-176.0	9.71	8.87	0.240	0.151	0.263	13.62
910513	0117	0.59	0.57	0.08	-18.0	156.0	9.71	11.98	0.144	0.074	0.254	12.91
910513	0700	0.52	0.50	0.10	-22.0	166.0	9.71	10.72	0.202	0.139	0.208	13.41
910515	1317	0.27	0.25	0.05	-42.0	-90.0	5.83	5.52	0.206	0.197	0.232	12.75
910515	1900	0.29	0.27	0.04	-52.0	-90.0	5.52	5.24	0.160	0.263	0.277	14.22
910516	0117	0.37	0.36	0.05	44.0	-90.0	4.17	6.59	0.140	0.132	0.234	12.85
910516	0700	0.53	0.50	0.13	18.0	90.0	4.54	4.35	0.270	0.273	0.300	13.83
910516	1300	0.48	0.45	0.07	12.0	90.0	4.35	4.35	0.153	0.152	0.152	12.80
910516	1900	0.59	0.56	0.08	-14.0	-90.0	5.83	5.52	0.139	0.136	0.216	14.08

(Continued)

(Sheet 16 of 18)

(Continued)

Date	Time EST	Wave Height H_{mo} m	$H_{mo,i}$ m	$H_{mo,r}$ m	Direction $\theta_{p,i}$ deg	$\theta_{p,r}$ deg	Period $T_{p,i}$ sec	$T_{p,r}$ sec	Reflection x_{mo}	$x_{p,i}$	$x_{p,r}$	Depth m
910517	0117	0.45	0.44	0.06	-4.0	-90.0	6.19	5.24	0.129	0.127	0.163	12.90
910517	0700	0.44	0.41	0.07	2.0	156.0	6.19	5.83	0.160	0.111	0.153	13.65
910517	1300	0.36	0.35	0.06	-10.0	-100.0	5.83	9.71	0.175	0.136	0.243	12.92
910517	1900	0.38	0.35	0.07	-8.0	-90.0	5.24	5.24	0.201	0.199	0.199	13.75
910518	0117	0.32	0.29	0.05	0.0	-90.0	8.87	5.52	0.159	0.146	0.209	13.05
910518	0700	0.31	0.28	0.06	-4.0	-100.0	8.87	8.16	0.193	0.176	0.227	13.35
910518	1300	1.38	1.36	0.16	6.0	90.0	4.98	4.17	0.115	0.135	0.185	13.37
910518	1900	2.20	2.17	0.27	26.0	90.0	7.04	4.35	0.123	0.058	0.249	13.81
910519	0117	2.22	2.18	0.24	12.0	90.0	8.87	4.17	0.109	0.059	0.202	13.80
910519	0700	2.47	2.45	0.21	6.0	90.0	6.19	4.17	0.087	0.055	0.203	13.55
910519	1300	2.30	2.26	0.25	16.0	90.0	7.04	4.17	0.110	0.045	0.216	13.83
910519	1900	1.85	1.82	0.20	14.0	90.0	6.59	5.52	0.108	0.053	0.136	13.46
910520	0100	1.65	1.60	0.21	4.0	90.0	10.72	4.35	0.129	0.072	0.213	13.96
910520	0700	1.54	1.51	0.15	-6.0	-90.0	10.72	5.52	0.102	0.064	0.126	13.21
910521	1300	0.99	0.95	0.13	0.0	-90.0	8.16	5.52	0.139	0.085	0.173	13.77
910521	1900	0.91	0.88	0.10	-14.0	-90.0	7.04	5.52	0.108	0.089	0.145	12.91
910522	0117	0.85	0.81	0.13	-40.0	-90.0	7.56	5.52	0.157	0.107	0.252	13.70
910522	0700	0.75	0.72	0.09	-8.0	-90.0	8.16	5.24	0.122	0.104	0.225	12.78
910522	1300	0.67	0.63	0.13	-8.0	-90.0	7.56	5.52	0.200	0.160	0.316	13.73
910522	1900	0.57	0.54	0.08	-48.0	-96.0	8.87	8.16	0.147	0.125	0.156	12.90
910523	0117	0.56	0.52	0.15	-44.0	-142.0	7.04	8.16	0.280	0.235	0.271	13.55
910523	0700	0.47	0.44	0.09	-34.0	-144.0	8.87	5.83	0.195	0.115	0.293	12.85
910523	1300	0.48	0.44	0.13	-34.0	-144.0	8.87	8.16	0.284	0.220	0.290	13.71
910523	1900	0.39	0.37	0.09	-50.0	-120.0	8.16	6.59	0.250	0.206	0.368	13.18
910524	0117	0.40	0.37	0.10	-50.0	-118.0	8.16	6.59	0.268	0.227	0.462	13.61
910524	0700	0.41	0.38	0.09	-16.0	-134.0	8.16	8.16	0.244	0.224	0.224	13.18
910524	1300	0.46	0.42	0.10	-38.0	-138.0	7.56	8.16	0.230	0.231	0.303	13.63
910524	1900	0.41	0.38	0.09	-48.0	-138.0	8.16	6.59	0.238	0.187	0.299	13.35
910525	0117	0.50	0.47	0.11	-48.0	-132.0	7.56	15.63	0.226	0.247	0.548	13.28
910525	0700	0.53	0.50	0.10	-50.0	-146.0	7.56	5.52	0.206	0.132	0.361	13.15
910525	1300	0.51	0.47	0.10	-44.0	-174.0	7.04	15.63	0.214	0.166	0.577	13.25
910525	1900	0.47	0.43	0.10	-44.0	-134.0	7.04	15.63	0.238	0.176	0.428	13.43
910526	0117	0.53	0.50	0.10	-50.0	-120.0	7.56	13.56	0.206	0.207	0.368	13.04
910526	0700	0.55	0.51	0.12	-46.0	-128.0	7.04	13.56	0.237	0.166	0.432	13.29
910526	1300	0.51	0.47	0.10	-42.0	-124.0	7.04	13.56	0.212	0.176	0.433	13.12
910526	1900	0.47	0.44	0.09	-48.0	140.0	7.04	13.56	0.210	0.178	0.274	13.68
910527	0117	0.47	0.43	0.09	-44.0	-176.0	7.04	13.56	0.212	0.164	0.374	13.05
910527	0700	0.47	0.43	0.12	-42.0	-120.0	7.04	6.59	0.273	0.198	0.348	13.55
910529	1317	0.38	0.35	0.07	-10.0	146.0	13.56	13.56	0.199	0.278	0.278	12.98
910529	1900	0.37	0.35	0.07	-22.0	-90.0	11.98	11.98	0.203	0.207	0.207	13.94
910530	0117	0.37	0.34	0.08	-16.0	142.0	11.98	11.98	0.228	0.282	0.282	12.91
910530	0700	0.40	0.36	0.08	-16.0	138.0	11.98	11.98	0.226	0.286	0.286	13.64
910530	1300	0.38	0.35	0.08	-22.0	136.0	11.98	11.98	0.215	0.245	0.245	12.91
910530	1900	0.34	0.32	0.07	-16.0	-158.0	11.98	11.98	0.217	0.299	0.299	13.80
910531	0117	0.32	0.29	0.08	-16.0	-152.0	11.98	11.98	0.272	0.291	0.291	12.84
910531	0700	0.33	0.31	0.06	-26.0	-138.0	10.72	7.56	0.194	0.193	0.265	13.52

(Continued)

(Concluded)

Date	Time EST	Wave Height H_{mo} m	$H_{mo,i}$ m	$H_{mo,r}$ m	Direction $\theta_{p,i}$ deg	$\theta_{p,r}$ deg	Period $T_{p,i}$ sec	$T_{p,r}$ sec	Reflection x_{mo}	$x_{p,i}$	$x_{p,r}$	Depth m
910531	1300	0.34	0.31	0.07	-6.0	-122.0	10.72	11.98	0.230	0.271	0.341	12.98
910531	1900	0.35	0.32	0.07	-20.0	-148.0	10.72	9.71	0.220	0.196	0.181	13.74
910601	0100	0.33	0.30	0.06	-6.0	-154.0	10.72	10.72	0.215	0.287	0.287	13.08
910601	0700	0.31	0.29	0.05	-10.0	-94.0	10.72	10.72	0.182	0.208	0.208	13.52
910601	1300	0.32	0.29	0.06	-30.0	148.0	10.72	11.98	0.200	0.194	0.286	13.15
910601	1900	0.29	0.27	0.05	-14.0	-96.0	10.72	10.72	0.178	0.220	0.220	13.70
910602	0117	0.31	0.28	0.06	-26.0	-154.0	10.72	10.72	0.213	0.245	0.245	13.18

Appendix B: Time Series Graphs of Bulk Spectral Parameters

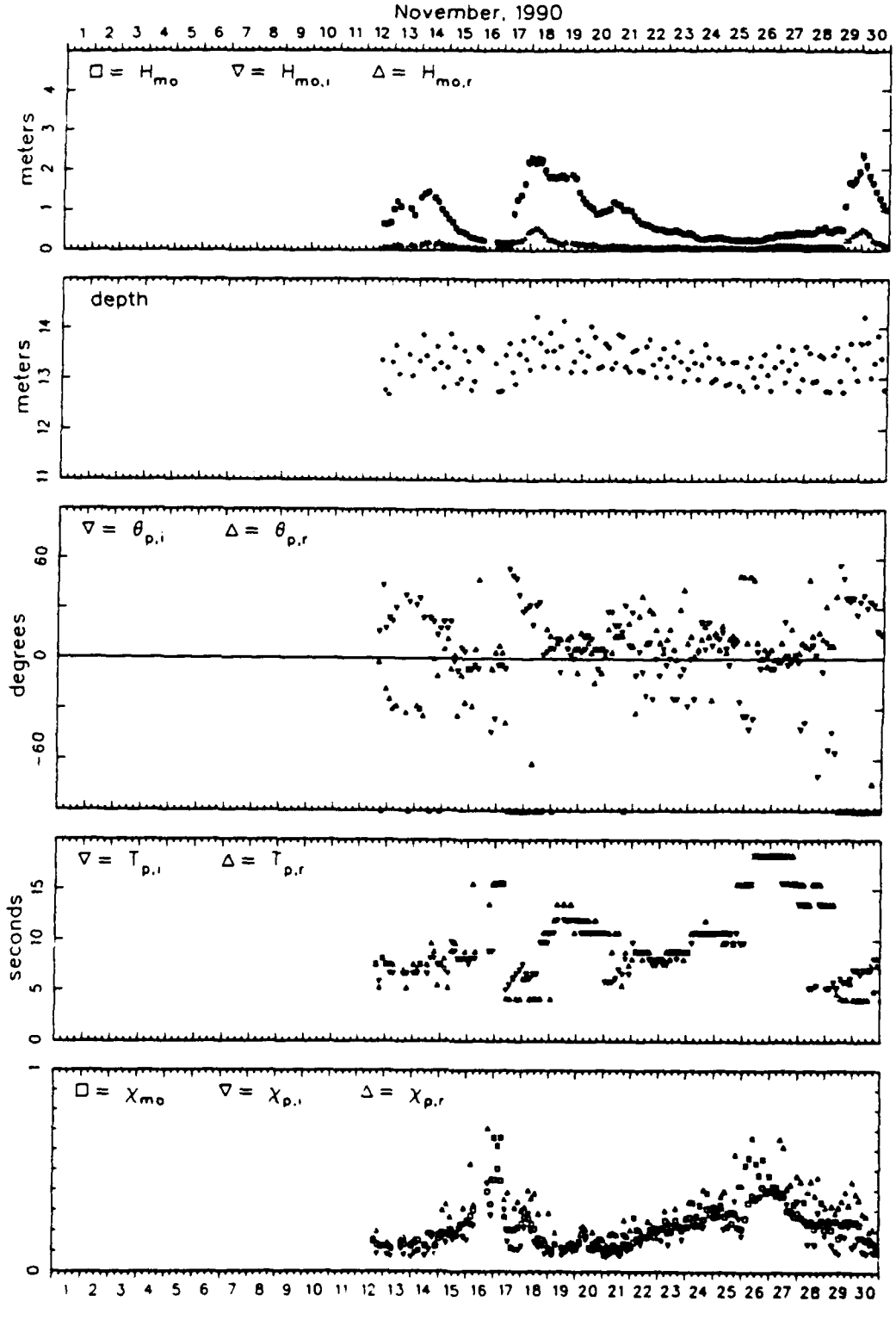

Figure B1. Bulk data for November 1990

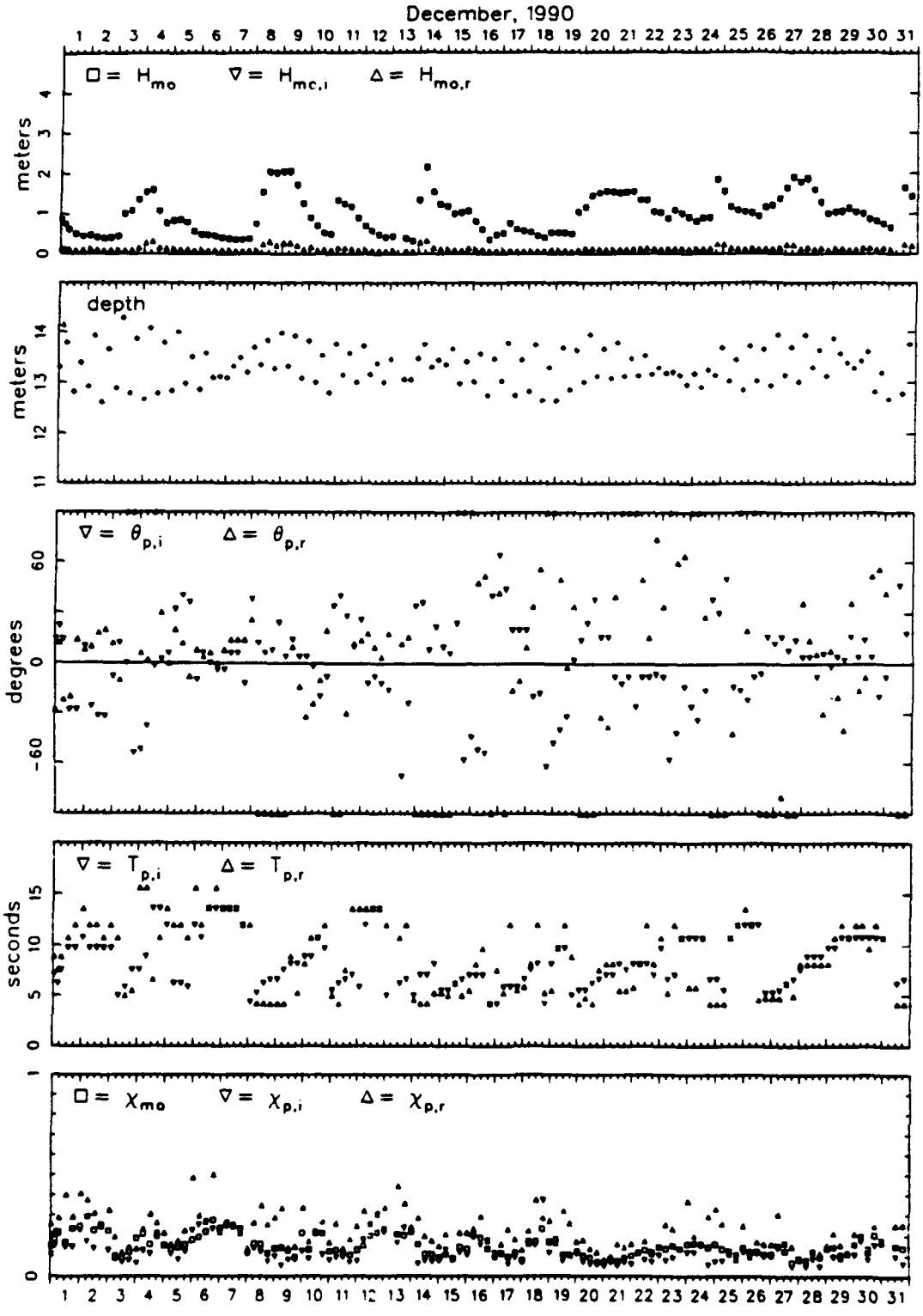

Figure B2. Bulk data for December 1990

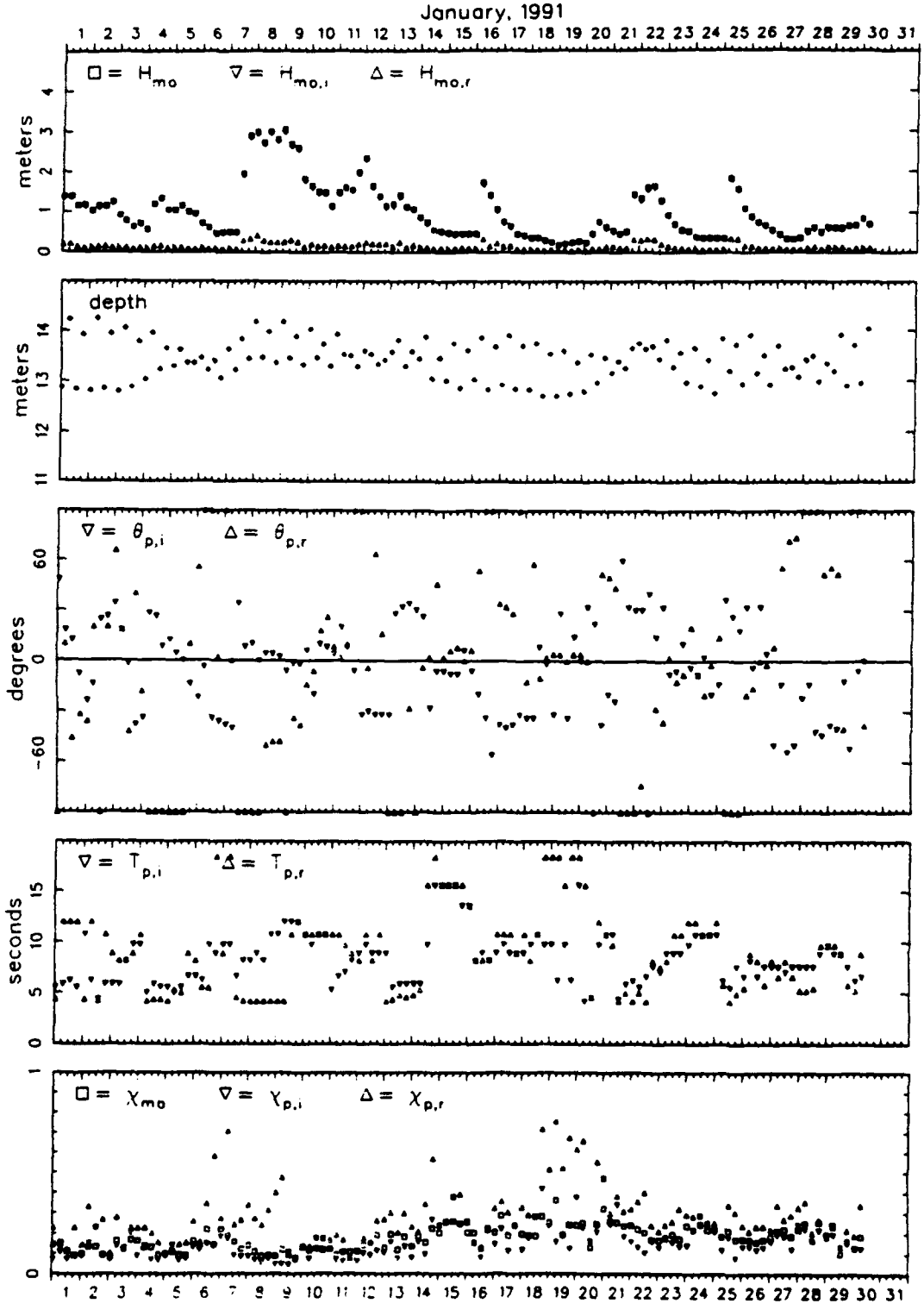

Figure B3. Bulk data for January 1991

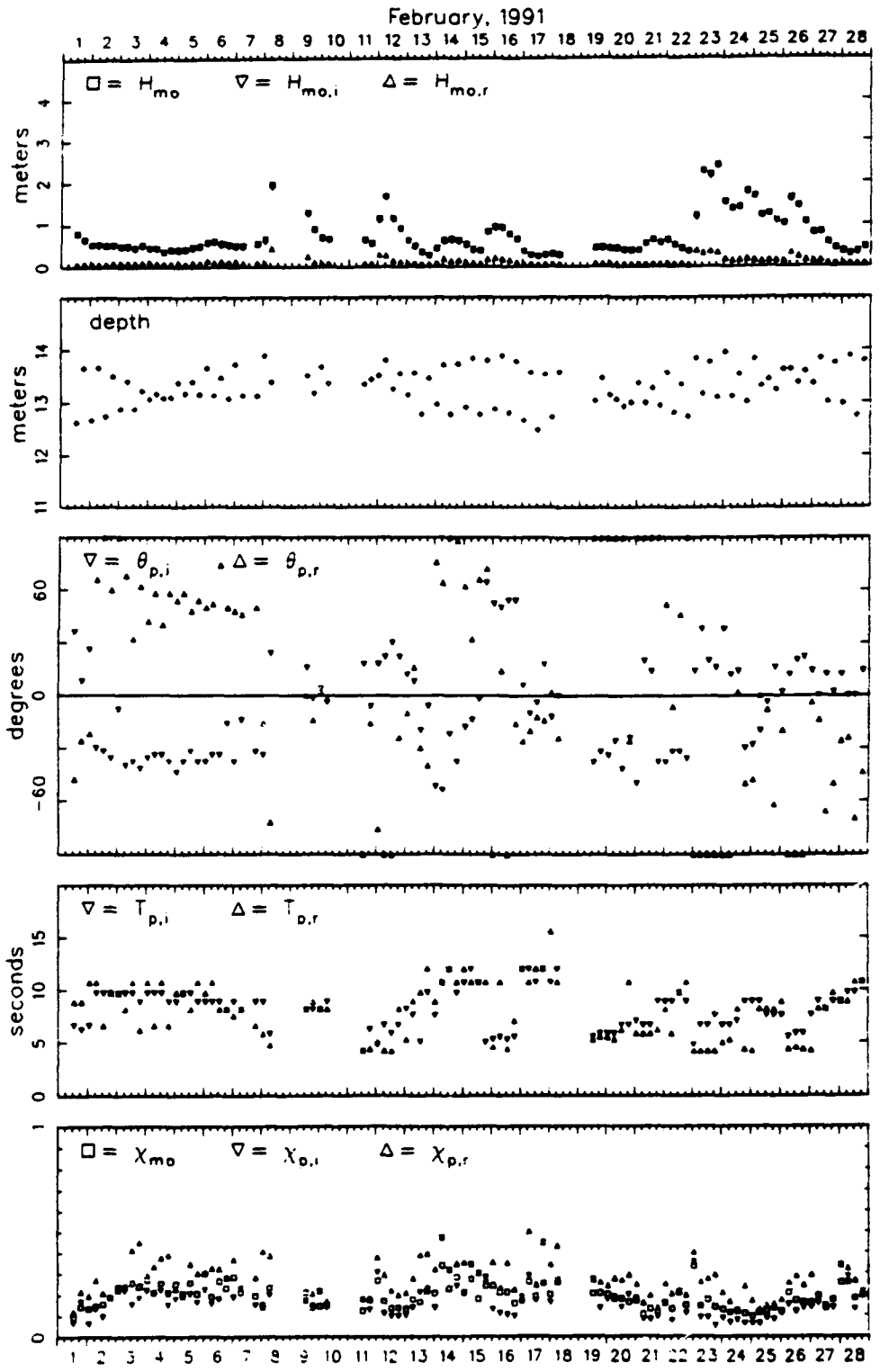

Figure B4. Bulk data for February 1991

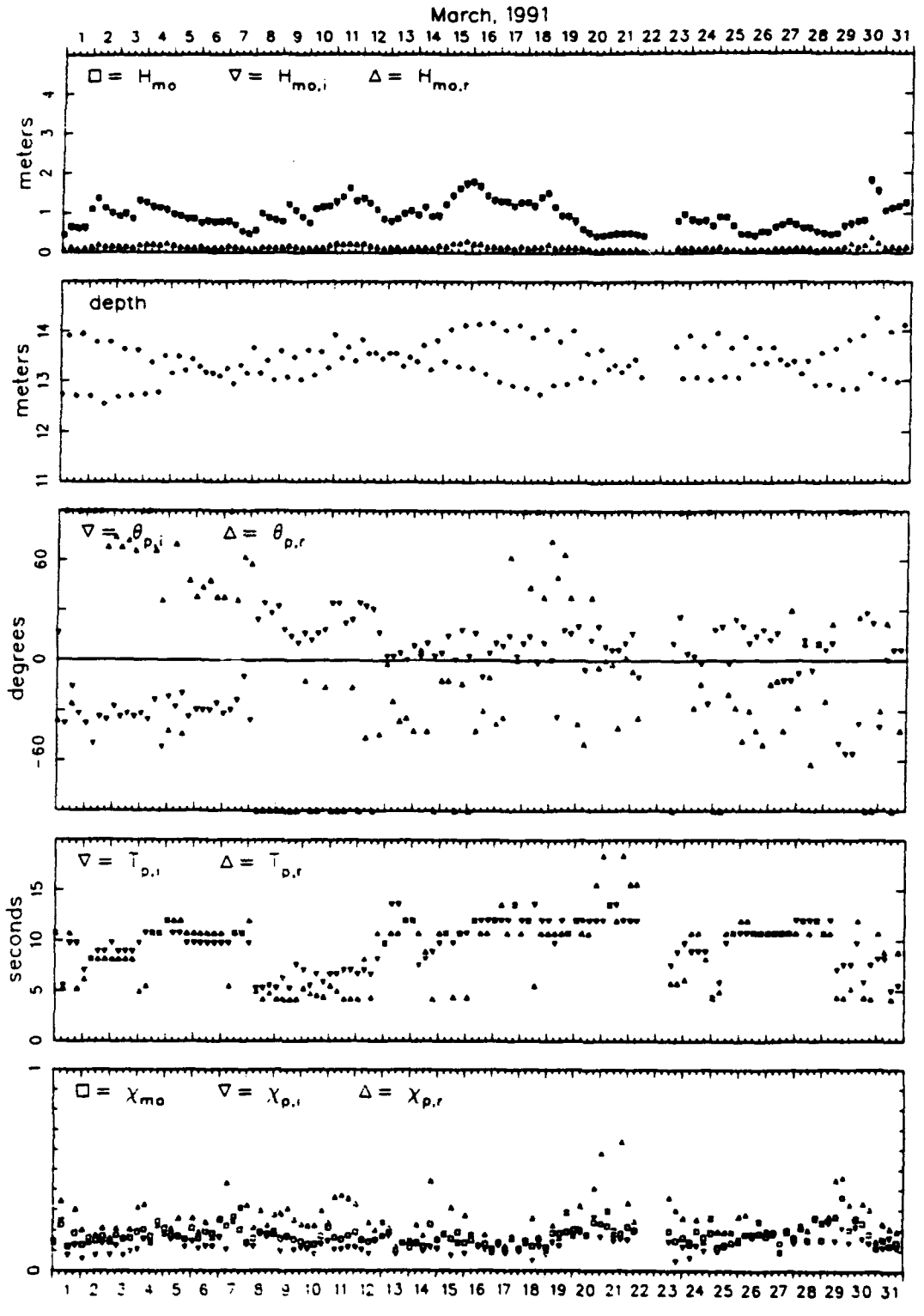

Figure B5. Bulk data for March 1991

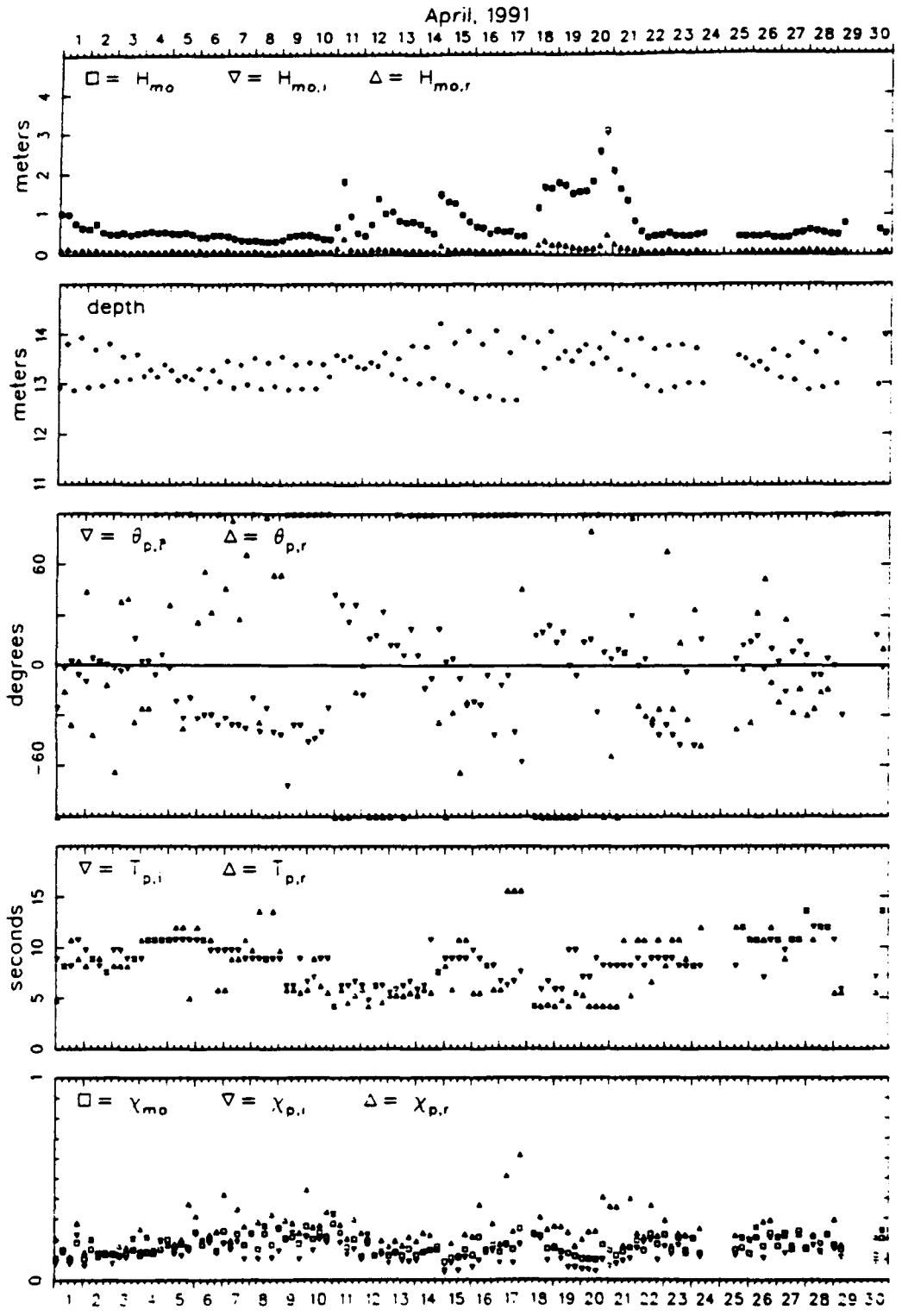

Figure B6. Bulk data for April 1991

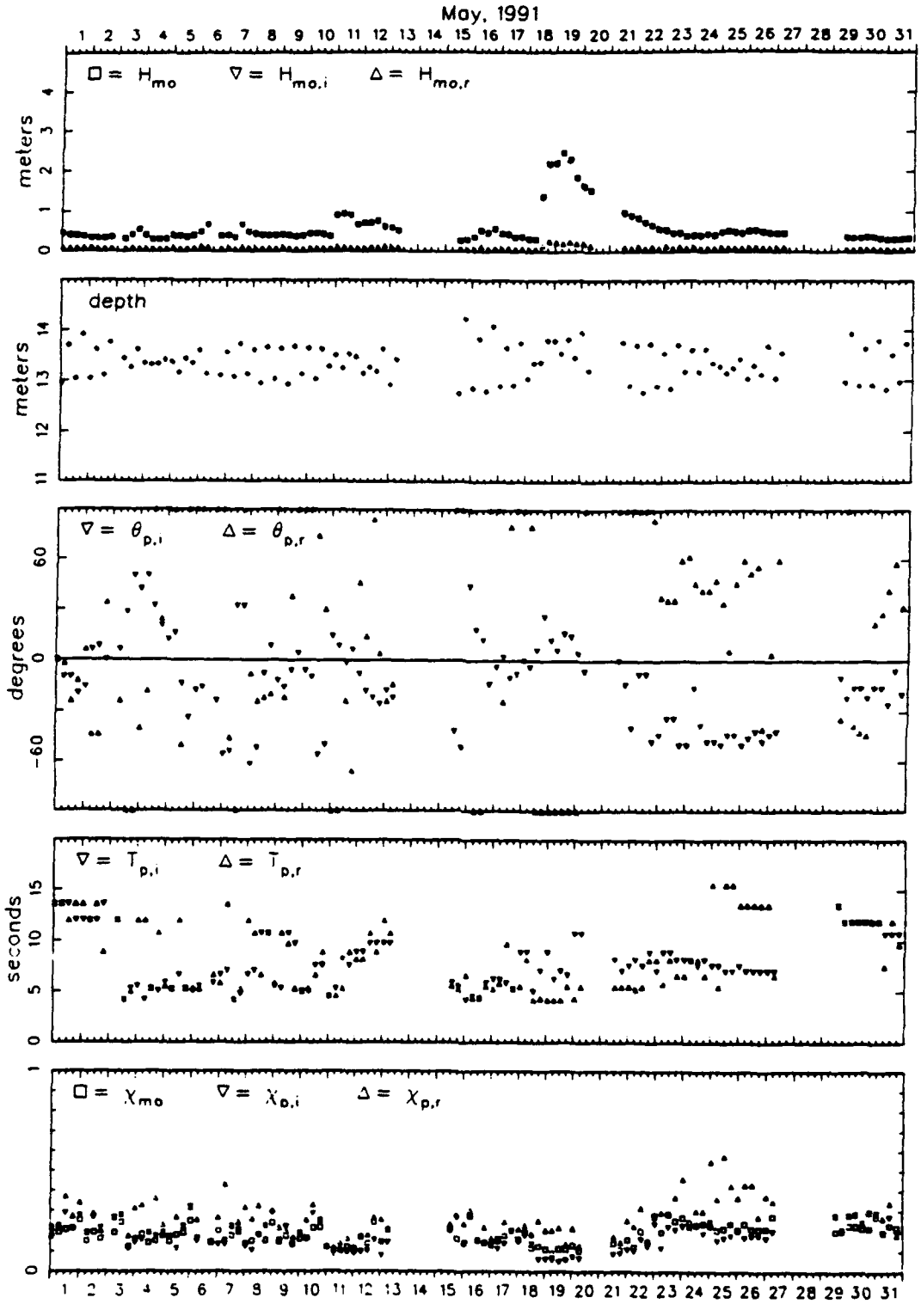

Figure B7. Bulk data for May 1991

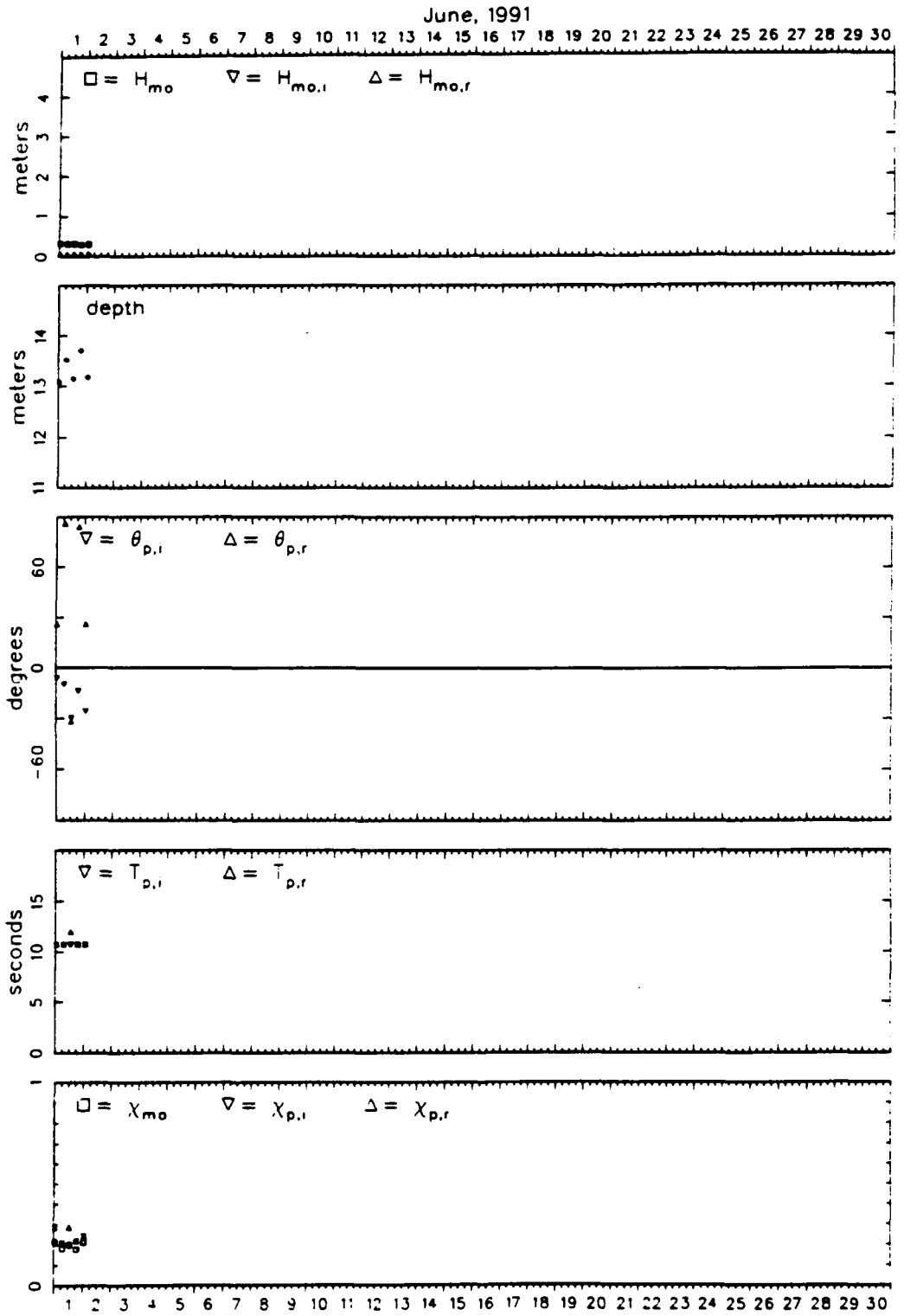

Figure B8. Bulk data for June 1991

Appendix C: Estimation of Error in Reflection Coefficients

Appendix C: Estimation of Error in Reflection Coefficients

1. To obtain some measure of reliability for the reflection coefficients deduced from the Sources of Ambient Micro-Seismic Noise (SAMSON) data, tests have been conducted using a variety of synthetic directional spectra in conjunction with the Iterative Maximum Likelihood Estimation (IMLE) algorithm and the geometry of the SAMSON array of gages. Artificial directional energy distributions are used to compute the cross-spectral matrices that would result from the SAMSON gages if the corresponding idealized wave fields had actually been measured. These cross-spectral matrices are then passed through the same directional estimation algorithm that was used to process the SAMSON field data. The resulting IMLE estimates of directional distributions are then compared to the original synthetic distributions to assess errors in the analysis algorithm.

2. To keep the test results tractable, synthetic distributions are necessarily kept simple. Consequently, the test distributions do not mimic exactly the structurally more complicated distributions detected in the field data reported in the main body of this report. As a result, these tests are only indicative of the viability of the analysis algorithm and are not specifically applicable to any particular real observation. Nonetheless, it is of immense value to have some quantitative measure of efficacy of the analysis system, and describing such a measure is the intent of this appendix.

3. Test spectra are single directional distributions constructed of two Gaussian-shaped modes, one representing incident waves and the other representing reflected waves, to which is added a white (constant with respect to direction) noise spectrum. A single directional distribution is equivalent to a directionwise slice at a particular frequency through a full frequency-direction spectrum, of which Figure 6 in the main text is an example. Frequency is specified for the tests because it determines the wavelengths of the (synthetic) waves that would pass through the array of gages, and it determines which sub-array of gages is used in analysis, following Table 1 in the main text. Computations are done at discrete directions* θ_m as in the main text, but with the direction increment $d\theta = 1$ deg instead of 2 deg, and increasing from -180 deg. Hence, directions are defined by

---

* A notation for this appendix is included in Appendix D.

$$\theta_m = -180^\circ + (m - 1)\, d\theta \quad , \qquad m = 1, 2, 3, \ldots , M \tag{C1}$$

where $M = 360$ is the total number of direction increments. In terms of these discrete directions, synthetic spectra take the form

$$S(\theta_m) = \frac{P_i}{\sqrt{2\pi}\,\delta\theta_i} e^{-\frac{1}{2}\left[\frac{\theta_m - \theta_{p,i}}{\delta\theta_i}\right]^2} + \frac{1 - P_i}{\sqrt{2\pi}\,\delta\theta_r} e^{-\frac{1}{2}\left[\frac{\theta_m - \theta_{p,r}}{\delta\theta_r}\right]^2} + \frac{1}{360} S_N \tag{C2}$$

where the first term on the right-hand side represents the incident mode, the second term on the right-hand side is the reflected mode, and the last term is the (constant) noise spectrum. The sum of the first two terms on the right-hand side is the signal. There are six variable parameters in Equation C2: P_i is the fraction of total signal energy in the incident mode, $\theta_{p,i}$ is the incident mode peak direction, $\delta\theta_i$ governs the directional spread of the incident mode, $\theta_{p,r}$ is the reflected mode peak direction, $\delta\theta_r$ determines the directional spread of the reflected mode, and S_N is the total variance in the noise spectrum. The coefficient $(1 - P_i)$ in the second term gives the fractional part of total signal energy in the reflected mode. Total noise S_N is divided by 360 in Equation C2 to give the proper variance density for each discrete direction θ_m. The parameters $\delta\theta_i$ and $\delta\theta_r$ are like the standard deviations in Gaussian probability density functions, and determine the rate at which the Gaussian curve decays from its peak. In practice, these two parameters are defined from the expressions

$$\delta\theta_i = \frac{\Delta\theta_i}{2} \qquad \text{and} \qquad \delta\theta_r = \frac{\Delta\theta_r}{2} \tag{C3}$$

and $\Delta\theta_i$ and $\Delta\theta_r$ are specified because they give the actual directional spreads at 1/e times the peak values of the Gaussian curves.

4. The total variance represented by Equation C2 is found by integration of both sides with respect to θ, which, in discrete form, is equivalent to summing the product $S(\theta_m)\, d\theta$ over all directions. The total signal variance has been arbitrarily set to 1 m^2. The coefficients have been defined so that this discrete summation over a finite range of directions very nearly approximates the integral of the continuous (in θ) form of Equation C2 over an infinite range of directions, i.e.,

$$\sum_{m=1}^{M} S(\theta_m)\, d\theta \approx P_i + (1 - P_i) + S_N \approx 1 + S_N \qquad \text{(C4)}$$

In this expression, the ratio of the total variance due to noise (S_N) to total signal variance (1 m^2) is simply S_N , so that the noise-to-signal ratio N/S is S_N identically. In computations with the spectrum of Equation C2, the area of the signal part of the spectrum is computed separately, and the first two terms on the right-hand side of Equation C2 are renormalized by this area to make Equation C4 exact (to computer accuracy).

5. The formulation of Equation C2 also allows some (approximate) control of reflection coefficients for the true spectra. If peak directions and directional spreads are such that the tails of neither incident nor reflected mode are significant on opposing sides of the ±90-deg boundary that separates incident and reflected wave energy, the wave-height-based reflection coefficient used here will be simply

$$\chi = \sqrt{\frac{1 - P_i}{P_i}} \qquad \text{(C5)}$$

However, because many of the test spectra do have extensive tail regions, reflection coefficients for true and estimated spectra are computed numerically in the same way as described in the main text, modified for the smaller direction increment $d\theta$. With that modification, and following the notation of Equation C2, the total incident energy plus noise is

$$S_i = \tfrac{1}{2} S(\theta_{91})\, d\theta + \sum_{m=92}^{270} S(\theta_m)\, d\theta + \tfrac{1}{2} S(\theta_{271})\, d\theta \qquad \text{(C6)}$$

and the total reflected energy plus noise is

$$S_r = \sum_{m=1}^{90} S(\theta_m)\, d\theta + \tfrac{1}{2}\left[S(\theta_{91}) + S(\theta_{271}) \right] d\theta + \sum_{m=272}^{360} S(\theta_m)\, d\theta \qquad \text{(C7)}$$

The reflection coefficient is then computed as

$$\chi = \left[\frac{S_r - \frac{1}{2} S_N}{S_i - \frac{1}{2} S_N} \right]^{\frac{1}{2}} \qquad \text{(C8)}$$

where half the noise variance is associated with the total incident energy and the other half is aligned with total reflected energy. For the true spectrum, S_N is specified exactly, so the true reflection coefficient can be computed with high accuracy. For spectra estimated with the Maximum Likelihood Estimation (MLE) or IMLE algorithms, S_N is estimated as the average of the smallest 10 discrete spectral values, just as was done with the SAMSON field data. The accuracy of reflection coefficients computed from either of the estimation algorithms thus depends strongly on how well they can resolve the noise, especially at high noise levels.

6. Variation of the six parameters P_i , $\theta_{p,i}$, $\theta_{p,r}$, $\delta\theta_i$, $\delta\theta_r$, and S_N allows considerable flexibility in test conditions for the estimation algorithms. Once these parameters are specified, Equation C2 can be evaluated. When a frequency and water depth are specified for the test condition, the set of gages in the sub-array can be identified as in Table 1 in the main text, and a wavelength λ can be found using the dispersion relation of linear wave theory. The true complex cross-spectral matrix element $C_{pq} - iQ_{pq}$ between one gage located at coordinates (x_p,y_p) and another gage located at coordinates (x_q,y_q) is computed from the expression

$$C_{pq} - i\,Q_{pq} = \sum_{m=1}^{M} S(\theta_m)\, e^{-ik[(x_p - x_q)\cos\theta_m + (y_p - y_q)\sin\theta_m]}\, d\theta \qquad \text{(C9)}$$

where $k = 2\pi/\lambda$ is the wave number and i is the square root of -1. Equation C9 is a discrete approximation of the exact sea-surface variance cross-spectral density derived from first principles by Munk et al. (1963)*. The inversion of Equation C9 to isolate $S(\theta_m)$ is fundamentally central to many directional estimation algorithms.

7. The complete cross-spectral matrix is formed when the computation of Equation C9 is performed for all pairs of gages in the sub-array. This matrix is then treated as if it was derived from field data, and processed with the IMLE algorithm described in the main text. The result is a discrete estimate $S_I(\theta_m)$ of the true spectrum of Equation C2, and various comparison tests can then be performed. In the computation of an IMLE estimate, the first iteration is an MLE estimate, denoted $S_M(\theta_m)$. It is useful to have this estimate as well, so it is included in some of the comparison tests described below.

---

* See References at the end of the main text.

8. An example of the type of results obtained with these computations is shown in Figure C1, where the MLE- and IMLE-estimated directional distributions are plotted with the true spectrum. Various parameters describe the goodness of fit of the two estimated curves and the behavior of the IMLE analysis algorithm. Parameters of the true spectrum are shown in the page header. Mode 1 information relates to the incident signal spectrum and mode 2 information is for the reflected signal spectrum. The entry in the column labeled "size" for mode 1 is the parameter P_i , and that for mode 2 is $1 - P_i$. The column labeled "peak" lists $\theta_{p,i}$ and $\theta_{p,r}$ for modes 1 and 2, respectively. The column labeled "spread" lists $\Delta\theta_i$ and $\Delta\theta_r$ for modes 1 and 2, respectively. The value shown for the N/S ratio is S_N . Frequency, depth, and the corresponding wavelength for this test case are shown in the first line of the page header.

9. The line labeled "gpats" contains two strings of letters, which are codes for subsets of gages from the SAMSON array. Each letter represents the gage number corresponding to that letter's ordinal position in the alphabet. Hence, the letter "A" represents gage 1, "B" represents gage 2, and so on through letter "X", which is gage 24. Gages 12 (letter ".") and 14 (letter "N") are not used in these tests because they were not used in processing the SAMSON field data. The first string of letters represents the initial subarray of gages appropriate for the wave frequency of this test, following Table 1 in the main text. The second string of letters represents the set of gages actually used to compute the estimated spectra shown. This second gage set was identified by the dynamic gage elimination procedure described in the main text. In the course of the test computations described here, it was commonly found that the initial gage set was reduced substantially through dynamic elimination. This behavior occurred because cross-spectral information tended to peak with relatively few gages for the simple shapes of test spectra used in these tests. The page header in Figure C1 indicates that after the final set of gages was identified, it took 25 iterations of the IMLE algorithm to converge to the result shown.

10. Computed parameters and parametric comparisons are shown in the header inside the graph frame. The column marked "χ" contains the true reflection coefficient χ , and the reflection coefficients from the MLE estimate χ_M and the IMLE estimate χ_I . Errors in estimated reflection coefficients are denoted $\Delta\chi$, and are computed as percentage differences from

freq = 0.10 Hz wavelength = 102.95 m depth = 13.00 m
gpats: ABCDFGHIJKMOPQRSTUWX CDGIOQ
N/S Ratio = 0.0001 Variance = 1.00 25 Iterations
True Curve is Synthetic

mode	size	peak(deg)	spread(deg)
1	0.900	20.0	20.0
2	0.100	160.0	20.0

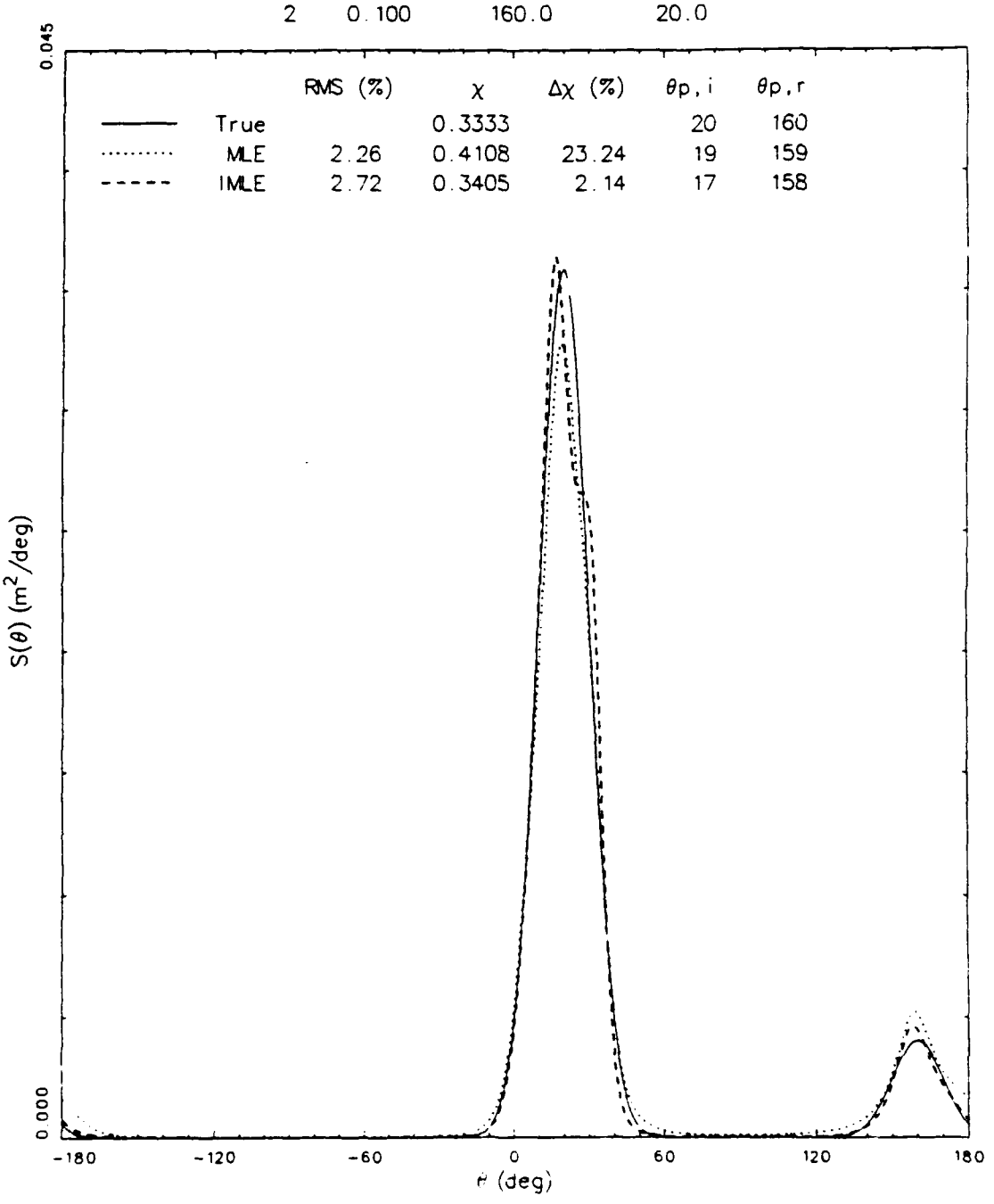

Figure C1. Sample comparison of $S_M(\theta_m)$ and $S_I(\theta_m)$ to true $S(\theta_m)$

the true reflection coefficient. Errors in the MLE estimate $\Delta\chi_M$ and IMLE estimate $\Delta\chi_I$ are computed from

$$\Delta\chi_M = \frac{\chi_M - \chi}{\chi} \cdot 100 \text{ percent} \quad \text{and} \quad \Delta\chi_I = \frac{\chi_I - \chi}{\chi} \cdot 100 \text{ percent} \tag{C10}$$

where χ , χ_M , and χ_I are found using Equations C6, C7, and C8. While reflection coefficient estimation is the subject of this appendix, some other measures of estimator quality are also given in Figure C1.

11. A measure of overall fidelity of an estimated spectrum to the true spectrum is indicated by the square root of the mean squared difference of two spectra, normalized by the peak of the true spectrum, and expressed as a percent. The column marked "RMS" shows the results of such a computation. If RMS_M and RMS_I denote these values for the MLE and IMLE estimates, respectively, the computation for RMS_I obeys

$$RMS_I = \frac{100\%}{S_{max}} \sqrt{\frac{1}{M} \sum_{m=1}^{M} \left[S_I(\theta_m) - S(\theta_m) \right]^2} \tag{C11}$$

where S_{max} [$= S(\theta_{p,i})$, in the tests reported here] is the peak value of the true spectrum. The computation for RMS_M also obeys Equation C11, but with S_M replacing S_I . Note that values for RMS_M and RMS_I can appear quite small if there are large regions of the spectrum with very low signal, as illustrated by Figure C1. Squared differences, sometimes large, in the signal parts of the spectra can be averaged with large numbers of small values where there is no signal, and the resulting computation can give a small number. Some caution is therefore required in interpreting this measure of error.

12. Because bimodal signal spectra are used in the tests reported here, the two estimated spectra can be searched for incident and reflected peak directions. The ability to resolve peak directions can be quantified by comparing estimated peaks to true peaks. The column marked "$\theta_{p,i}$" in Figure C1 shows the true incident peak direction and the peak incident directions of the *MLE and IMLE estimates*. The column marked "$\theta_{p,r}$" shows the corresponding reflected peak directions. The true incident and reflected peak directions are the modal peak directions defined in the page header, and can always be specified. In some test cases, the modes can be combined in such a way that there is no specific peak for the reflected spectrum, and, if one or both

of the estimated spectra faithfully represent the true spectrum, no peak reflected direction can be found. In such cases, an entry of "999" is used in the column for peak reflected directions.

13. Examination of some of the test parameters shown in Figure C1 suggests that the MLE estimate may be slightly better than the IMLE estimate for this case. The RMS error is slightly smaller and differences between true and estimated incident and reflected peak directions are smaller for the MLE estimate. However, the reflection coefficient estimate is much worse for the MLE estimate than for the IMLE estimate. This is because the IMLE algorithm is better at distributing the estimated energy in direction, i.e., it is better at getting the right amounts of energy in the semicircles defined as incident and reflection. As can be seen in Figure C1, the MLE curve underestimates the area in the incident peak and overestimates the area in the reflected peak more than the IMLE estimate does. Consequently, the ratio of these two areas (which leads to the reflection coefficient in low-noise cases) is much better represented by the IMLE estimate, which, in the case of Figure C1, yields a reflection coefficient only about 2 percent different than the true one.

14. If the noise level is raised for the case depicted in Figure C1, some effects of a finite, directionally white, background signal on reflection coefficient estimation can be seen. Figure C2 shows a case where the true signal properties are the same as in Figure C1 but N/S is raised from 0.0001 to 0.1, a level high enough to be seen as the nearly constant intermodal line at the bottom of the figure. The IMLE estimated spectrum rather faithfully reproduces the whole true spectrum, and overpredicts the reflection coefficient by only about 5 percent. Part of the reason for this error is that the IMLE estimate undulates slightly about the background noise level. The method of using the average of the smallest 10 points of the discrete estimated spectrum to estimate the noise is probably biased low by the low points in the undulations. Consequently, the true noise level is underestimated, the difference makes a greater contribution to the estimate of reflected area, and the reflection coefficient is slightly overestimated. That the error is small is somewhat remarkable. The area under the noise spectrum is 10 percent of the signal, and the area under the reflected peak (0.1) is 10 percent of the total signal (1.0), so the ratio of noise to reflected signal is 1.0, which is rather high. On the other hand, the reflection coefficient is moderately

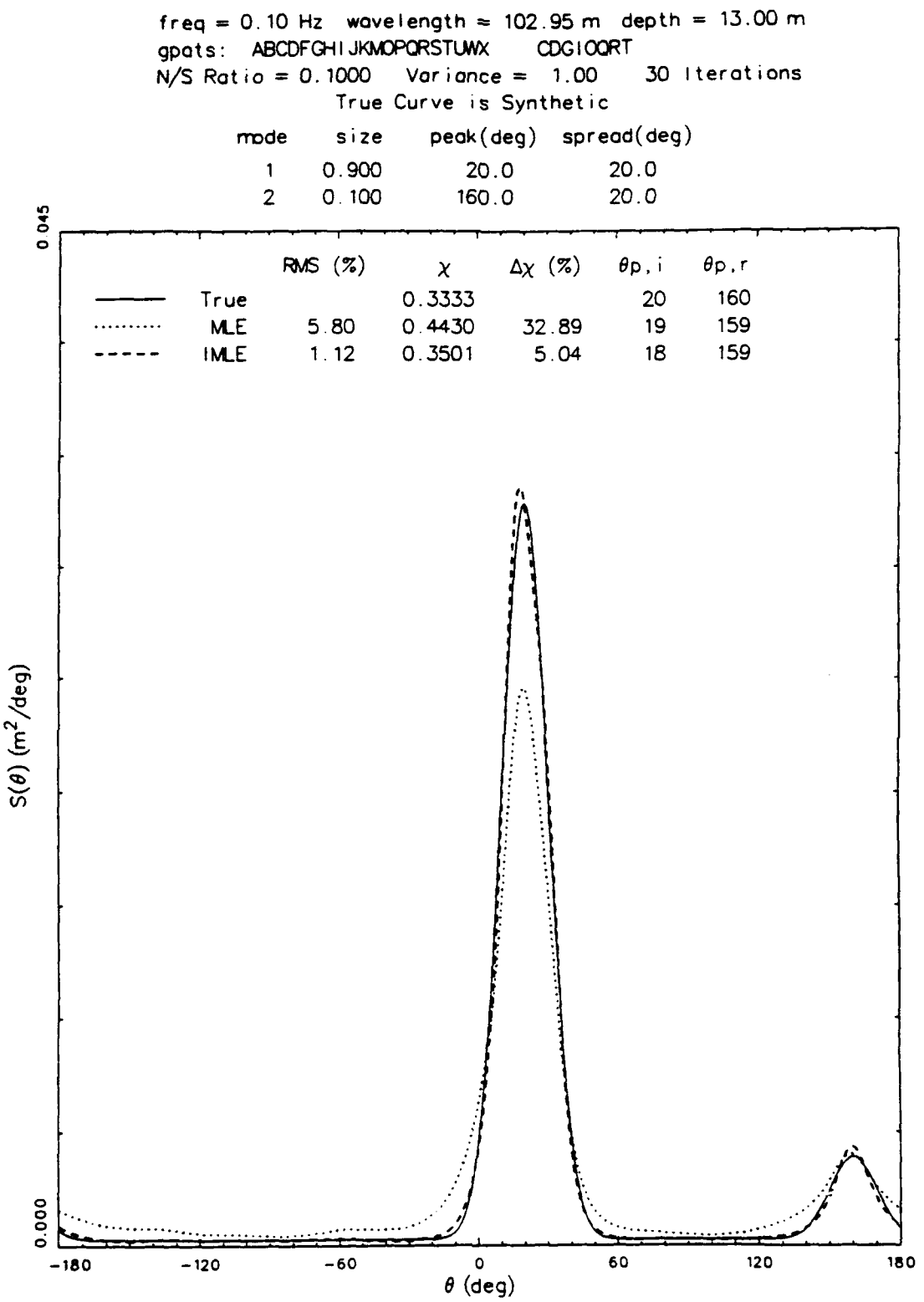

Figure C2. Same conditions as in Figure C1, but with increased noise

high, given the range of reflection coefficients listed in Appendix A and depicted in Appendix B.

15. Many of the values listed in Appendix A are nearer to 0.1 than 0.3, so the test conditions shown in Figure C2 can be modified by changing the relative sizes of incident and reflected energies, keeping all other governing parameters the same. Figure C3 shows such a case where the incident energy is raised to 98 percent of the total signal, the reflected energy is 2 percent of the total signal, and the true reflection coefficient becomes approximately 0.14. The behavior of the IMLE estimate in Figure C3 is largely the same as in Figure C2, but now the slight errors mentioned in the last paragraph have a larger effect on the estimate of the reflected energy, and the reflection coefficient is overpredicted by about 22 percent.

16. When the modal peaks are close together, it is sometimes more difficult for the IMLE algorithm to resolve the true spectral structure. Figure C4 shows a rather extreme case where the modal spreads stay the same as in Figure C3, but the peak directions are moved to within 60 deg of each other. Also, the area of the reflected mode is halved from the value used in Figure C3, reducing the true reflection coefficient to about 0.11. The small variations in the IMLE estimate from the true spectrum result in an over-prediction of the reflection coefficient by about 42 percent. This result is not surprising because, in this case, the area of the noise spectrum is 10 times the area of the reflected signal. This suggests that field data having estimated reflection coefficients of order 0.1, under low energy (high N/S) conditions, and having high incident angles of attack will be subject to this much error, at least. Additional errors (e.g., those due to uncertainty in cross-spectral estimates) in field data and not evaluated here will likely increase errors in reflection coefficients.

17. The errors shown in Figure C4 are extreme for the set of test conditions evaluated at this frequency and noise level. If the modal peaks remain close together, but the modal spreads increase so that modal tail regions both overlap and cross the nominal 90-deg boundary that distinguishes "incident" from "reflected" energy, the errors decrease again. Figure C5 shows a low-noise (N/S = 0.0001) case with modal peaks separated by 60 deg, modal spreads increased to 40 deg (from 20 deg in Figure C4) and the reflected mode given 10 percent of total signal variance. Both modal tail regions cross the 90-deg boundary, so the reflection coefficient is somewhat higher

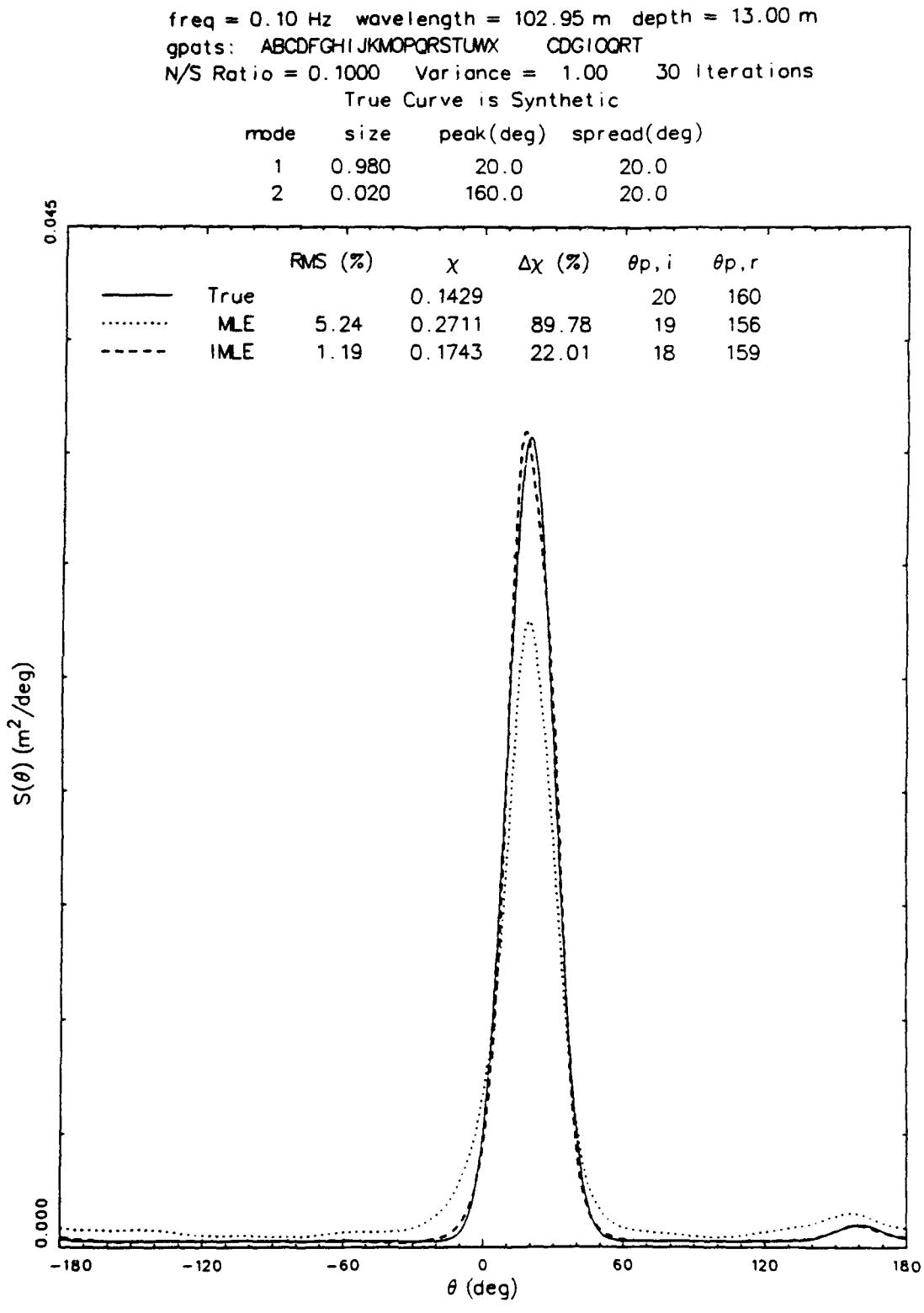

Figure C3. As in Figure C2, but with a smaller reflection coefficient

freq = 0.10 Hz wavelength = 102.95 m depth = 13.00 m
gpats: ABCDFGHIJKMOPQRSTUWX CDGIOQRT
N/S Ratio = 0.1000 Variance = 1.00 30 Iterations
True Curve is Synthetic

mode	size	peak(deg)	spread(deg)
1	0.990	60.0	20.0
2	0.010	120.0	20.0

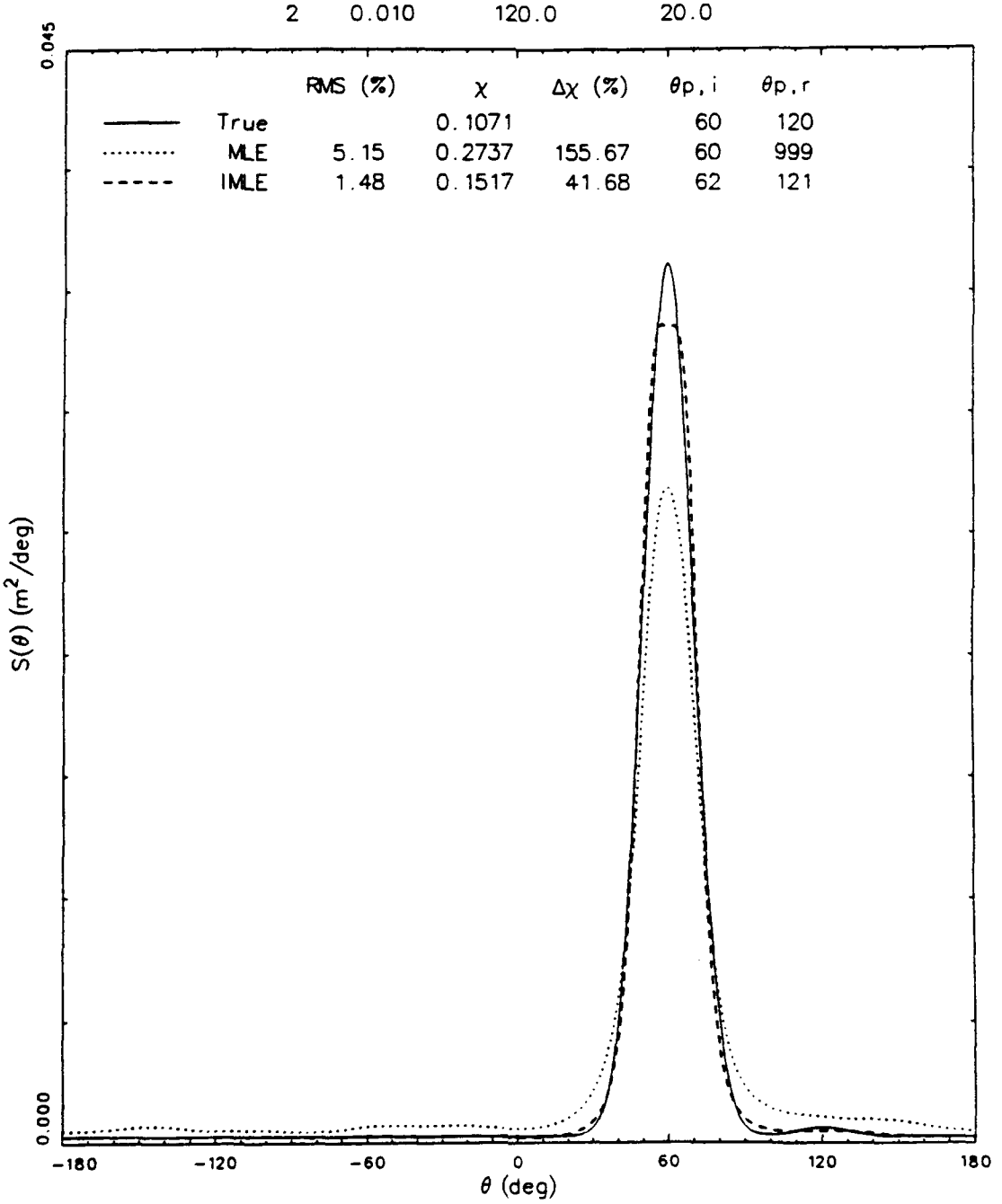

Figure C4. As in Figure C3, but with small reflection coefficient and modal peaks in close proximity

freq = 0.10 Hz wavelength = 102.95 m depth = 13.00 m
gpats: ABCDFGHIJKMOPQRSTUWX CDGIOQ
N/S Ratio = 0.0001 Variance = 1.00 30 Iterations
True Curve is Synthetic

mode	size	peak(deg)	spread(deg)
1	0.900	60.0	40.0
2	0.100	120.0	40.0

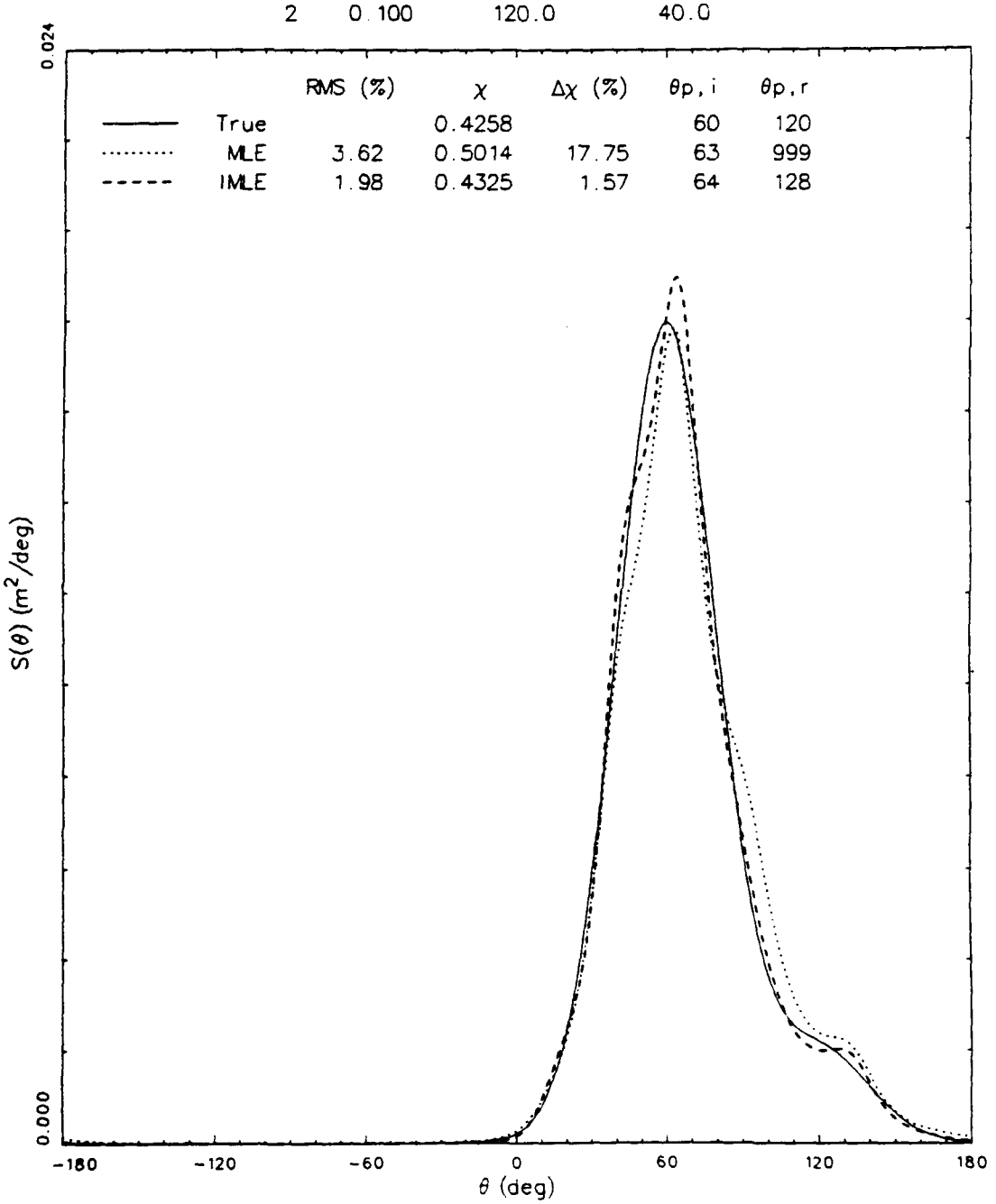

Figure C5. A case with modal peaks in close proximity, broad modal spreads, low noise, and moderate reflection coefficient

(χ = 0.43) than the case where the modes are well isolated (χ = 0.33). As can be seen in Figure C5, variations of the IMLE estimate about the true spectrum do not have a large effect on the reflection coefficient because both modal regions have large areas and the noise level is low. Consequently, the estimated reflection coefficient is only in error by about 2 percent.

18. If the noise level is increased for the case shown in Figure C5, error estimates remain small, partly because both incident and reflected signals remain relatively high. Figure C6 shows a case where N/S = 0.1, and all other conditions are the same as in Figure C5. The IMLE estimated spectrum matches the true spectrum almost perfectly, and the error in the reflection coefficient is less than 1 percent. Part of the reason for this very good result is somewhat fortuitous in that the structure of the true spectrum is rather well matched to the array geometry. Consequently, fewer gages are lost in the dynamic elimination process, leaving more gages with viable information to resolve the true spectral shape. In this case 11 gages are used, whereas in the other cases shown in this appendix, only 6 to 8 gages are used.

19. If the amount of energy in the reflected mode is reduced from the case shown in Figure C6, there is very little change in the result. Figure C7 shows a case where the reflected mode has only 2 percent of total signal energy, a condition where the reflection coefficient would be about 0.14 if the modes were well separated. In Figure C7, the true reflection coefficient is about 0.30, mostly because the tail of the incident mode dominates the calculation. The IMLE estimate remains good, with the error in reflection coefficient being less than 3 percent.

20. Clearly, Figures C1 to C7 show that there is great variety in the quality of reflection coefficients derivable from the SAMSON array with the IMLE algorithm. Results depend strongly on the nature of the overall spectral shape, the amount of energy in the reflected mode, and the amount of noise. There is also a likely dependence on wave frequency because short-wave (high-frequency) spectra tend to be better resolved than long-wave (low-frequency) spectra with an array of finite spatial extent. To gain a broader view of the ability to resolve reflection coefficients, a number of calculations were done, varying the test frequency and all six of the parameters governing the shape of the true spectrum.

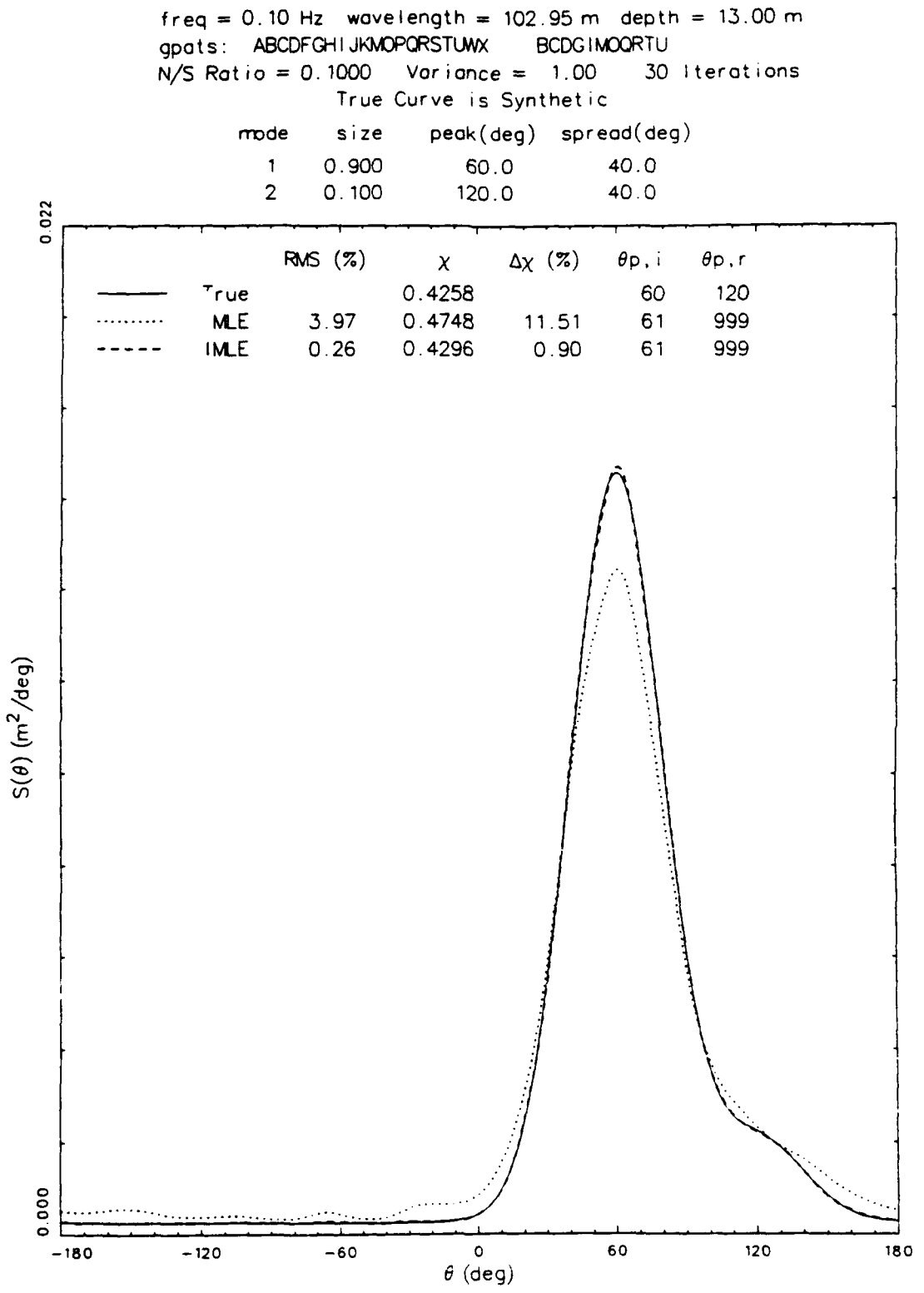

Figure C6. As in Figure C5, but with increased noise

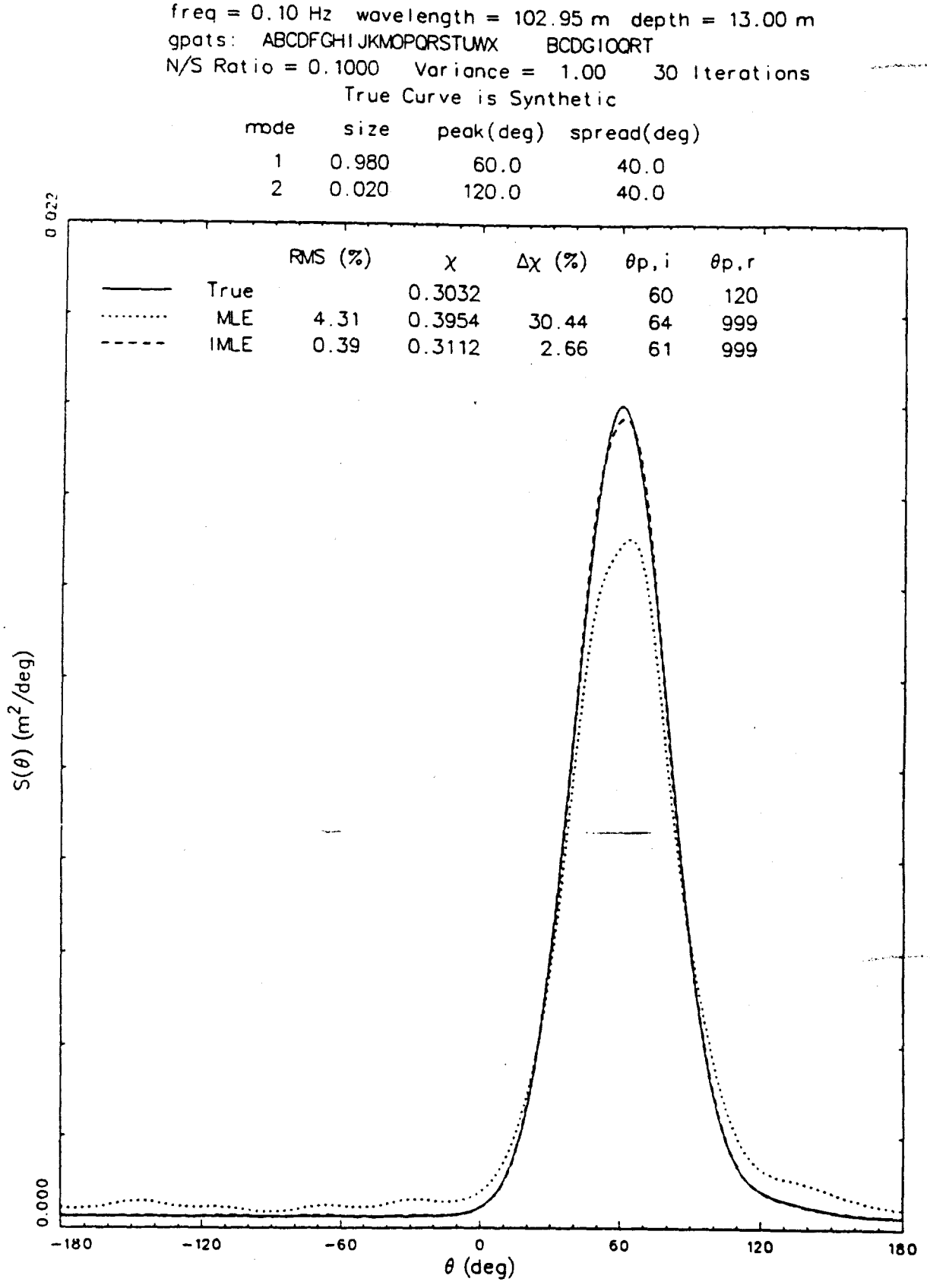

Figure C7. As in Figure C6, but with less energy in the reflected mode

21. To obtain more realistic results, ranges of values for background noise were approximated from the SAMSON spectral parameters listed in Appendix A. As discussed in paragraphs 38 to 41 in the body of this report, overall characteristic wave height H_{mo} was found from the total volume of the frequency-direction spectrum, and so included any noise that was present, whereas the wave heights that characterized incident ($H_{mo,i}$) and reflected ($H_{mo,r}$) energy were computed after first removing the noise, which was estimated by averaging the smallest 10 values of the integrated direction spectrum $S(\theta_m)$, defined by Equation 3 in the main text. Signal variance plus noise is then 16 times the square of H_{mo}, and signal variance alone is estimated as 16 times the sum of the squares of $H_{mo,i}$ and $H_{mo,r}$. An estimate of the noise-to-signal ratio is thus found from

$$N/S = \frac{16 H_{mo}^2 - 16 (H_{mo,i}^2 + H_{mo,r}^2)}{16 (H_{mo,i}^2 + H_{mo,r}^2)} \tag{C12}$$

or, more simply,

$$N/S = \frac{H_{mo}^2}{H_{mo,i}^2 + H_{mo,r}^2} - 1 \tag{C13}$$

Figure C8 shows the set of N/S values computed from Equation C13 plotted as a function of H_{mo}. For moderate and high H_{mo}, the estimated N/S values in Figure C8 lie mostly in the range 0.01 to 0.1. Significant, but not surprising, is that N/S tends to increase for small wave heights (i.e., small signal). For $H_{mo} < 0.5$ m, the upper limit of the range increases to about 0.3. While the numbers shown in Figure C8 are only approximate, they do suggest the order-of-magnitude range for N/S to use in synthetic data tests.

22. Based on these results, tests were conducted using four values for N/S: 0.0001, 0.01, 0.1, and 0.3, with the first one being a very low value to act as the control for essentially no noise. The signal part of the synthetic spectrum was defined by varying the remaining five governing parameters. The parameter set consisted of: five P_i = 0.99, 0.98, 0.95, 0.90, and 0.80; four $\theta_{p,i}$ = 0, 20, 40, and 60 deg; four $\theta_{p,r}$ = 120, 140, 160, and 180 deg; five $\Delta\theta_i$ = 10, 20, 30, 40, and 50 deg; and four $\Delta\theta_r$ = 10, 20, 30, and 40 deg. All combinations of all parameters were employed, resulting in 1,600 different

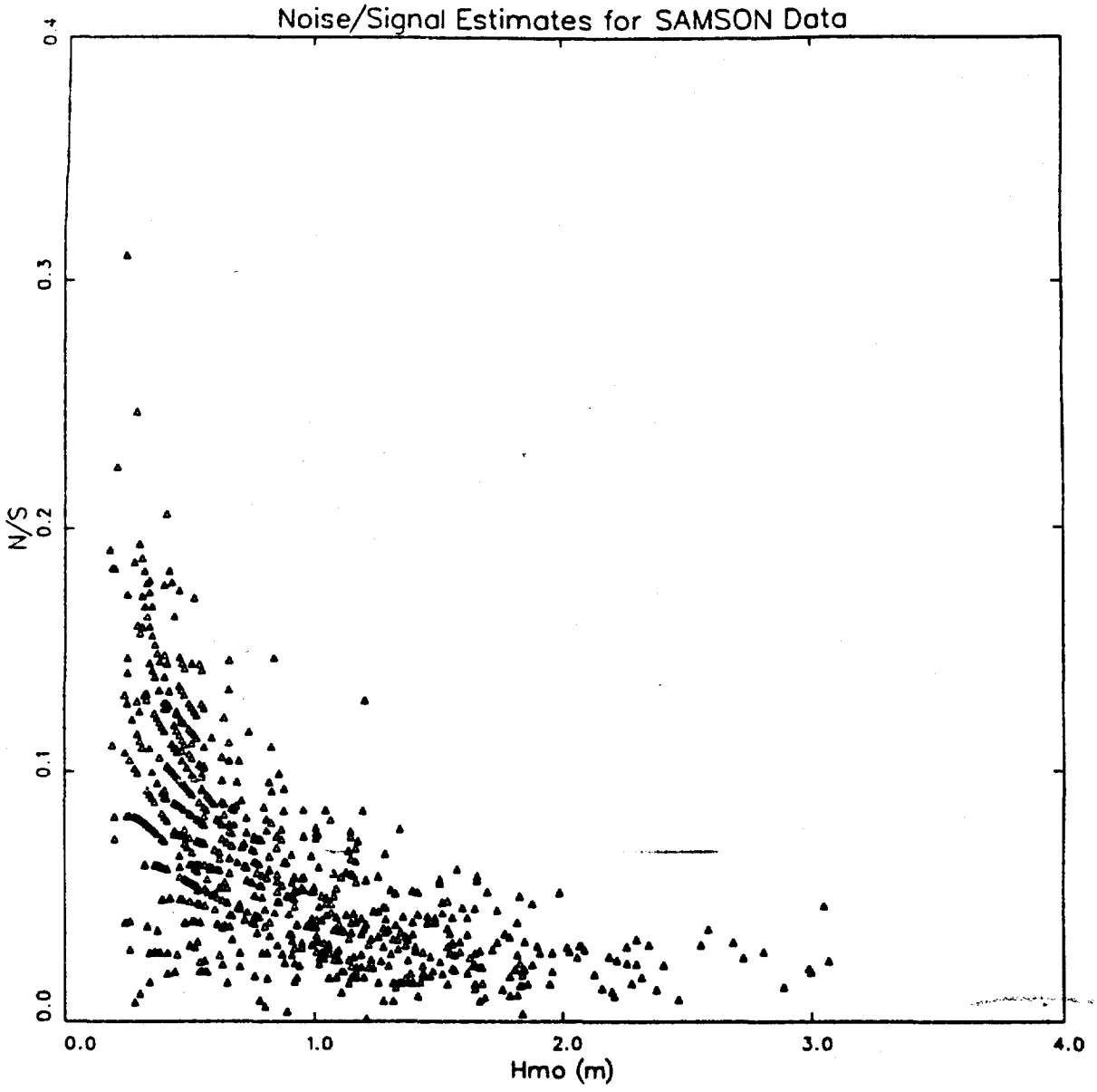

Figure C8. Guidance for N/S ratios to use in synthetic spectra

shapes for the signal spectra. An additional dependency on wavelength was also examined by using four wave frequencies equal to 0.06, 0.10, 0.14, and 0.21 Hz. A constant water depth of 13 m was used for all cases. Altogether, 25,600 test cases were evaluated for error in reflection coefficient.

23. Resulting estimates of error were grouped both by frequency and N/S ratio. Groups were then plotted (Figures C9 to C12) as scatter diagrams of error as a function of true reflection coefficient. Results for 0.06-Hz waves are shown in Figure C9; those for 0.10-Hz waves are shown in Figure C10; those

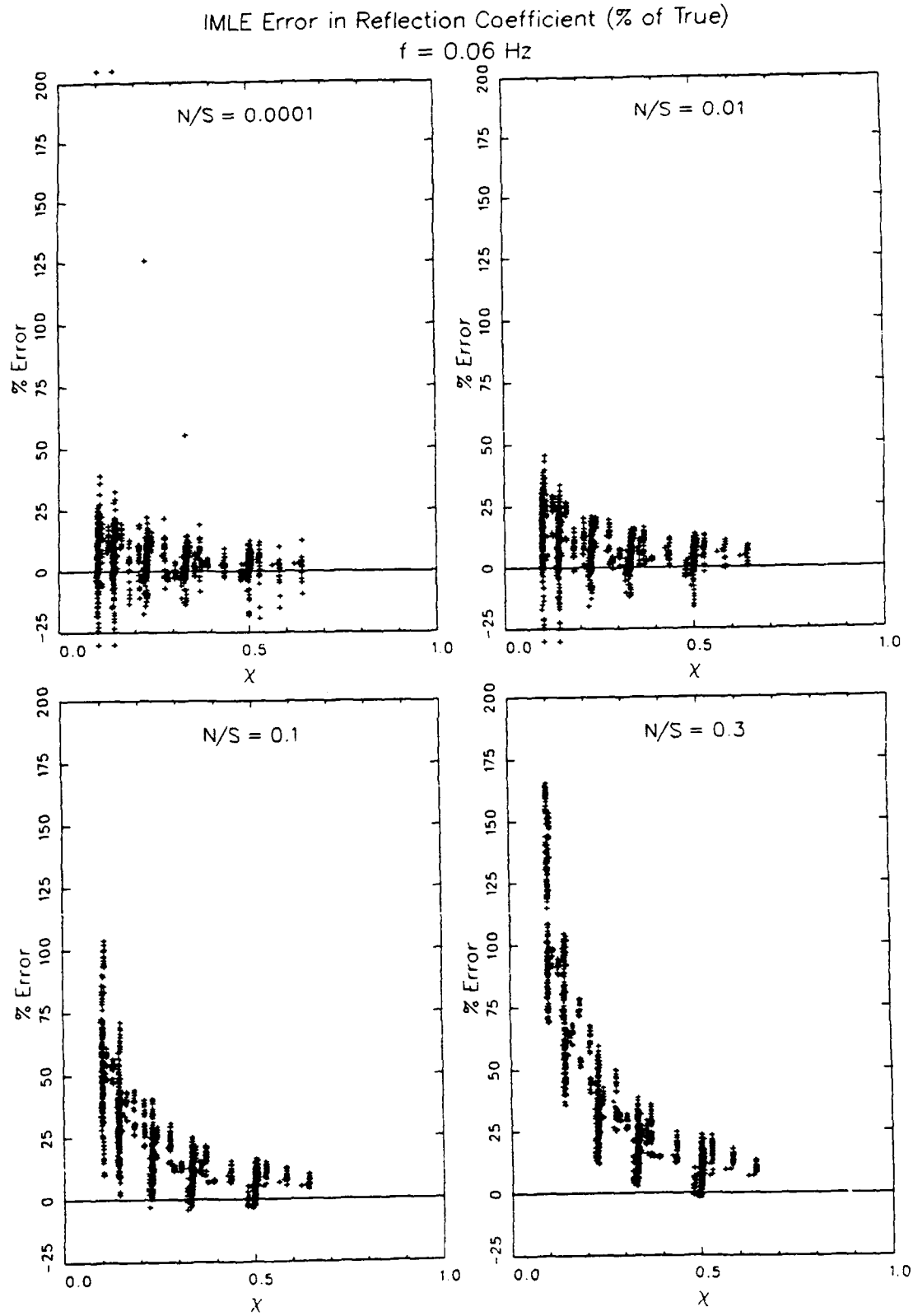

Figure C9. Test results for 0.06-Hz waves

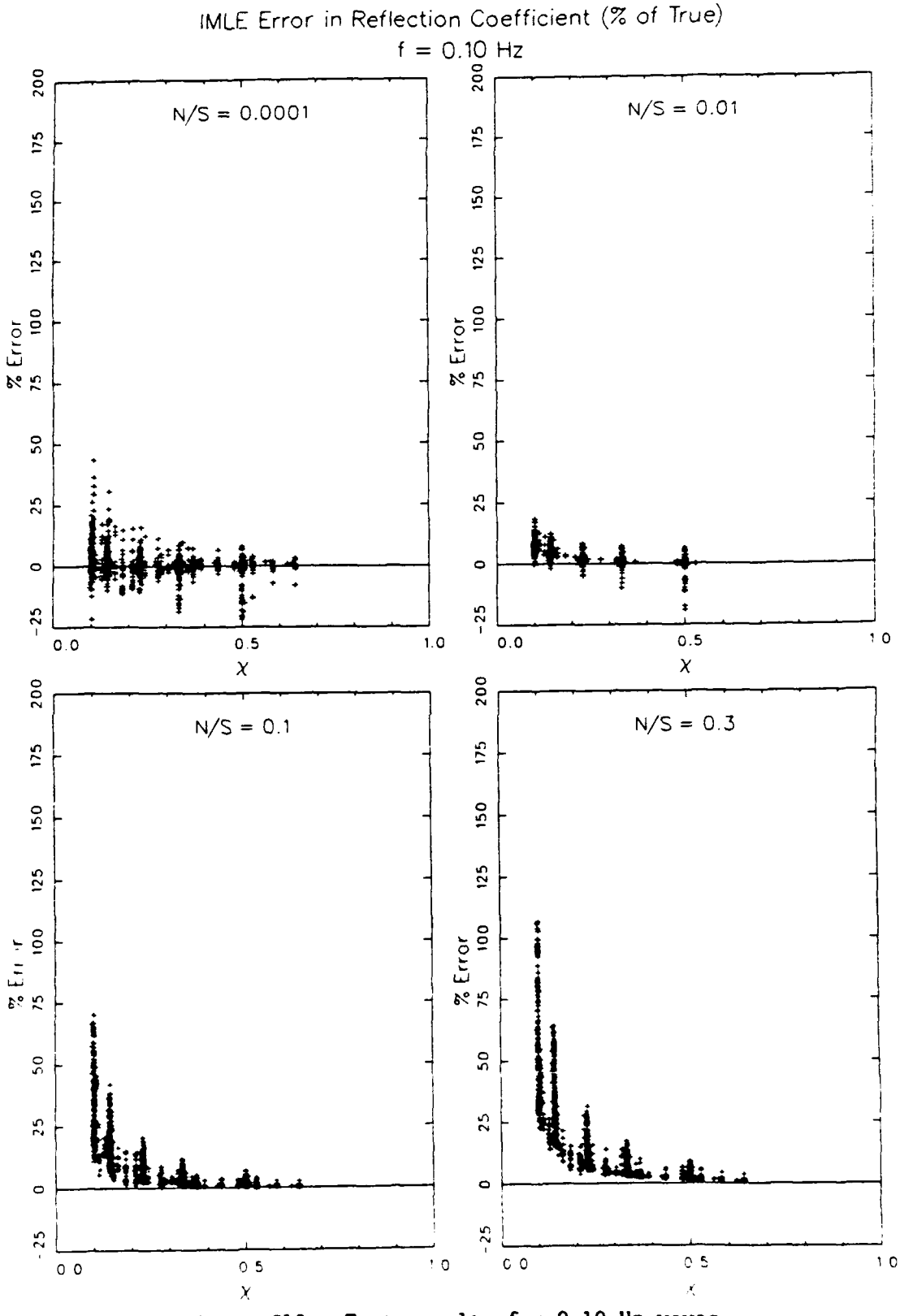

Figure C10. Test results for 0.10-Hz waves

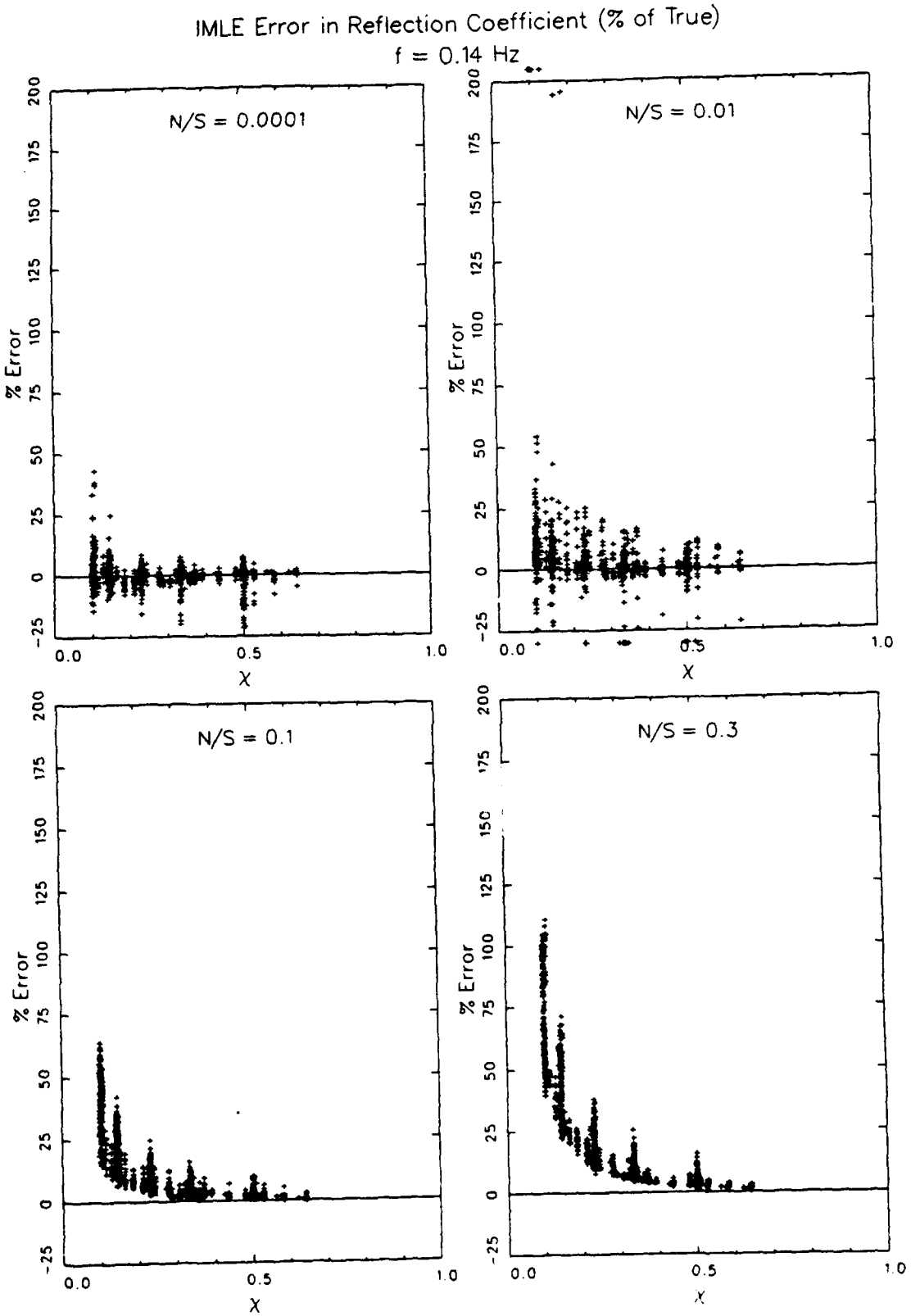

Figure C11. Test results for 0.14-Hz waves

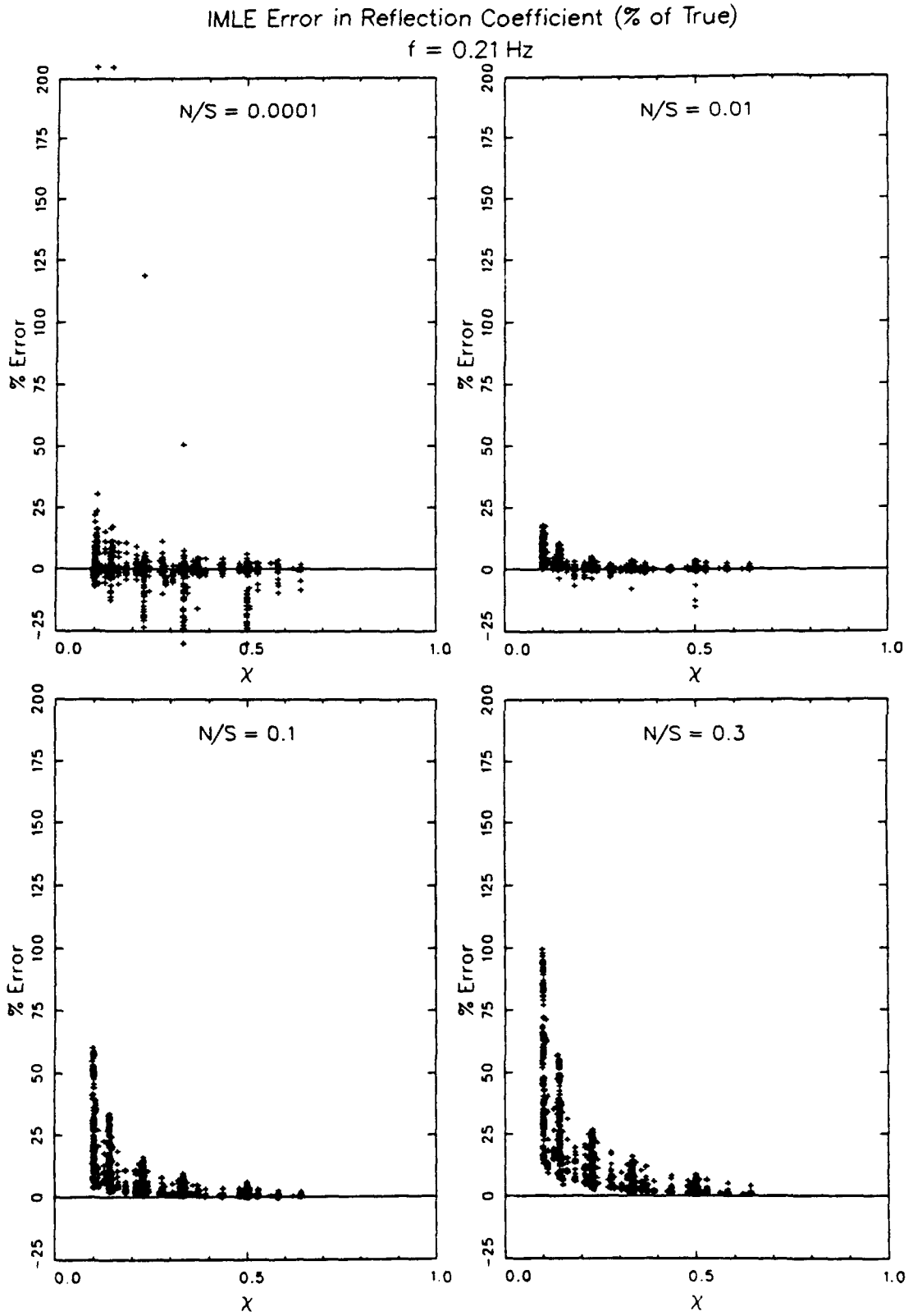

Figure C12. Test results for 0.21-Hz waves

for 0.14-Hz waves are shown in Figure C11; and results for 0.21-Hz waves are shown in Figure C12. A few (< 10) extreme outlier errors (near 400 percent) for some values of χ are not plotted in Figures C9 to C12 so that the major point groupings could all be plotted at the same scale. Collectively, Figures C9 to C12 show tendencies for the error in reflection coefficient to increase with increasing N/S, increase with decreasing wave frequency, and increase with decreasing true reflection coefficient. The plots also show a strong tendency for the algorithm used here to overpredict the true reflection coefficient, probably because the noise level tends to be underestimated, as mentioned in the discussion of Figures C3 and C4, above.

24. A summary of the results of this analysis is obtained by computing means and standard deviations for subsets of the error analysis results (including the outlier points not shown in Figures C9 to C12). A strong banding of data is seen in Figures C9 to C12 for the five values of χ corresponding to the result of Equation C5 for the five P_i used in these tests. Each band contains about 250 data points, so reasonably representative means and standard deviations can be computed for these five χ. Errors for intermediate values of χ follow the same distribution patterns as the five main clusters in all of the figures, so the summary results are properly representative of the whole data set.

25. Figure C13 illustrates the summary statistics. Nominal ranges of frequency and noise-to-signal ratio in which reflection coefficients computed from the SAMSON data are reasonably reliable can be deduced from this figure. Both the bias and range of error are largest for small χ at all noise levels. The high range of error suggests that results are highly dependent on specific structures of the true spectra. This result means that evaluating errors for low-χ SAMSON data would have to be done on a case-by-case basis because the spectral shapes vary considerably. Such an analysis is beyond the scope of this report, but it seems that reflection coefficients near 0.1 or less are likely to be considerably in error. If background noise levels are high, the cutoff for reliable reflection coefficients increases. At $N/S = 0.3$, the expected (i.e., the mean) error does not drop below 20 percent until χ is about 0.3 or higher.

26. For low to moderate noise levels, for all frequencies tested, and for $\chi \geq 0.2$, the expected error is less than about 20 percent and the scatter of error estimates is small, suggesting that results are not too

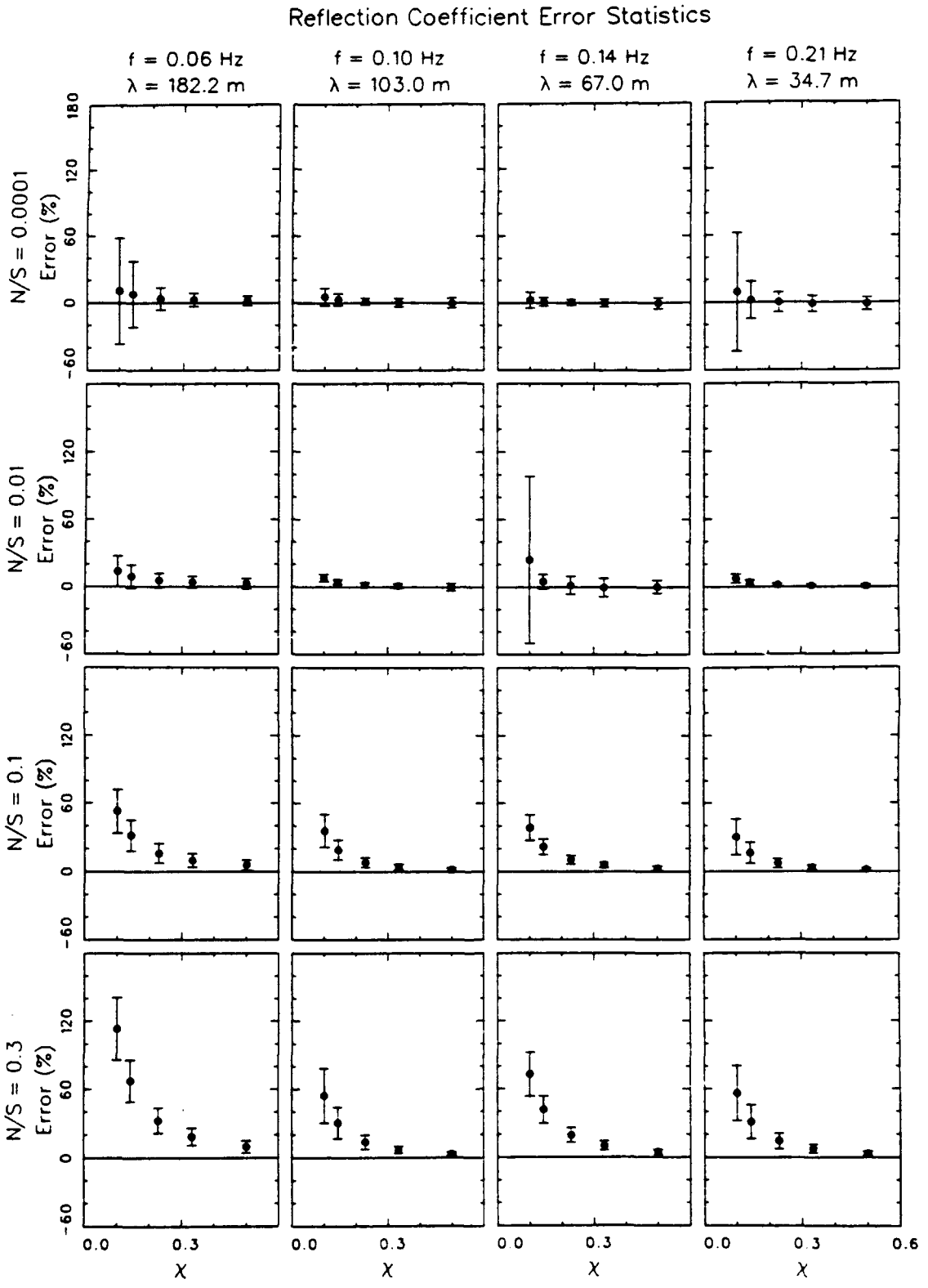

Figure C13. Means and standard deviations of errors in χ

dependent on specific spectral shape. In the SAMSON data, estimated noise levels are reasonably low for H_{mo} greater than about 0.5 m. Consequently, reported reflection coefficients are expected to be good at the 20-percent level for $\chi > 0.2$ and $H_{mo} > 0.5$ m. An uncertainty of a factor of 2 or more can be expected for $\chi \approx 0.1$.

Appendix D: Notation

Appendix D: Notation

C_{pq}	Coincident spectral density between gages at coordinates x_p, y_p and x_q, y_q
dd	Mnemonic for two-digit day of the month
df	Increment of frequency
$d\theta$	Increment of direction
$D(f_n, \theta_m)$	Element of directional distribution function at n^{th} frequency and m^{th} direction
f_n	n^{th} discrete frequency of a set of N frequencies
f_p	Spectral peak frequency
$f_{p,i}$	Peak frequency of incident spectrum
$f_{p,r}$	Peak frequency of reflected spectrum
H_{mo}	Spectrum-based characteristic wave height
$H_{mo,i}$	Characteristic height of incident spectrum
$H_{mo,r}$	Characteristic height of reflected spectrum
i	Complex notation, $\sqrt{-1}$
k	Radian wave number
m	Index integer
mm	Mnemonic for two-digit representation of month in a calender year
M	Upper limit of indices denoted m
N	Upper limit of indices denoted n
N/S	Noise-to-signal ratio
P_i	Fraction of total signal variance in the incident mode of a bimodal test spectrum
Q_{pq}	Quadrature spectral density between gages at coordinates x_p, y_p and x_q, y_q
RMS	Root-mean-square difference of true and estimated spectra expressed as a percentage of S_{max}

RMS_I	Root-mean-square difference of IMLE spectrum and true spectrum expressed as a percentage of S_{max}
RMS_M	Root-mean-square difference of MLE spectrum and true spectrum expressed as a percentage of S_{max}
$S(f_n)$	Frequency spectral density at n^{th} discrete frequency
$S(\theta_m)$	Direction spectral density at m^{th} discrete direction
$S(f_n,\theta_m)$	Frequency-direction spectral density at n^{th} discrete frequency and m^{th} discrete direction
$S(f_{p,i},\theta_m)$	Frequency-direction spectral density at peak frequency of the incident spectrum and at m^{th} discrete direction
$S(f_{p,r},\theta_m)$	Frequency-direction spectral density at peak frequency of the reflected spectrum and at m^{th} discrete direction
$S_a(f_n)$	Auxiliary frequency spectral density at n^{th} discrete frequency
S_i	Estimate of total incident variance
$S_i(f_n)$	Incident frequency spectral density at n^{th} discrete frequency
$S_I(\theta_m)$	Spectrum at m^{th} discrete direction estimated with the IMLE algorithm
S_{max}	Maximum value of true spectrum
$S_M(\theta_m)$	Spectrum at m^{th} discrete direction estimated with the MLE algorithm
S_N	Total variance in noise spectrum
$S_N(f_{p,i})$	Estimated total variance in noise spectrum at the peak frequency of the incident spectrum
$S_N(f_{p,r})$	Estimated total variance in noise spectrum at the peak frequency of the reflected spectrum
S_r	Estimate of total reflected variance
$S_r(f_n)$	Reflected frequency spectral density at n^{th} discrete frequency
T_p	Spectral peak period
$T_{p,i}$	Peak period of incident spectrum
$T_{p,r}$	Peak period of reflected spectrum
yy	Mnemonic for two-digit representation of year

yymmdd	Date mnemonic, a concatenation of year, month, and day mnemonics
$\delta\theta_i$	Directional half-width of the incident signal mode of a bimodal test spectrum
$\delta\theta_r$	Directional half-width of the reflected signal mode of a bimodal test spectrum
$\Delta\theta_i$	Directional width parameter of the incident signal mode of a bimodal test spectrum
$\Delta\theta_r$	Directional width parameter of the reflected signal mode of a bimodal test spectrum
$\Delta\chi$	Error in estimated reflection coefficient as a percentage of the true reflection coefficient
$\Delta\chi_I$	Error in reflection coefficient estimated with the IMLE algorithm as a percentage of the true reflection coefficient
$\Delta\chi_M$	Error in reflection coefficient estimated with the MLE algorithm as a percentage of the true reflection coefficient
λ	Wavelength
θ_m	Element m of a discrete set of wave directions
θ_p	Peak wave direction
$\theta_{p,i}$	Peak direction of incident wave spectrum
$\theta_{p,r}$	Peak direction of reflected wave spectrum
χ	Reflection coefficient based on wave heights
χ_I	Reflection coefficient of a spectrum estimated with the IMLE algorithm
χ_{mo}	Reflection coefficient based on characteristic wave heights
χ_M	Reflection coefficient of a spectrum estimated with the MLE algorithm
$\chi_{p,i}$	Reflection coefficient at the peak frequency of the incident wave spectrum
$\chi_{p,r}$	Reflection coefficient at the peak frequency of the reflected wave spectrum